BNL-61859
INFORMAL

ATF CO_2 Laser System Upgrade to Terawatt Peak Power

I.V. Pogorelsky

ATF, NSLS

Brookhaven National Laboratory

725C, P.O.B. 5000, Upton, NY 11973

Tel: (516) 282-5801, Fax: (516) 282-3115

Abstract

This document describes the proposed upgrade of the 10-GW peak power 50-ps CO_2 laser presently operational at the ATF to the 1 TW level at a shorter, 3-10 ps, pulse duration. The approach adopted is based on state of the art CO_2 laser technology and an experience gained in the course of the ATF laser design and application for the laser accelerator experiment. The proposed upgrade is an economical way for the ATF to become in a short time among leading users facilities available for next generation (≥100 MeV) laser accelerator studies.

Acknowledgments

The author wishes to thank I. Ben-Zvi for encouraging and guiding of this study, J. Skaritka, T. Rao, M. Babzien, K. Batchelor , K. Kusche who are putting there expertise and enthusiasm into this project and N. Kurnit and L. DiMauro for helpful discussions. This work was performed under the auspices of the U.S. Dept. of Energy, Contract No. DE-ACO2-76CH00016.

Contents

Section **Page**

Figures and Tables

Figure — Page

Table — Page

Section 1

Executive summary

Laser-driven particle acceleration is an emerging application area for high-power lasers. The fundamental motivation for studying laser-driven particle accelerators is the ultra-high fields attainable with high-intensity pulsed lasers. High-power, picosecond CO_2 lasers would be attractive candidates for novel particle accelerator drivers. However, it should be understood that the technology of picosecond CO_2 lasers has yet to mature. That is why the development of such a system involved a massive research effort started in 1986 at the Los Alamos National Laboratory, a contractor for the major components of the ATF (Accelerator Test Facility) laser system. Since 1990, R&D work was continued at the ATF during the assembling and commissioning of this laser system. The R&D work resulted in an operable table-top CO_2 laser system of 10 GW peak power delivered in a pulse envelope of 50-ps duration.

A CO_2 laser system is now one of the principal components of the ATF which also includes a 65-MeV RF linac and a picosecond Nd:YAG laser. This assembly of basic components represents the prime goal of the ATF: to serve the scientific community as a user's facility for testing various novel strong-field-physics concepts based on using a high-brightness relativistic e-beam and high-power laser radiation in combination.

The present program of experiments at the ATF, based on using the interaction of a CO_2 laser with e-bunch, includes:

Laser-driven electron acceleration:

- Inverse Cherenkov Laser Acceleration (STI, UCSB, Stanford, BNL),
- Inverse Free Electron Laser Acceleration (BNL, Yale, UCLA),
- Grating Accelerator (BNL, LANL, Princeton, UCLA).

Generation of high-brightness electromagnetic radiation:

- High Gain Harmonic Generation FEL (BNL, Grumman).

While already under way or being scheduled to start using the existing 10-GW CO_2 laser system, most of these experiments will greatly benefit from further laser power increase. The above listed laser acceleration schemes are potentially scalable to long acceleration distances and high acceleration energies. However, a 100 GW or higher peak power CO_2 laser is needed to comply with priority items announced by DOE for laser accelerator studies: 100 MeV demonstration and, based on it, 1 GeV accelerator design. Based on state of the art laser technology as well as on experience gained in the course of development and operation of the present ATF CO_2 laser, we show that a relatively compact single-beam picosecond CO_2 laser system is scalable to the terawatt peak power level. Physical principles of the terawatt CO_2 laser design concept are presented in Section 3.

In Section 4, we describe a proposed conceptual design for the ATF CO_2 laser system upgrade to a terawatt level where the present 3-atm UV preionized 1-*l* CO_2 amplifier will be replaced with a 5-atm x-ray preionized 8-*l* amplifier with a 250 GW output. At the next stage of the power upgrade, we switch to the multi-isotope gas mixture. That should permit a further peak power increase to the several terawatt level via laser pulse shortening.

In Section 5 we describe the proposed management plan, including project organization, schedule, procurement plan and cost estimate.

The Appendix presents Specifications for design, manufacturing and tests of a high-power large-aperture CO_2 amplifier as they appear in the Request for Proposal which is a part of the procurement process for the amplifier components.

Section 2

INTRODUCTION. Present status of ATF CO_2 laser and upgrade requirements

High-power CO_2 lasers are traditionally attractive for strong-field physics applications. Such interest is based upon the ability to build fairly economical large-aperture, large-volume CO_2 lasers with high-energy output and high repetition rates. The relatively long wavelength of CO_2 lasers (~10 μm) is also desirable for certain laser particle acceleration concepts. However, because of the relatively narrow rotational structure typical for molecular gas spectra (~10^{10} Hz), picosecond pulse formation via a mode-locking technique has not been as successfully obtained with CO_2 lasers as with solid state lasers, which have wide crystal-host broadening of the individual ion spectral lines (10^{11}-10^{12} Hz).

Over the years alternative ways to produce CO_2 pulses with picosecond time scales have been developed including: optical free-induction decay, optical parametric oscillation, and semiconductor switching. The last method is based on modulating the reflective and transmissive properties of a semiconductor by optically controlling the free-carrier charge density. Subpicosecond CO_2 pulses have been demonstrated by this method. A train of 1.5 GW peak power, 2-ps pulses was produced in a 1-mm^2 beam from a regenerative CO_2 amplifier. However, the potential for high-peak-power extraction in a short single picosecond pulse from a big-volume gas-discharge amplifier has not been capitalized so far.

This approach to a picosecond high-peak power CO_2 laser is further persued at the ATF, where a 10-GW table-top CO_2 laser system is in operation to test several laser acceleration schemes.

Fig.1 presents a diagram of the ATF. The laser system consists of Nd:YAG and CO_2 lasers. The YAG laser with 30 mJ, 15 ps, 3 Hz, λ=1.06 μm output controls picosecond slicing in the CO_2 laser and serves as the linac photocathode driver. A ~15 ps FWHM bunch of electrons is produced by a laser photocathode electron gun and is accelerated to 70 MeV by two RF traveling-wave linac sections. The CO_2 laser beam is transported to several locations in the experimental hall where it interacts with electron bunches to test different laser acceleration schemes.

The CO_2 laser system, a block-diagram of which is presented in Fig.2, consists of a hybrid TEA oscillator, picosecond semiconductor switch, and a UV-preionized multipass TE amplifier. CO_2 laser delivers pulses of IR radiation synchronized with the electron bunches. Such synchronization is automatically achieved by optical switching of the 100-ns CO_2 oscillator output by the same YAG pulse which is ultimately used to drive the photocathode. Following the optical gating, the 1-MW oscillator pulse, now several picosecond long, is amplified in 8 passes through a 1.2 m long 3-atm UV-preionized discharge. The Fourier transform of its pressure broadened rotational lines gives 50 ps. That is about the shortest pulse that we can efficiently amplify with this amplifier.

After being amplified to 20 GW peak power, the 50-ps pulse is transported to the experimental hall where it is used for electron acceleration experiments. The first under way is Inverse Cherenkov Accelerator (ICA) experiment which is also illustrated by a block-diagram in Fig.2. Using an axicon mirror, a radially polarized laser beam is converged to the e-beam axis. Because of the wave-front inclination, a longitudinal accelerating component of the electric field is developed. When the phase-matching condition is satisfied, by filling the interaction cell with hydrogen, the

injected electron bunch propagates in phase with the optical field and experiences an acceleration. This process is complementary to coherent Cherenkov radiation. That is why this acceleration scheme is called the Inverse Cherenkov Accelerator.

In the first ICA run using a 0.7 GW CO_2 laser beam, up to 3.5 MeV peak acceleration has been observed. Up to 12 MeV acceleration over a 20 cm interaction distance is predicted by computer simulations for 5 GW of laser drive power.

The Grating Linac and IFEL are two other laser accelerator experiments scheduled at the ATF. The Grating Linac scheme is based on excitation of an evanescent surface field when a laser beam is cylindrically focused onto a periodic structure. 1 GV/m acceleration is predicted for this scheme with a cylindrically focused CO_2 beam of 700 GW/cm^2 intensity.

Another, IFEL scheme, is based on the accelerating action of a linearly polarized laser beam onto electrons having an oscillating trajectory inside a wiggler. Model simulation predicts 100 MeV/m acceleration with a 200 GW CO_2 laser beam in a properly tapered wiggler.

The experimental demonstration of 100 MeV electron acceleration and, based on it, a 1 GeV accelerator design are set as the next milestones in laser accelerator development. The ATF laser accelerator schemes are potentially scalable to ΔW=100 MeV if at least 200 GW of a CO_2 laser peak power is provided.

Other intensively and world wide studied electron acceleration schemes, such as laser wake field and laser beat wave accelerators, are based on the interaction of electron beams with laser-produced plasma wake fields. Recently demonstrated record high-gradients of electron acceleration give promise for further advancement of these laser accelerator concepts towards practical devices.

CO_2 lasers are potentially attractive as plasma-based accelerator drivers because of the 100 times stronger pondermotive action of its radiation compared with more extensively used 1-μm lasers. Note that the pondermotive action is the foundation of such key processes in plasma accelerators as avalanche and tunnel ionization, relativistic self-focusing, and plasma wake excitation. Despite this advantage, CO_2 lasers were not specified so far for the ultra-high acceleration experiments due to their relatively long, typically of the order of 1 ns, pulse duration.

The proposed here terawatt-class picosecond CO_2 laser, with its short, down to 3 ps pulse duration, solves this problem and **presents new opportunities in laser acceleration study.**

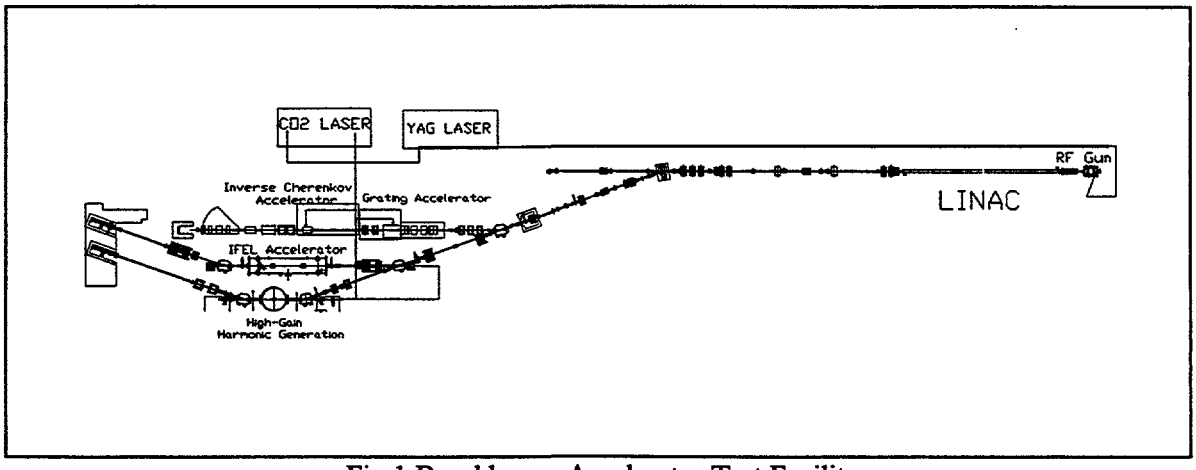

Fig.1 Brookhaven Accelerator Test Facility

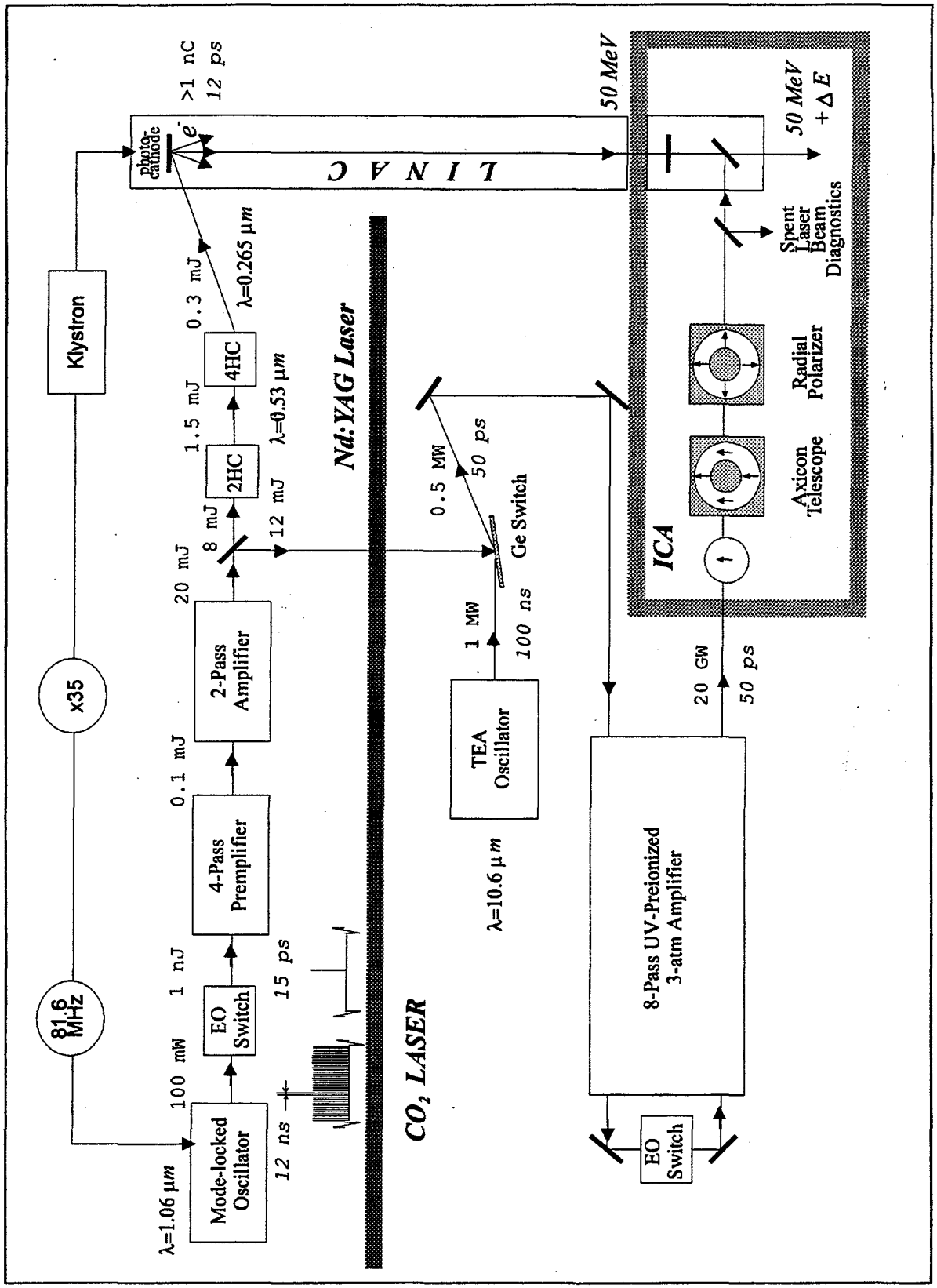

Fig.2
ATF laser system

Section 3

Physical approach to compact terawatt CO_2 laser

In this Section, we discuss physical principles and considerations specific for the design of the high-power picosecond CO_2 laser system. The following subjects have been selected for this discussion:

1) A high peak laser power may be attained in two ways: by energy increase or by reduction of the laser pulse duration. The second approach is a natural way to build a compact high-peak power laser. Pulse shortening also helps to relieve energy-proportional optic damage constraints. Short pulse duration is similarly important for a number of potential applications such as plasma accelerators. In Paragraph 3.1, we will see how bandwidth of a CO_2 amplifier defines requirements on the amplifier medium (pressure, isotopic content) and imposes a 3 ps minimum to the amplified laser pulse duration.

2) In Paragraph 3.2 we show that low peak power CO_2 laser pulses of down to 3 ps duration, required as a seed signal for the high-power amplifier, may be produced with a semiconductor switching method controlled by a picosecond Nd:YAG laser which is available at the ATF.

3) By reviewing in Paragraph 3.3 data on optical breakdown thresholds in gases and optical materials, we define the minimum aperture of the discharge area and output optic window for the terawatt CO_2 amplifier.

4) Small signal gain and saturation define the laser beam size and distance to be traveled through the amplifier before attaining the required power and energy. In Paragraph 3.4, we use computer simulations of picosecond CO_2 laser pulse amplification to find laser beam parameters that ultimately determine optical configuration and physical dimensions of the amplifier.

5) The design of the picosecond terawatt-class CO_2 laser amplifier suggested in this proposal is based on present state of the art laser technology. However, no prototype to such device exists and may be directly reproduced. The choice of design parameters for such an amplifier is not straightforward. That is why we devote Paragraph 3.5 to describe the methods for the amplifier configuration and parameters selection. We start the paragraph justifying the choice of x-ray preionization for the high-pressure, large-aperture laser amplifier and then give guidelines towards choosing the appropriate parameters for discharge circuit.

3.1 Bandwidth Limitations in Picosecond Pulse Amplification

In this paragraph we are going to highlight specifics of picosecond laser pulse amplification in a molecular gas discharge when spectral gain is periodically modulated by a rotational structure. When a short laser pulse propagates in a resonant-amplifying molecular medium, two characteristic spectral parameters and their corresponding time constants should be taken into consideration. The first is time, δt, corresponding to a frequency interval between the centers of V-R lines, which is 18 ps for the P-branch of the 10-μm band. The other is a collisionally induced dipole dephasing time, T_2, related to a Lorenzian line shape of a V-R transition by the ratio $\delta\nu^1 =$

πT_2, where T_2 is inversely proportional to the gas pressure. For 1-atm CO_2-laser gas mixture, $T_2 \approx$ 100 ps.

Let us consider, how the amplification of the CO_2 laser pulse with the initial duration τ_0 depends upon the time constants δt and T_2.

a) $\delta t < \tau_0 < T_2$:

If the input laser pulse width, τ_0, is longer than δt, then just one rotational line is involved in the amplification. During the amplification, the spectrum of the input pulse is filtered by the gain spectrum and, eventually, pulse duration increases as illustrated by Fig.3(e).

Pulse broadening is most pronounced at atmospheric or lower pressure, when the spectral width of the individual V-R transition is much less than the spectral separation between the rotational lines, and the gain spectrum may be considered as discrete.

b) $\tau_0 > T_2$:

Pressure broadening of the individual rotational lines helps to minimize the pulse shape distortion. Because T_2 is inversely proportional to the gas pressure, it becomes ~10 ps at 10 atm. Fig.3(f) gives the illustration for τ_0=30 ps pulse amplification.

In a 3-atm amplifier filled with a regular gas mixture, pulses of τ=60 ps may be amplified without appreciable distortions. A shorter pulse will experience less small signal gain (SSG), due to worse bandwidth matching to the gain spectrum, and gradual expansion of the pulse duration to $\tau \approx T_2(g_o l_s)^{1/2}$ occurs, where l_s - distance at which gain reaches saturation. In typical case, $(g_o l_s)^{1/2} \approx 3$. These considerations, together with a natural reduction of the initial energy for shorter sliced pulses, make seed pulses shorter than ~60 ps unattractive to use in a 3-atm amplifier. That correlates with experimental results obtained at the ATF, when performance degradation has been observed when 30 ps sliced pulses were injected into the amplifier.

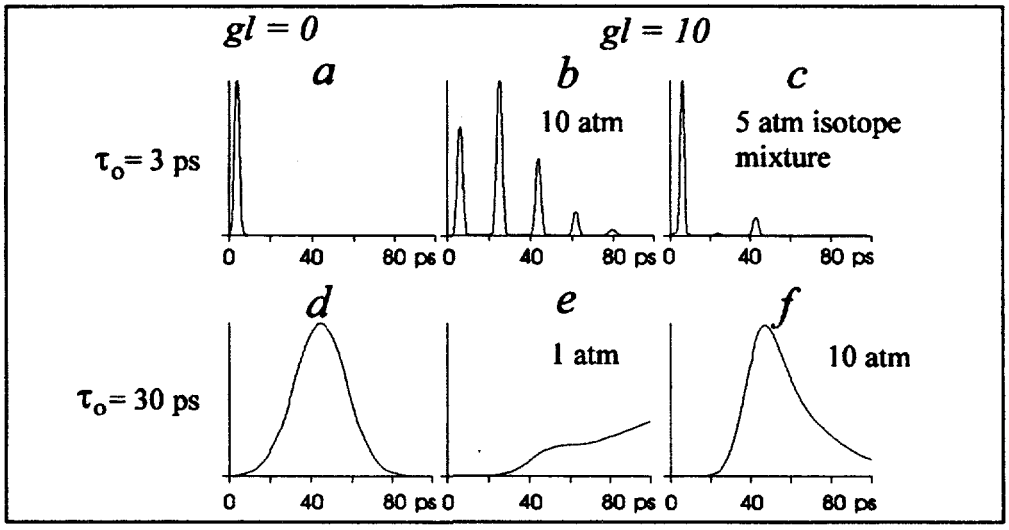

Fig. 3

Picosecond pulse propagation in the CO_2 amplifier with a total gain $g_o l$=10 (initial intensity 1 MW/cm^2) (by P. Kannari, Keio University, Yokohama) a) initial 3-ps pulse; b) same after amplification in a regular 10-atm mixture; c) same in a 4-atm isotopic mixture; d) initial 30-ps pulse shape; e)same after amplification in a 1-atm regular mixture;. f) same after amplification in a 10-atm regular mixture.

c) $\tau_0 < \delta t < T_2$:

The spectral width of a short laser pulse (less than ~20 ps) may cover several discrete transition lines. The electric field of such an input pulse excites a polarization in CO_2 molecules, which are in various V-R states. Since molecules in different states are characterized by different frequencies, these polarization components eventually become dephased. As a result, the spectral and time structure of the induced radiation will not remain equal to those of the initial pulse. At a low, ~1 atm, gas pressure the discrete gain spectrum transforms the spectrum of the input pulse from continuous to discrete, and its Fourier transform corresponds to a pulse train with a δt period. At higher pressure, the broadening effect smoothes the discrete gain spectrum. As a result, for the same pulse width a 10-atm amplifier causes smaller pulse splitting (see Fig.3(b)). Somewhat less splitting has been obtained in similar simulations for the 10-atm case by N. Kurnit, et.al. in LANL and by V. Platonenko in Moscow State University. Selective enhancement of the leading pulse is predicted due to saturation at larger $g_o l$ products.

An alternative to achieve gain smoothing is a reduction of the spectrum modulation period using an isotopic gas mixture. Replacement of one of the oxygen nuclei by that of a different isotope destroys the symmetry of the CO_2 molecule. That means that twice as many V-R transitions are allowed and the gain spectrum becomes twice as dense as with a regular CO_2 molecule. If we consider a mixture $^{12}C^{16}O_2$:$^{12}C^{16}O^{18}O$:$^{12}C^{18}O_2$ = 1:2:1, then, due to isotopic shifts, the combined spectrum will have an approximately 4-times denser rotational line structure in overlap regions than with a regular CO_2 molecule. Computer modeling shows that the reduction in spectral line interval results in considerably less short-pulse distortion during amplification (see Fig.3(c)). The technical advantage of this approach relates to the greater ease of establishing a large-aperture stable discharge at 3-4 atm in comparison to 10 atm.

Design-impact conclusions to the paragraph:

Spectral bandwidth sets 3 ps limitation to the minimum duration of a pulse amplified in a CO_2 laser. For 10 ps and shorter pulses 10 atm amplifier may be required. Using multi-isotope CO_2 mixture, 4-5 atm pressure would be adequate for amplification of 3 ps pulses.

3.2 Picosecond Pulse Generation

The picosecond switching method used in the ATF CO_2 laser system is based upon the modulation of the reflective and transmissive properties of a semiconductor by optically controlling the free-carrier charge density. A short-wavelength picosecond laser pulse with a photon energy above the band gap of the semiconductor creates a highly reflective electron-hole plasma in the surface layer of a semiconductor, such as germanium, which is normally transparent to 10-μm radiation. The free-electron density, N_e, at the semiconductor surface is linearly proportional to the absorbed control pulse fluence E by the relation

$$N_e = \alpha E / h\nu, \qquad (1)$$

where α is the absorption coefficient and $h\nu$ is the photon energy. For a Nd:YAG control laser, α^{-1}=1 μm, and, for a characteristic pulse fluence of $E \approx 2$ mJ/cm^2, the density of excess free carriers, N_e, created in Ge is more than the critical density of N_{cr}=1.6x10^{19}/cm^3 defined by

$$N_{cr} = \omega^2 m_e n_0^2 / 4\pi e^2, \qquad (2)$$

where ω is the radiation frequency, m_e- reduced free carrier mass, n_0- refractive index at normal conditions. The refractive index drops due to free carriers according to the equation

$$n=n_0(1-N_e/N_{cr})^{1/2} \qquad (3)$$

and turns imaginary at $N_e>N_{cr}$. At this moment, the Ge slab switches from a window at 10 μm to a highly reflective mirror due to its "metallization" by a picosecond Nd:YAG control pulse.

After the termination of the control pulse, the main process governing the time evolution of the excess free carriers at the surface, and hence the reflectivity, will be ambipolar diffusion having a characteristic time constant of 150 ps in Ge. To define the trailing edge of the pulse, shortening it to a few picoseconds, the complement to reflection switching, transmission switching, is used for a second stage. An optically delayed control pulse cuts off the trailing edge of the transient pulse by initiating reflection and absorption with a $\sigma=6\times10^{-16}$ cm^2. Absorption makes the Ge slab opaque for 10-μm radiation during the ~50 ns time-interval while the electron-hole recombination takes place. The resulting "sliced" transmitted pulse has the desired few-picosecond length determined by optical delay adjustment of the control radiation before the transmission switch.

It would be convenient to have control pulses of a duration shorter than the desirable switched pulse duration. However, due to a very critical dependence of the reflectivity upon N_e in the vicinity of N_{cr} (see Fig.4), duration of the switched CO_2 laser pulse may be even shorter than the control Nd:YAG pulse. Indeed, as shown in Fig.4, reflectivity change from 10% to 90% occurs while N_e changing from 1×10^{19} cm^{-3} to 2×10^{19} cm^{-3}, correspondingly. These numbers are attained at the absorbed control laser fluence, correspondingly, 1 mJ/cm^2 and 2 mJ/cm^2. Hence the pace of the reflectivity change, and therefore the ultimate switched pulse duration, will be determined not as much by the total control pulse duration but by the time interval when the required energy density is delivered. For instance, for the ideal rectangular shaped control pulses delivering 10 mJ/cm^2 of the total absorbed fluence (still below the damage threshold), the switching time will be one tenth of the pulse duration. In this way, with 30-ps control pulses down to 3 ps switched pulses may be obtained.

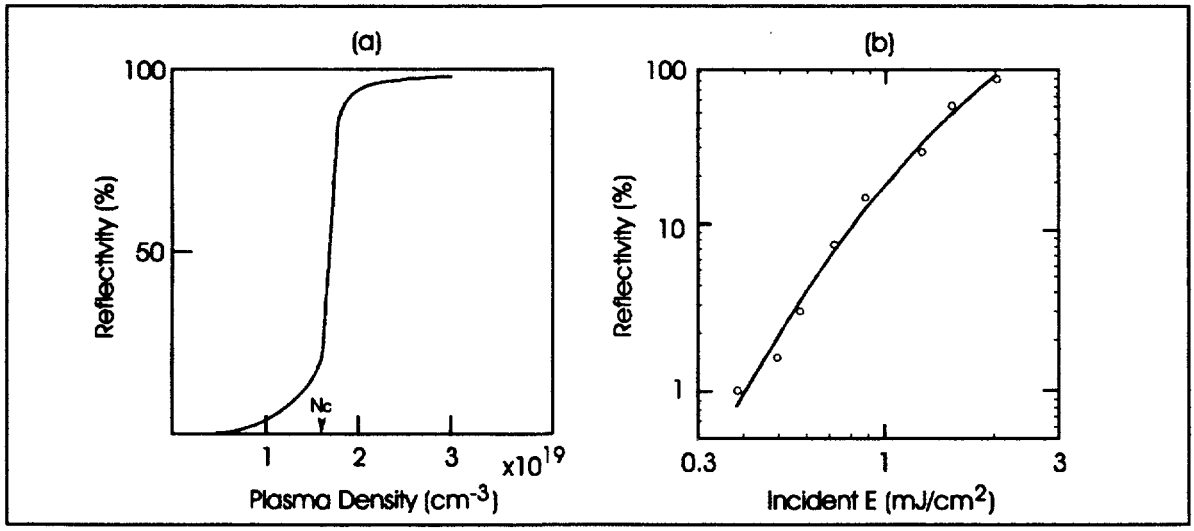

Fig.4

Optical switching of a Ge Brewster window normally transparent for a p-polarized CO_2 laser beam: a) theoretical reflectivity as a function of free-carrier density (after A. Alcock and P. Corkum); b) reflectivity measured as a function of a picosecond Nd:YAG laser energy absorbed (after S. Jamison et. al.)

For further sharpening and contrast increase of the switched laser pulse, the transient response of a thin etalon can be exploited as suggested by P. Corkum. It is quite obvious that an etalon tuned to minimum reflectivity will serve as a differentiator transmitting radiation with constant or slowly changing intensity and reflecting signals in a time scale shorter than a double optical thickness of the etalon. For instance, a 100-μm thick Ge etalon may serve for efficient differentiating and background subtraction for 3-ps switched pulses.

Design-impact conclusions to the paragraph:

With the available 20-mJ, 15-ps control pulses from the ATF Nd:YAG laser, 10 ps and even 3 ps short, background-free CO_2 laser pulses may be sliced using a semiconductor switching technique.

3.3 Optical Breakdown Limitations

The practical limits to intensity increases in picosecond CO_2 laser beams are set by such detrimental effects as optical component (windows, mirrors) damage and gas breakdown. Relevant data collected with the ATF CO_2 laser system and compiled from other publications is presented in Table 1. We list there materials most commonly used in CO_2 laser technology as windows or beamsplitters (NaCl, ZnSe), mirrors (Cu), Pockels cells (CdTe), as well as laser gas medium and ambient air.

TABLE 1

Optical breakdown thresholds.

Material/Gas	Pulse Length	E_{th} (J/cm^2)
Cu	1.7 ns 50 ps	11 4
NaCl	2 ns 2 ps	7.5 0.5
ZnSe	1.5 ns 200 ps 50 ps	1.2 0.5 0.5
CdTe	50 ps	0.2
Air (1 atm)	1 ns 200 ps	10 10
CO_2:N_2:He (10 atm)	7 ps	>1.5 (estimated)

Limited experimental data available on gas breakdown and optical material damage with picosecond CO_2 laser pulses may be supplemented with theoretical considerations under the assumption that, at I<1 TW/cm^2, both effects are described by the avalanche electron multiplication mechanism. This mechanism assumes the inverse proportionality between the breakdown threshold flux, I_{th}, and laser pulse duration, τ, i.e., $I_{th}\sim\tau^{-1}$, or the invariance of the threshold fluence, E_{th}, with τ. That is why the $E_{th}\sim\sqrt{\tau}$ relation, typical in a nanosecond time scale where a thermal damage mechanism is valid, flattens when approaching 100 ps and shorter pulse widths. Consequently, we can expect E_{th} levels similar to those presented in Table 1 for shorter CO_2 laser pulses as well.

Analyzing the data in Table 1, we come to the conclusion that optical window damage may be a primary limitation to energy scaling of picosecond CO_2 lasers. However, the laser pulse shortening

should provide nearly proportional increase of the finite power density that may be transmitted through the window without its damage.

Design-impact conclusions to the paragraph:

Assuming $E_{th}/2$ figure as a damage-safe fluence through a window and an additional 2.5 safety factor due to spatial nonuniformity of the output laser beam (presumably Gaussian) we estimate a *surface-averaged* fluence deliverable through a NaCl or ZnSe window at the level of 0.1 J/cm^2. That means that a 30 cm^2 aperture window will be required to extract a 1-TW, 3-ps pulse from the amplifier and, correspondingly, a 100 cm^2 window to transmit 1-TW, 10-ps or 3-TW, 3-ps pulses. Approximately 2-times reduction of the clear aperture will be permissible when using Brewster optical windows due to larger surface illumination at the oblique incidence.

3.4 Amplification of Picosecond Pulses

In this paragraph we consider how fast and efficiently a picosecond CO_2 laser pulse extracts energy from the amplifier and, hence, how long of a beam path is needed for a realistically sized laser beam to attain the terawatt power level. By answering these questions, we specify the optical configuration and physical parameters of the amplifier.

When estimating performance of CO_2 amplifier, the following two intrinsic physical parameters play the major role:

- a small signal gain $g_o=\sigma N^*$, where σ - gain cross-section, and N^* - population of upper laser level;
- saturation fluence $E_s=h\nu/2\sigma$.

Parameters g_o and E_s regulate the energy amplification process described by the Franz-Nodvik equation

$$E_{out} = E_s \ln\{1 + \exp(g_o l)[\exp(E_{in}/E_s) - 1]\}. \quad (4)$$

The product of these parameters gives an estimate of the potentially extractable energy from the amplifier in a single pass in a strongly saturated regime:

$$\varepsilon_{max} = g_o E_s l S, \quad (5)$$

where l and S, are the length and aperture of the amplifier, correspondingly. Ratio ε_{max}/τ gives the upper estimate of the peak power.

It was already shown in Paragraph 3.3, that the amplifier pressure, P, is critical in determining the minimal pulse duration, τ, supported by the amplifier. Hence, in order to estimate the peak power extractable from the amplifier, we just need to know how ε_{max} depends upon the pressure or, referring to Eq.(5), how g_o and E_s change with pressure.

Due to pressure broadening of the gain spectrum, there is a dependence of g_o and E_s upon pressure via the parameter σ. In addition, g_o depends upon N^* which is subject to the electric discharge conditions. Assuming the current density, i, constant, the electron-molecule collision frequency and, hence, the pump rate rise proportional to the pressure. The assumption of constant current is close to be true because in order to maintain stable discharge conditions the electric field, V/d, must be increased together with the pressure; but the electron mobility and, hence, the electrical conductivity of the discharge plasma drops with the pressure. If the discharge is faster than collisional quenching of the inversion (this is about true for pulsed discharges shorter than $t[\mu s]\approx$

$3/P$[atm]), then we may consider $N^* \sim P$ and g_o invariant with pressure. Ultimately, we come to the conclusion, that $\varepsilon_{max} \sim P$.

However, this simplified approach, more applicable to atomic two-level systems, is complicated for molecular gases such as CO_2. Because of the rotational-vibrational structure of the CO_2 energy levels, two kinds of saturation energies must be considered:

$$E_s = h\nu/2\sigma \text{ and } E_s^v = E_s/Z[j_{max}],$$

where $Z[j_{max}]$ is the maximum relative population of the rotational level in the upper laser level. These quantities correspond, respectively, to the single rotational line saturation energy and to saturation of all rotational lines, i.e., the total vibrational level.

If the initial pulse duration τ_0 is much longer than the characteristic time constant for rotational relaxation, τ_R, the amplification process is governed by the vibrational level saturation energy, E_s^v. Note, that τ_R is inversely proportional to gas pressure, and at 3 atm is equal to 50 ps. For a Boltzman thermal distribution in the discharge, $Z[j_{max}]=0.065$, and using the value $\sigma=5\times10^{-19}$ cm^2 for the 10P(20) line at 1 atm, we obtain $E_s^v=350$ mJ/cm^2.

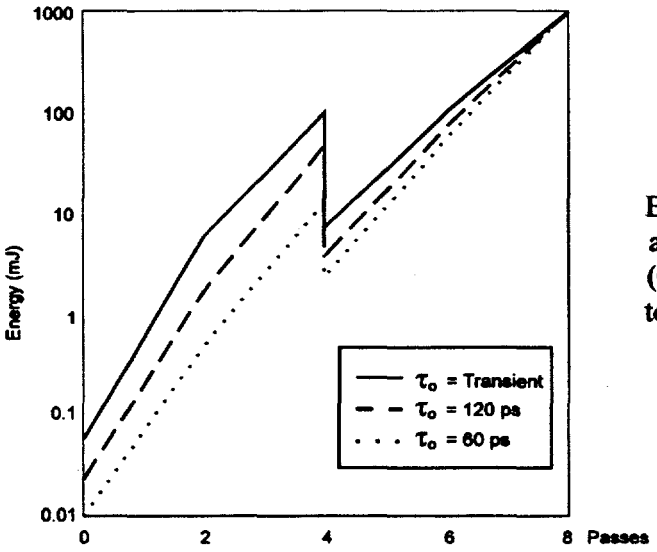

Fig.5
Experimental curves for energy evolution of a laser pulse in 8-pass ATF CO_2 amplifier. (Observed after 4 passes energy drop is due to losses in Pockels cell and plasma shutters used to prevent the amplifier against self-lasing.)

In the situation when τ_0 becomes comparable with τ_R, the effective saturation energy, E_s^*, lies between E_s and E_s^v. The E_s^* value may be obtained in this case via the best fit of Eq.(4), where E_s is substituted by E_s^*, to a computer simulated curve obtained by direct solution of Maxwell-Bloch system of equations that describe the interaction of the laser radiation with excited CO_2 energy levels. Such an approach is used to model several high-power amplifier options. For example, for a 50-ps pulse amplification in a 3-atm discharge, $E_s^*=50$ mJ/cm^2 was obtained for this case as a best fit of Eq.(4) to the experimental curve obtained with the ATF 3-atm amplifier and presented in Fig.5. This figure is close to E_s presuming an efficient energy extraction from just one rotational energy level. For shorter pulses and higher pressure, E_s^* increases for several reasons: pressure-proportional drop of σ (however, g_o stays constant because $N^* \sim P$), faster collisionally induced energy exchange between rotational levels, and interaction of a broad-bandwidth short pulse (remember, the Fourier transform spectrum of a 3-ps pulse covers all rotational lines of the CO_2 laser transition) with many rotational lines.

The computer model used for plotting Fig.6-7 has been verified by comparing curves on Fig.5 with modeling results. The good agreement gives us confidence in using these data for modeling larger

aperture amplifiers. In the considered examples we presume an amplifier module having a moderately large, 32 (4x8) cm^2 optical aperture and the same length, l=1.2 m, and small signal gain, g_o=2.5%/cm, as in the present ATF 3-atm amplifier.

In the first example, as the input to the 3-atm amplifier, we assume a 50-ps, 5-GW, single-rotational-line, 8 cm^2 aperture (3-cm diameter) collimated beam. Such a beam is available from the present ATF CO_2 laser system. After the second pass, it is expanded to 32 cm^2 and stays collimated during the third pass. To determine the energy evolution of the laser pulse after every pass we use the measured gain curve presented in Fig.5 and assume optical losses of 20% per pass. For simplicity, the intensity is considered uniform across the beam diameter. The dynamics of the energy amplification determined in this way are presented in Table 2. As mentioned previously, E_s^*=50 mJ/cm^2 is determined by the best fit of Eq.(4) to the energy gain curve. Considering no pulse duration change during the amplification process, the output power in a 50-ps pulse after the 3-pass amplifier is equal to 160 GW. Close to 100 GW may be extracted without optical window damage.

Table 2

3-passes of 50-ps pulse in 3-atm amplifier

($g_o l$=3, E_s^*=50 mJ/cm^2).

Pass	Size(cm^2)		W(GW)		E (mJ/cm^2)		Amplification	Extraction (%)
	in	out	in	out	in	out	$\mathcal{E}out/\mathcal{E}in$	$\Delta E/E_s^* g_o l$
1	8	8	5	17	31	105	3.5	56
2	8	32	17	60	105	95	3.5	
3	32	32	60	160	95	315	2.7	83

Increase of the amplifier pressure to 5 atm results in E_s^* increasing to 100 mJ/cm^2, via a decrease of σ due to pressure broadening. Some reduction of the initial pulse duration is also possible without distortion when the amplifier pressure is increased. Due to these factors, up to 300 GW peak power in a 30-ps pulse can be expected out of the 5-atm amplifier with the same 5 GW input signal (see Table 3). However, optical damage may limit extractable power to 200 GW.

Table 3

3-passes of 30-ps pulse in 5-atm amplifier

($g_o l$=3, E_s^*=100 mJ/cm^2).

Pass	Size(cm^2)		W(GW)		E (mJ/cm^2)		Amplification	Extraction (%)
	in	out	in	out	in	out	$\mathcal{E}out/\mathcal{E}in$	$\Delta E/E_s^* g_o l$
1	8	8	5	25	20	95	5.0	25
2	8	32	25	100	95	100	4.0	
3	32	32	100	300	100	300	3.0	50

A 10-atm CO_2 discharge module is a better candidate as a final amplifier, providing the prospect for even higher peak power via a combination of output energy increase and pulse shortening. Faster rotational relaxation, $\tau_R \approx 20$ ps, and higher saturation fluence, $E^*_s \approx 500$ mJ/cm^2 (best fit of Eq.(4) to the energy gain curve in Fig.6), complete the argument in favor of the energetic feasibility to reach up to $I = 60$ GW/cm^2 flux at the output of a 3-pass 10-atm amplifier with a 10-ps, 5-GW seed pulse (see Table 4). However, again optical window damage may limit the total extractable power to ~600 GW.

Table 4

3-passes of 10-ps pulse in 10-atm amplifier

($g_o l = 3$, $E_s^* = 500$ mJ/cm^2).

Pass	Size(cm^2)		W(GW)		E (mJ/cm^2)		Amplification	Extraction (%)
	in	out	in	out	in	out	$\mathcal{E}out/\mathcal{E}in$	$\Delta E/E_s^* g_o l$
1	8	8	5	70	6	90	15	15
2	8	32	70	560	90	180	8	
3	32	32	560	1800	180	580	3.2	80

In order to amplify pulses as short as a few picoseconds, a multi-isotope laser gas mixture, e.g., $^{12}C^{16}O_2$:$^{12}C^{16}O^{18}O$:$^{12}C^{18}O_2$ = 1:2:1, should be used (see Paragraph 3.3). Such a mixture is of interest for picosecond pulse amplification due to its nearly filled-in gain spectrum. According to computer simulations, pulses as short as 3 ps can be amplified without significant distortions in a 5-atm multi-isotope discharge. The bandwidth of a 3-ps pulse covers the total 10P CO_2 branch, resulting in efficient energy extraction from all rotational sublevels of the (001) vibrational level.

However, this smoothing of the spectrum results also in a significant SSG drop when compared with the most intense 10P(20) $^{12}C^{16}O_2$ rotational line. $^{12}C^{16}O_2$ molecules constitute only 25% of the total CO_2 molecules in the multi-isotope mixture resulting in a proportional 4-times SSG drop for an individual rotational line. For a 5-atm multi-isotope mixture, the pressure broadened overlapping lines increase the effective SSG at this wavelength by a factor of 1.8. That means that the effective SSG of the multi-isotope mixture is smaller than in a regular mixture by a factor of 2.2.

Because of the considerably lower gain (the single-pass linear gain, $g_o l$, drops from 18 for a regular mixture to 4 for a 5-atm multi-isotope mixture) at least 5 passes through the amplifier would be needed to approach the optical-damage-limited output power, if starting with a 5 GW input. Due to a high saturation energy of $E_s \approx 600$ mJ/cm^2 (best fit to the curve in Fig.7), typical for a multi-isotope mixture, the peak power will be increased to the ~2 TW level in a nearly linear regime, as seen in Table 5. Due to the short pulse duration, we do not reach the optic damage threshold when using a Brewster output window.

Design-impact conclusions to the paragraph:

We considered here several physical options for short CO_2 laser pulse amplification. We have shown that CO_2 amplifiers of 5-10 atm pressure, with ~2.5%/cm small signal gain, and of ~5x10x100 cm^3 or bigger discharge volume are suitable to boost 3-10 ps laser pulses from 5 GW, attained at the ATF so far, to the terawatt level. Although parameters in simulations may change in

wide ranges, the examples given above are not just illustrative. They have been deliberately chosen to fit to the realistically feasible state-of-the-art laser devices the principles of which are discussed in the next paragraph.

Table 5

5-passes of 3-ps pulse in 5-atm multi-isotope amplifier

($g_0 l$=1.35, E_s*=600 mJ/cm^2).

Pass	Size(cm^2)		W(GW)		E (mJ/cm^2)		Amplification	Extraction (%)
	in	out	in	out	in	out	$\mathcal{E}out/\mathcal{E}in$	$\Delta E/E_s^* g_0 l$
1	4	4	5	16	4	12	3.3	3
2	4	4	16	53	12	40	3.3	10
3	8	8	53	175	20	65	3.3	10
4	8	32	175	570	65	57	3.3	15
5	32	32	570	1900	57	190	3.2	20

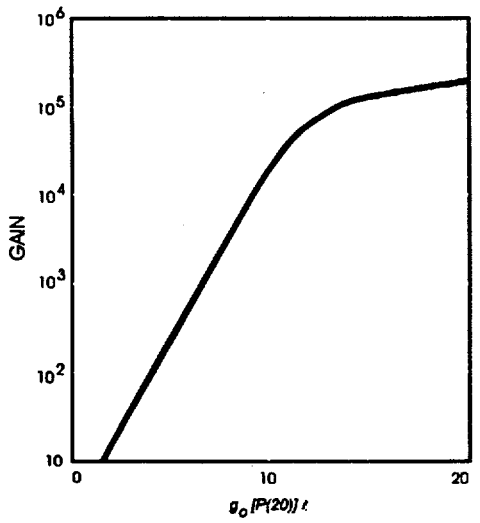

Fig,6

Energy gain modeling (30 ps, 10 atm, E_0= 23 μJ/cm^2)

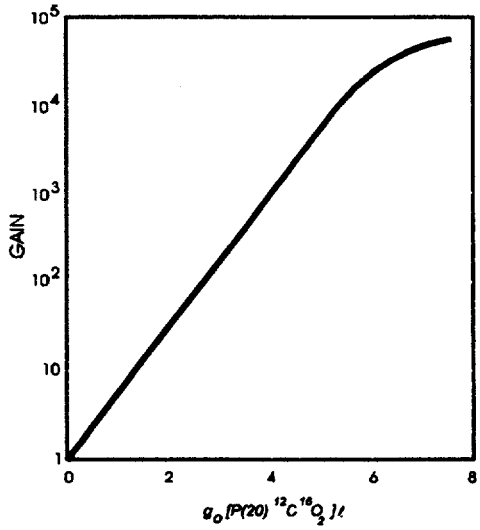

Fig,7

Energy gain modeling(3 ps, 5 atm, multi-isotope, E_0= 23 μJ/cm^2)

3.5 Choice of Discharge Parameters

In our simulations of picosecond pulse amplification made in Paragraph 3.4 we presumed availability of CO_2 amplifiers with 5-10 atm pressure and with 5 *l* or more discharge volume. Such devices are considered technically feasible. However, the design of discharge lasers with such

parameters is not straightforward. That is why we consider it relevant to analyze in this paragraph the principles of excitation of such discharges.

Electric discharge is used to excite CO_2 molecules producing population inversion and optical gain in the 10 μm spectral transition. The electric energy transfer to CO_2 molecules in discharges is via nonelastic collisions with discharge electrons. To facilitate this transfer, relatively light-weight He buffer gas is regularly used as an intermediate agent. Another auxiliary component of the laser mixture, N_2, is necessary for selective resonance excitation of the denoted (001) vibration level of CO_2 molecule, which is the upper level of the laser transition. While the CO_2:N_2:He mixture composition is basically predetermined, the proportion of molecular components to helium, ξ, may vary typically between ξ=15-30%. Rich mixtures are characterized by higher gain, but with lean mixtures it is easier to maintain a uniform volume discharge. We will return to the ξ selection criteria later.

There is a certain choice of the discharge techniques. A self-sustained glow discharge can exist at $dP \leq 0.1$ cm•atm. Above this point, an additional external uniform ionization should be applied to prevent pinching instabilityin the discharge. The simplest corona and UV-preionization methods work well up to $dP \approx 15$-20 cm•atm. Above that level, more intense and volume-penetrating x-ray and e-beam preionizers are used. High ionization efficiency of e-beams makes it possible even to reduce the discharge voltage two times below the self-glow level (so called, e-beam sustained discharge). This helps to maintain the discharge at the optimum normalized field strength, V/dP, resulting in high efficiency of the upper laser level excitation. However, a high probability of e-beam window failure (usually thin metal foils), especially at a high pressure, makes e-guns a bad choice for our application.

In terms of efficiency, x-ray preionizer is in an intermediate position between UV and e-beam ionization. X-ray preionized discharge pumping, while somewhat more complex than UV-preionization, has many advantages for large-aperture high-pressure discharge applications. Because of strong absorption of the preionizing UV radiation by CO_2 molecules, it is difficult to implement even for $dP > 25$ cm•atm (e.g., P=5 atm and d=5 cm). The range for 30-50 keV x-rays is much larger than the dimensions desired here. In addition, the x-ray photoelectron production increases with gas density. This higher photoelectron production coupled with the long x-ray range ensures that the entire discharge volume is filled with initial electrons at a high and uniform density required for stable discharge formation. The photoelectron cross section is higher for CO_2 than for He, ensuring good preionization even for the richer CO_2 mixtures desired for short pulse amplification.

Another important advantage of x-ray preionization is the elimination of spark discharges associated with the UV preionization method, or high energy electron beams associated with e-beam preionization, both of which contribute significantly to the dissociation of CO_2, thus shortening gas lifetime. The x-rays are produced in a separate chamber from the laser gas thus eliminating the hot gas regions associated with sparks. In addition, the x-rays have high enough energy for reasonable transmission through a thin metal electrode, facilitating the use of a smooth electrode rather than a mesh as required for transmission of UV radiation or e-beams. The combination of smooth electrodes and uniform volumetric preionization contributes to more stable discharge formation for a larger range of conditions.

With relatively simple corona-cathode e-guns, collimated "sheets" of x-rays with a cross-section of 0.1 m^2 or more can be readily produced. At an applied cathode voltage of ~100 kV and a typical cathode-target discharge resistance of ~100 Ohm, e-beam with a current density of ~1 A/cm^2 maintained over ~1 μs is adequate to generate in the interelectrode space an x-ray dosage of~20

mrad. Corresponding to this dose, the initial photoelectron concentration of ~10^8 cm^{-3} will be adequate for starting a uniform volumetric discharge at $dP \approx 50$ cm•atm or even higher.

Having made our choice on the preionization mechanism to use, the next key decision would be regarding the parameters of the main discharge. The main externally set parameter of the discharge is voltage. To avoid confusion, we should first clearly define terminology used. We define output voltage, V_{out}, of the high-voltage (HV) pulser as a shock potential developed at the moment of spark gaps triggering. For instance, for the typical Marx-type pulse generator, V_{out} is a single-stage charge voltage multiplied by the number of stages. The voltage step propagating along the current lead toward the load (discharge) is $\frac{1}{2}V_{out}$. When the voltage step reaches the high-voltage electrode in the discharge cell, the conductivity of the plasma, that has been produced to this moment by the preionizer, is low and the discharge gap may be considered as an open end. Because of the signal reflection, double-step potential equal to V_{out} will be erected at the HV electrode. If this voltage is above the breakdown potential determined by d, P, and ξ, the discharge plasma will be fully developed in several (20-40) nanoseconds and plasma active resistance drops to a typical value of 3-5 Ohm (again depends upon d, P, ξ, and electrode surface area S). For normally impedance-matched discharges, the HV electrode potential drops to half of the output voltage and further slowly varies in accordance with the capacitor bank discharging. To support a glow discharge during this phase, the electrode potential should be equal or higher than the discharge sustain voltage, V_s.Hence, V_{out} shall comply with requirements to breakdown and sustain potentials set by parameters d, P, and ξ. Based on available data, we can draw a semi-empirical law for the reduced sustain voltage, V_s/dP, dependence upon ξ:

$$V_s/dP[\text{kV/cm•atm}]=2.5(1+0.1\xi[\%]) \qquad (6)$$

resulting in V_s/dP=6.25 kV/cm•atm @ ξ=15% and V_s/dP=10.0 kV/cm•atm @ ξ=30%. It also turns out that the breakdown voltage is less than 2 times above the sustain voltage (e.g., it is ~10 kV/cm•atm @ ξ=15%). Hence, the pulser suitable to sustain discharge at given d, P, and ξ parameters is automatically good to produce a breakdown at the open circuit conditions. As follows from Eq.(6), technically feasible HV pulse generators having output voltage in the range of 500-1000 kV are capable to maintain a discharge in ξ=15% mixture at dP ranging between 40-80 cm•atm and, correspondingly, dP=25-50 cm•atm @ ξ=30%.

Let us stop for a moment. We already have four primary parameters that characterize the discharge: V, d, P, and ξ. How do we choose the proper setting of this parameters for a design? The following considerations will be relevant:

V- this is the primary restriction in choosing high dP values desirable for high-power picosecond amplifiers. Hence, the higher V - the better. As mentioned previously, technical complications in generating and delivering high electric potentials may restrict the choice by $V_{out} \leq 1000$ kV limit.

ξ - defines dP by Eq.(6), as long as V value is already set. As mentioned previously, the compromise between the discharge stability and a high optical gain is between 15-30%. Which value for ξ to choose depends upon the consideration: what is the limiting factor in energy extraction from the amplifier. If gain is high enough to reach the saturation fluence but the output window damage is the limiting factor (as in the 10-atm example in Paragraph 3.4), it may be reasonable to reduce ξ and, thereby, increase d and the window aperture. If because of low gain the output fluence is much below the optic damage threshold (situation close to the multi-isotope example in Paragraph 3.4), ξ increase should be considered. (Note, that gain used in simulations in Paragraph 3.4 corresponds to ξ=15%.)

P increase leads to higher peak power output because of higher specific stored and extractable energy and shorter sustained pulse duration.. As discussed previously, as high as 10 atm pressure is required for 10-ps amplifier. Multi-isotope gas mixture gives a possibility to reduce the pressure, and as short as 3-ps laser pulse may be amplified at 5 atm pressure. What pulse duration to use may depend upon such factors as the particular application or capability to generate a short pulse. For generic application, it is desirable to reduce pulse duration as close to 3 ps as possible in order to avoid optics damage.

d - For given V and ξ, product dP is invariant. As we discussed previously, as long as the increase of P leads to the pulse reduction, P should be set to the maximum technically feasible level. We consider such maximum to be ~10 atm. Hence, d will be actually predetermined by other listed above parameters. Practical considerations limit maximum d value to ≤10 cm.

Finally, let us illustrate the above considerations with the cumulative Table 6. Similarly to simulations in Paragraph 3.4, we consider the input power to the amplifier at 5 GW and estimate the estimated window damage-limited output after 3 passes through the discharge arranged between electrodes of 10 cm wide and 120 cm long flat area. The output aperture is assumed $8\times(d-1)$ cm^2

Included into the Table 6 is the estimate for electric energy deposited into discharge, E_{dep}. This estimate is based on the semi-empirical requirement for specific energy loading at the level of ~120 J/l•atm in order to attain SSG at the level 2.5%/cm using regular mixture with ξ=15%. In other words, the engineering formula for the required E_{dep} looks

$$E_{dep}[\text{kJ}]\geq 0.12PSd[\text{atm}\bullet l]. \qquad (7)$$

Equation $E_{dep}=C_{shock}V_{out}^2/2$, together with Eq.(7), help to specify the minimum value of the shock capacitance, C_{shock}, of the HV pulser as

$$C_{shock}[\text{nF}]\geq 0.24PSd[\text{atm}\bullet l]/V_{out}^2[\text{MV}]. \qquad (8)$$

In a Marx generator with a number of stages m, C_{shock} is related to the single stage capacitance, C, as $C_{shock}=C/m$.

Table 6

Design Choices for Picosecond CO_2 Laser Amplifier

τ(ps)	P(atm)	Mixture	V_{out}(MV)	ξ(%)	d(cm)	E_{dep}(kJ)	W(TW)
30	5	Regular	0.5	15	8	6	0.35
30	5	Regular	1.0	30	10	7	0.5
10	10	Regular	0.5	15	4	6	0.5
10	10	Regular	1.0	15 (30)	8 (5)	12 (7)	1.1 (0.6)
3	5	Multi-isotope	0.5	30	5	3.5	2.0
3	5	Multi-isotope	1.0	30	10	7	4.5

While defining the stored electric energy, C_{shock} is also an important parameter that regulates the discharge duration. We should note here, that the glow discharge is a transient phenomenon at $P\leq$ 0.1 atm, and contracts into a streamer channel in a time interval decreasing inversely proportional to the gas pressure. While the desirable discharge duration should be less than instabilities onset

and gain depletion time, it should be also high enough to permit an efficient excitation transfer from N_2 to CO_2 molecules. In their combination, all these requirements set the optimum discharge duration at

$$\tau_{10\text{-}90}[\mu s] \approx 3/P[\text{atm}]. \quad (9)$$

Here we define the discharge duration as the time interval when 80% of the stored electric energy is deposited into the discharge. For impedance-matched discharges,

$$\tau_{10-90} \approx 2\sqrt{LC_{sh}} \quad (10)$$

(see Fig.8), where L is the inductance of the discharge circuit. Thus, we can draw a condition that specifies the allowed C_{shock} at the level of

$$C_{shock}[\mu F] \leq 2.25/P^2[\text{atm}]L[\mu H]. \quad (11)$$

Finally, we need to satisfy the impedance-matching condition

$$\sqrt{L/C_{shock}} \approx R_{disch}, \quad (12)$$

were R_{disch} is the active discharge resistance. Combining Eq.(11) and (12), we arrive at a simple condition

$$C_{shock}[\mu F] \leq 1.5/P[\text{atm}]R_{disch}[\text{Ohm}]. \quad (13)$$

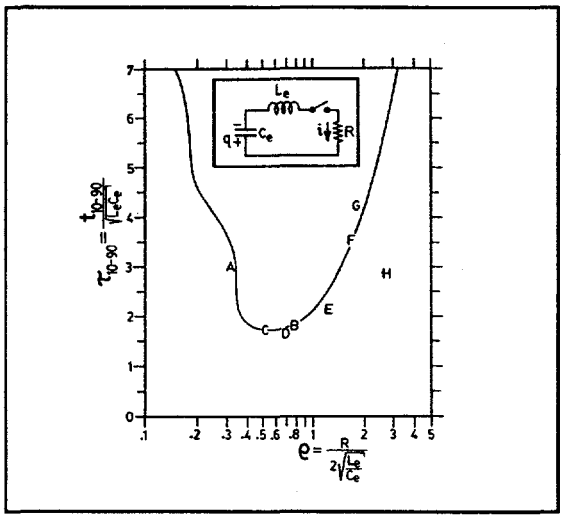

Fig.8

Energy deposition time vs damping constant ρ (Rev. Sci. Instrum., 64 (4), p. 839, 1993).

Assuming typical values of R_{disch}=3-5 Ohm, we conclude that for P in the range of 5-10 atm, C_{shock} shall be chosen between 30-90 nF with lower values more relevant to the higher pressure. Voltage increase in a proportion $V_{out} \sim P^{3/2}$ will help to maintain the required energy loading compensating for C_{shock} reduction. According to Eq.(12), L should be kept close to 500 nH. It is easy to verify, that requirements of high energy loading, Eq.(8), and short discharge duration, Eq.(12), are not in mutual contradiction for practically reasonable sets of the specified above parameters: P=5-10 atm, discharge volume 5-10 l, V_{out}=0.5-1.0 MV.

Design-impact conclusions to the paragraph:

Here, we have justified the choice of x-ray preionization for the high-pressure, large-aperture laser amplifier and have given guidelines towards choosing the appropriate parameters for discharge circuit.

Section 4

Conceptual design of terawatt CO_2 laser system

After specifying in Section 3 the basic physical principles of the high-power picosecond CO_2 laser system design, we proceed here toward the description of technical details of the proposed ATF CO_2 laser system upgrade to the terawatt level. We give emphasis to the design of the high-aperture amplifier, which is the major upgrade task.

The optic diagram in Fig.9 shows the set up of primary components of the proposed laser system. The system includes: oscillator, picosecond pulse slicer, regenerative amplifier, and large-aperture final amplifier. As shown in the floor plan in Fig.10, the system occupies two rooms in the ATF Bldg. 820. By means of vacuum laser beam transport lines, the CO_2 laser system is optically connected with experiments located in the ATF Experimental Hall and with the control Nd:YAG laser that will be moved close to the e-gun. Partitions in Fig.10 are positioned according to the present ATF floor plan. After more detailed design, when actual dimensions of the system are defined, the partitions may be moved or eliminated and/or the laser system components may change places. Present tentative positioning of the high-pressure amplifier in Room #1 helps to better isolate this potential source of EM noise from the computer-interfaced sensitive control and diagnostics equipment located in Rooms #2 and #3. When the amplifier is placed in Room #1, we have a possibility to put some auxiliary amplifier components outside the room, in the High-Bay Area. Such components may include: recirculating gas compressor, catalyst oven, heat exchanger with a water chillier, DC power supplies. These components, being environmentally safe, but bulky, generating heat and mechanical vibrations, are not welcome in the close proximity to the precise optical set-up in Rooms #1 and #2 where climate and noise control is required. We may consider also, as an option, to place a HV pulse power supply outside the laser rooms. It may be electrically connected to the amplifier discharge cell by a bundle of low-inductance HV cables. In addition to saving valuable floor space in laser rooms, such an option may help to avoid costly wall demolishing and rebuilding that is necessary if the bulky HV pulser does not fit into the doorways.

As illustrated by Fig.10, Room #1 accommodates the amplifier with the regenerative and multi-pass amplification optical set-up positioned on two optical tables. The oscillator and picosecond pulse slicer are located on one of the optical tables in Room #2. Another optical table accommodates optical control equipment (autocorrelator, spectrograph, etc.). Some space on the table is also reserved for users equipment permitting local experimentation with the high-power CO_2 laser beam or its testing and conditioning before transporting to the experimental hall. A good example of such a need is the Inverse Cherenkov Accelerator experiment where a double Max-Zander interferometer with spiral phase delay plates is used for radial polarization conversion of the initially linearly polarized laser beam. It is unlikely that such a converter may be used with a terawatt laser beam. A more promising approach is when the polarization converter is placed after the preamplifier. Then, the amplified radially polarized laser beam will be relay imaged to the interaction chamber in the experimental hall.

Control electronics and computer racks are placed in Room #2 and/or, for better noise protection, in Room #3. Pressurized gas cylinders and vacuum pumps are positioned in the outside gas hutch and vacuum cabinet.

The conceptual design of principal components of the CO_2 laser system is discussed below.

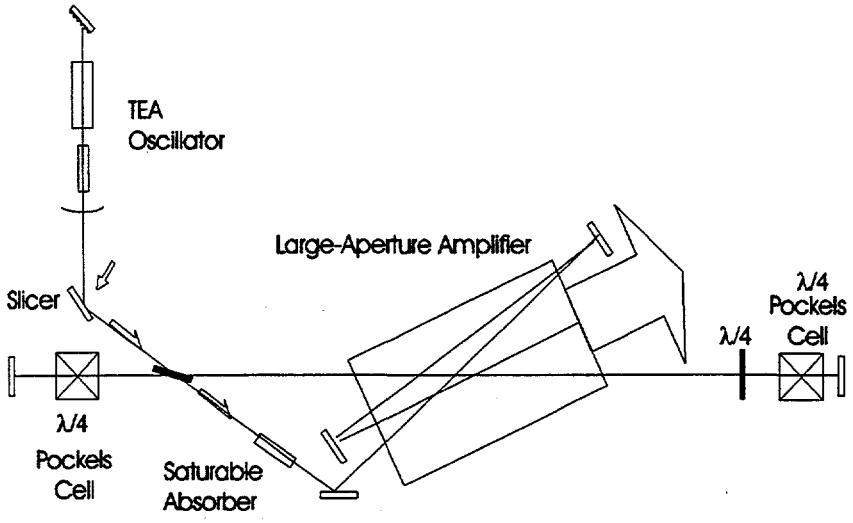

Fig.9

Principal optical diagram of the proposed CO_2 laser system

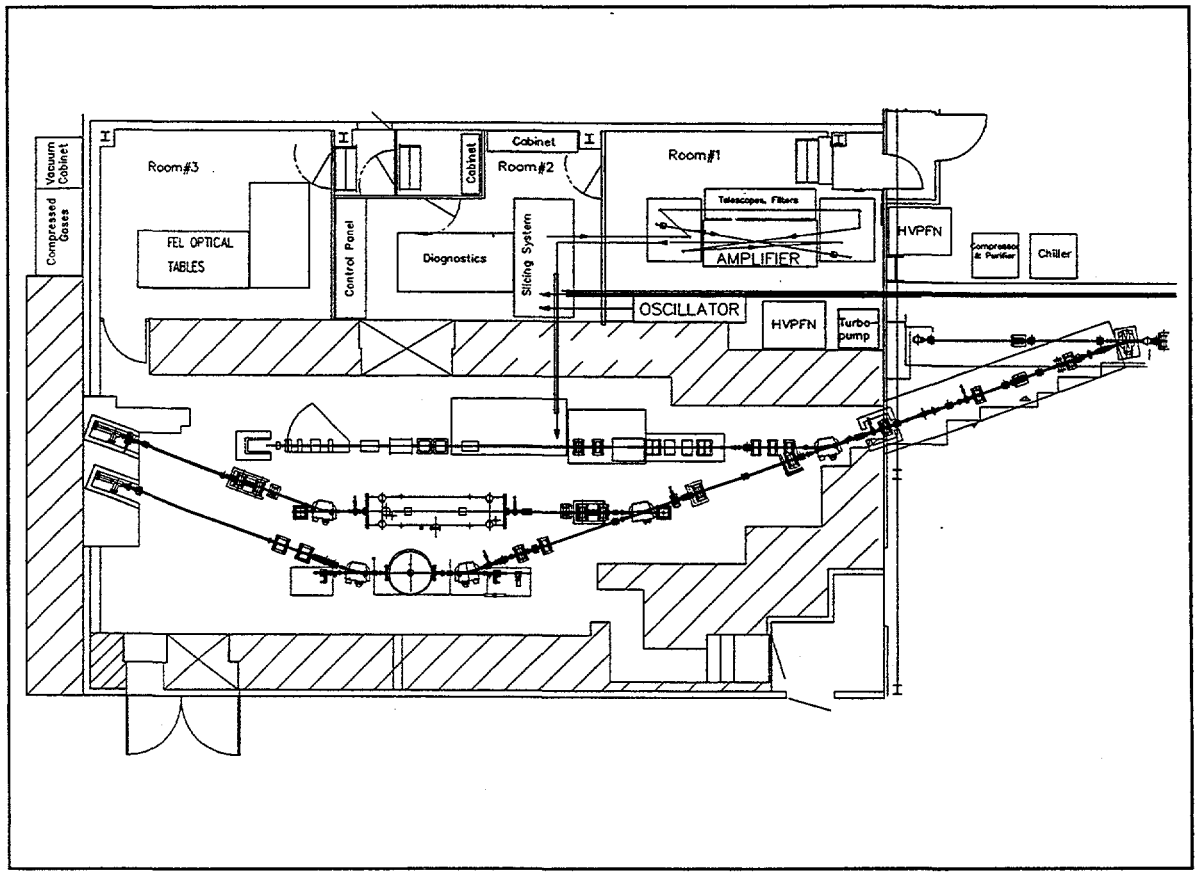

Fig.10

Fragment of the ATF floor plan with a location of the primary components of the proposed CO_2 laser system

We do not discuss in this Section the design of the optical transport lines from the Nd:YAG hutch and to the experimental hall. Their development will be a straightforward modification of the existing CO_2 and Nd:YAG laser beam transport lines according to the new laser locations and the increased power to deliver. However, this task is anticipated in Section 5, Project Structure and Management.

4.1 Oscillator

As the source of the 10-μm beam for the upgraded ATF CO_2 laser system the presently operational hybrid single-longitudinal zero-transverse mode TEA laser oscillator will be used without any major alterations. Oscillator is assembled on an optical table in Room #2 as a single self-contained unit with a 35-kV DC power supply and controls positioned outside the oscillator enclosure.

A block-diagram of this device is presented in Fig.11. Single-longitudinal-mode operation of the oscillator is due to a combination of a low-pressure auxiliary discharge tube, used to provide a narrow peak in the gain spectrum, and piezo-electric fine tuning of the oscillator cavity length. Such design permits delivering pulses of a smooth temporal envelope, without mode beating, that is needed for reproducible picosecond slicing. A diffraction grating, used as an end reflector in the laser cavity, selects a predetermined line in the CO_2 rotational spectrum. When the diffraction grating is replaced by a Cu mirror, the oscillator operates predominantly at the 10P(20) 10.59 μm line.

Principal electrical diagram of the oscillator is presented in Fig.12. The energy for a TEA discharge is supplied from a Blumlein network assembled inside the oscillator enclosure and charged up to 25 kV. A thyratron, triggered from the SRS pulse generator initiates the discharge. Automatic UV preionization is produced by branching a portion of the discharge current onto a preionizer structure inside TEA discharge head. A low-pressure (18 torr) discharge for the smoothing tube is triggered by the SRS pulser 0.2 ms in advance of the main discharge.

Premixed CO_2:N_2:He gases from a high-pressure cylinder are used for the smoothing tube. A slow gas flow rate at 18 Torr pressure is maintained by using a rotary roughing pump and micrometer-controlled leak valves before and after the discharge tube. The 1-atm pressure inside the TEA discharge head does not require using a vacuum pump, and the gas mixture (after passing the discharge tube) is vented directly to the atmosphere. Regulated flow meters are used to control the absolute flow rates and proportion of every gas component supplied from different gas cylinders.

The output laser pulse energy is ~150 mJ, about 50% of which is contained in the leading short pulse with a FWHM duration of 75-100 ns. The maximum 15 ppm repetition rate of the oscillator greatly exceeds the repetition rate feasible with the present and proposed amplifiers. The output beam has a Gaussian spatial profile with a 6 mm diameter at the $1/e^2$ level and a 1.2 mrad angular divergence.

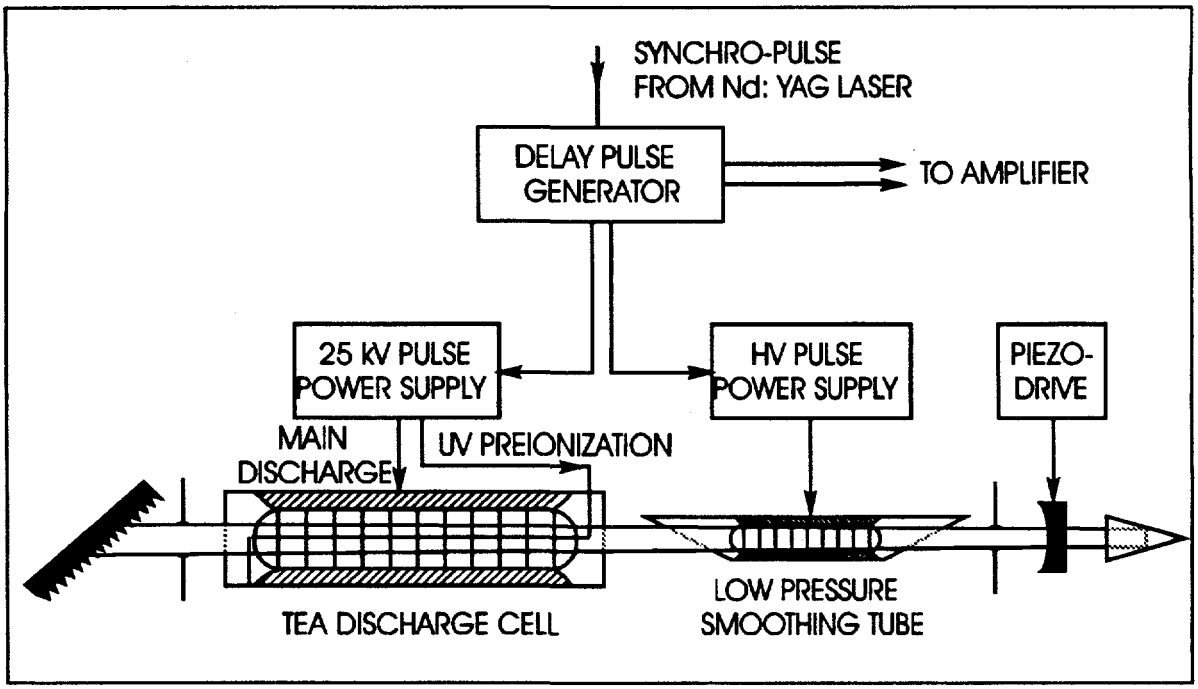

Fig.11

Block diagram of TEA CO_2 oscillator

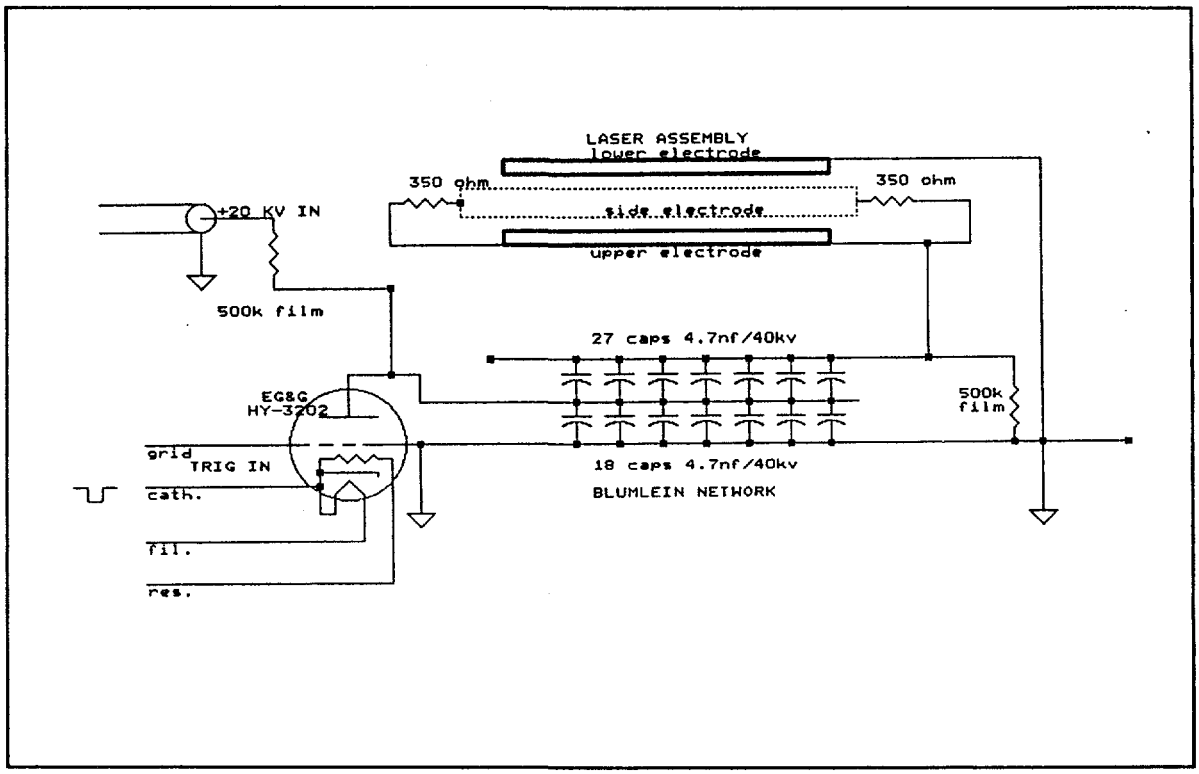

Fig.12

Electric diagram of the main discharge pulser for CO_2 oscillator

4.2 Picosecond Pulse Slicer

To slice the picosecond pulse from the oscillator output, a similar system to that presently operational at the ATF will be used. The system is based on a semiconductor switching method the principles of which have been described in Paragraph 3.2. The schematic of the optical set up of the picosecond slicer is presented in Fig.13. The control beam for the CO_2 oscillator pulse semiconductor switching is provided by a picosecond Nd:YAG laser system that includes: an actively-mode-locked diode-pumped CW oscillator and a two-stage multi-pass amplifier.

The 30-mJ output pulse is frequency-quadrupled to drive the photocathode of the ATF linac's electron gun. The unconverted 1.06-μm beam, about 70% of the initial laser pulse energy, is sent to the switching system. The use of the same Nd:YAG pulse to control both the linac and the CO_2 slicing system ensures an adequate synchronization of the e-beam and CO_2 laser pulse on the picosecond time scale necessary for the ATF laser acceleration experiments.

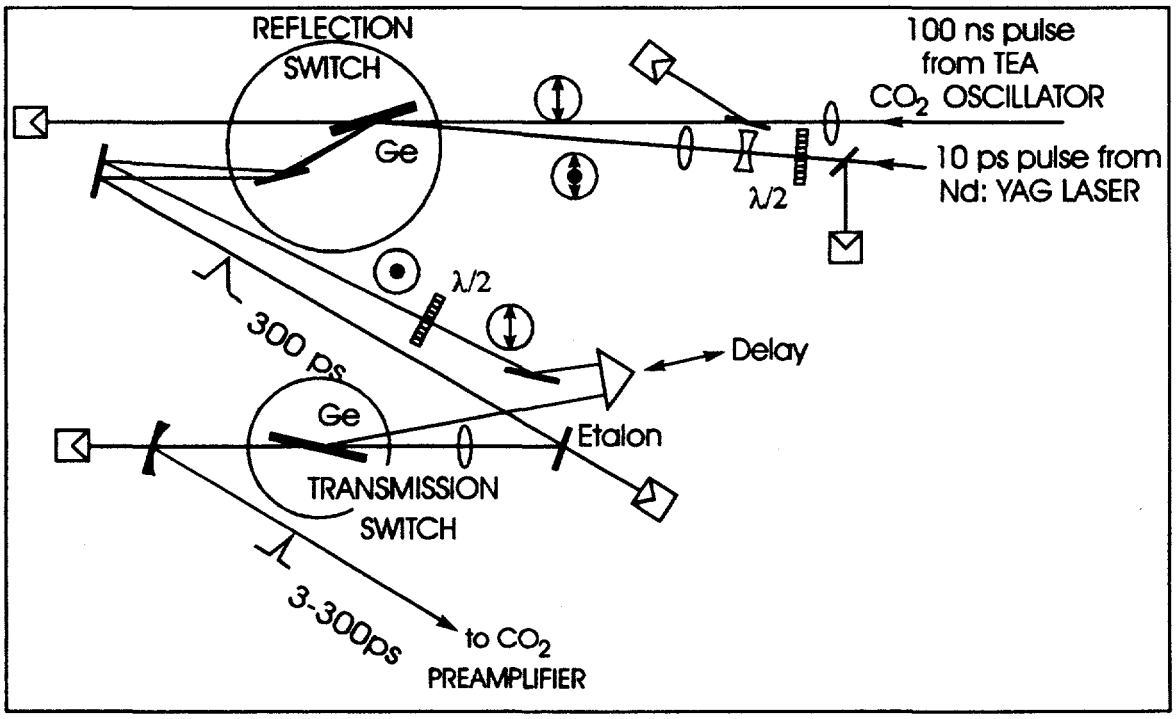

Fig.13

Principal diagram of the picosecond slicing set-up

The main elements of the system are two active semiconductor (Ge) switches and an optional passive etalon placed between the stages. The polarization rotation of the input Nd:YAG beam by λ/2-plates provides the optimal redistribution of the control pulse energy between the reflection and transmission switches. By utilizing the large difference in absorption for a p- and s-polarized Nd:YAG laser radiation, we can arrange to absorb a variable portion of the energy at the reflection switch and, after an additional polarization rotation, absorb the remainder at the transmission switch. The angular spread between the 1-μm and 10-μm beams is kept close to 1° to ensure that the sliced pulse front has no appreciable tilt.

The reflection switch is placed on two perpendicularly-oriented rotary stages of 0.3 arc-sec accuracy. After precise angular alignment of the reflection switch at the Brewster angle, background reflection does not exceed 10^{-5} of the incident CO_2 oscillator intensity. An etalon,

placed after the reflection switch should help to increase the contrast in the sliced signal at least an order of magnitude. A mirror placed on the same stage as the Ge plate automatically conserves overall alignment of the slicing system during the reflection switch angular adjustment. A $\lambda/2$ retardation plate in the path of the incident control beam regulates Nd:YAG energy deposition at the first Ge plate between 20% and 100%. Regularly, it is set to ~80% absorption. This is because of a much lower Nd:YAG energy requirement to control the second, transmission switch where the low-energy transient CO_2 pulse is tightly focused. The s-polarized Nd:YAG beam reflected by the Ge plate is transformed into a p-polarized beam after passing the second half-wave plate. After a variable time-delay introduced by a prism, the Nd:YAG pulse is directed to the second Ge switch, onto the spot irradiated by the transient CO_2 pulse, where it truncates the CO_2 tail by means of both reflection and absorption which remains after the plasma has diffused to below critical density.

The spots illuminated by both, CO_2 and Nd:YAG, overlapping laser beams on the reflection and transmission switches are, correspondingly, 4 and 1 mm high and approximately 4 times longer horizontally due to the oblique incidence at Brewster angle equal to 74°. Spherical mirrors in the path of the laser beam are used to match CO_2 and Nd:YAG laser beam spot sizes on the reflection switch and to reduce requirements of the control energy by focusing the beams on the transmission switch where the energy loading is small. After recollimation by a spherical mirror, the picosecond sliced pulse is sent to the regenerative amplifier.

In preceding experimental tests, up to 5×10^{-4} of the incident CO_2 oscillator energy has been reflected when ~5 mJ of the control energy was absorbed on the first Ge switch. CO_2 and Nd:YAG beams had close to Gaussian spatial distributions on the reflection switch with diameters (at $1/e^2$ level) of 3 mm and 5 mm, respectively. Direct time measurements of the picosecond CO_2 pulses immediately after slicing are not possible with presently available techniques. (The autocorrelator we built requires amplified pulses.) But monitoring the CO_2 energy after the transmission switch as a function of the delay time of the control pulse arrival, and differentiating the resulting energy curve, allows conclusions about the shape of the transient CO_2 pulse after the reflection switch. On the basis of these measurements, the transient pulse rise-time is close to the control pulse duration (~20 ps in this test). Assuming the similar falling edge duration in the double switching process, we were able to slice pulses down to ~30 ps. As has been discussed in Paragraph 3.2, with shorter and higher-energy control pulses used together with a thin etalon, as short as 10 ps and even 3 ps CO_2 laser pulses may be readily sliced using the described switching setup. The required pulse duration will be determined by the pressure in the regenerative preamplifier as discussed in Paragraph 3.1.

4.3 Regenerative Preamplifier

In the present ATF laser system, the peak power of the sliced CO_2 laser pulse is boosted from 0.5 MW to ~10 GW level via 8 passes through the amplifier. A regenerative amplifier is another, more compact, approach to attain the similar power level in a short picosecond pulse. In this case, the seed laser pulse is trapped inside the optic cavity, e.g., by means of a fast Pockels cell, and is amplified during the predetermined number of round trips until it is released in a similar manner as it has been trapped. The output of the regenerative preamplifier (RP) will be limited primarily by the optic damage threshold of the Pockels cell crystal (CdTe) that, for picosecond pulses, may be taken at 100 mJ/cm^2. Hence, the energy of ~30 mJ may be safely transmitted through the crystal of 1x1 cm^2 aperture resulting in a ~10 GW peak power in a 3-ps pulse or ~1 GW in a 30-ps pulse. The requirements on the pressure inside RP are similar to those discussed in Paragraph 3.1. Although in some sense it would be convenient to have RP as a separate unit, the real estate and

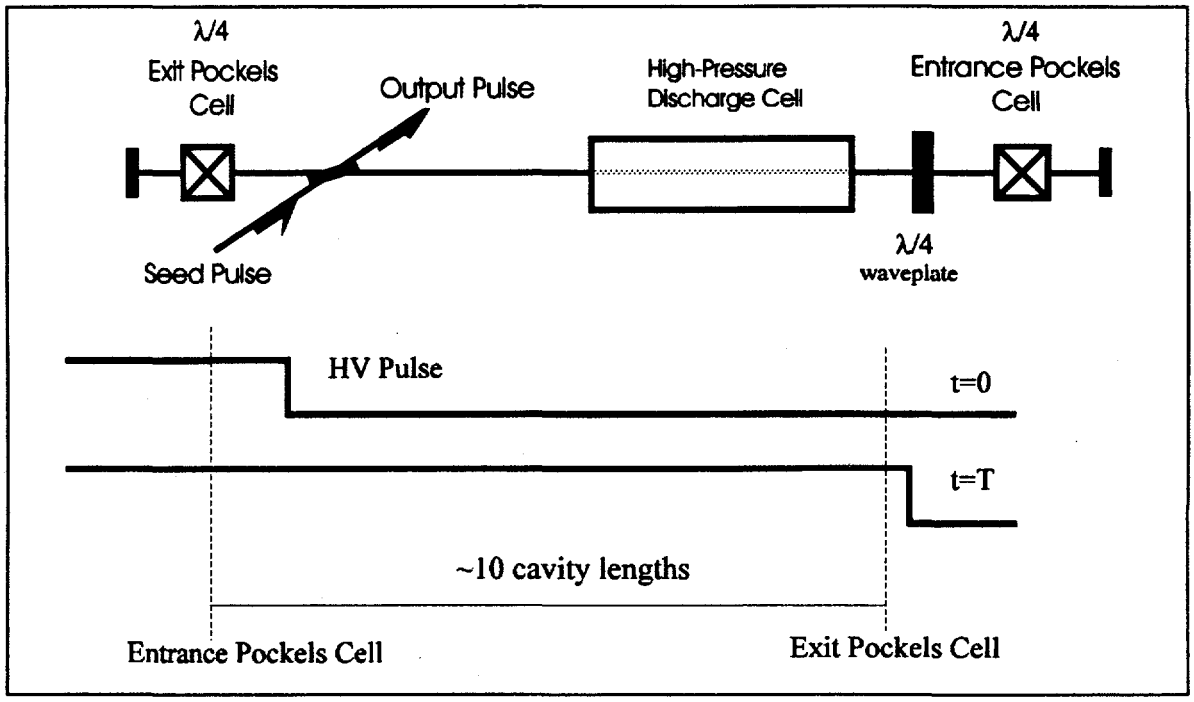

Fig.14

Principle of regenerative amplifier operation

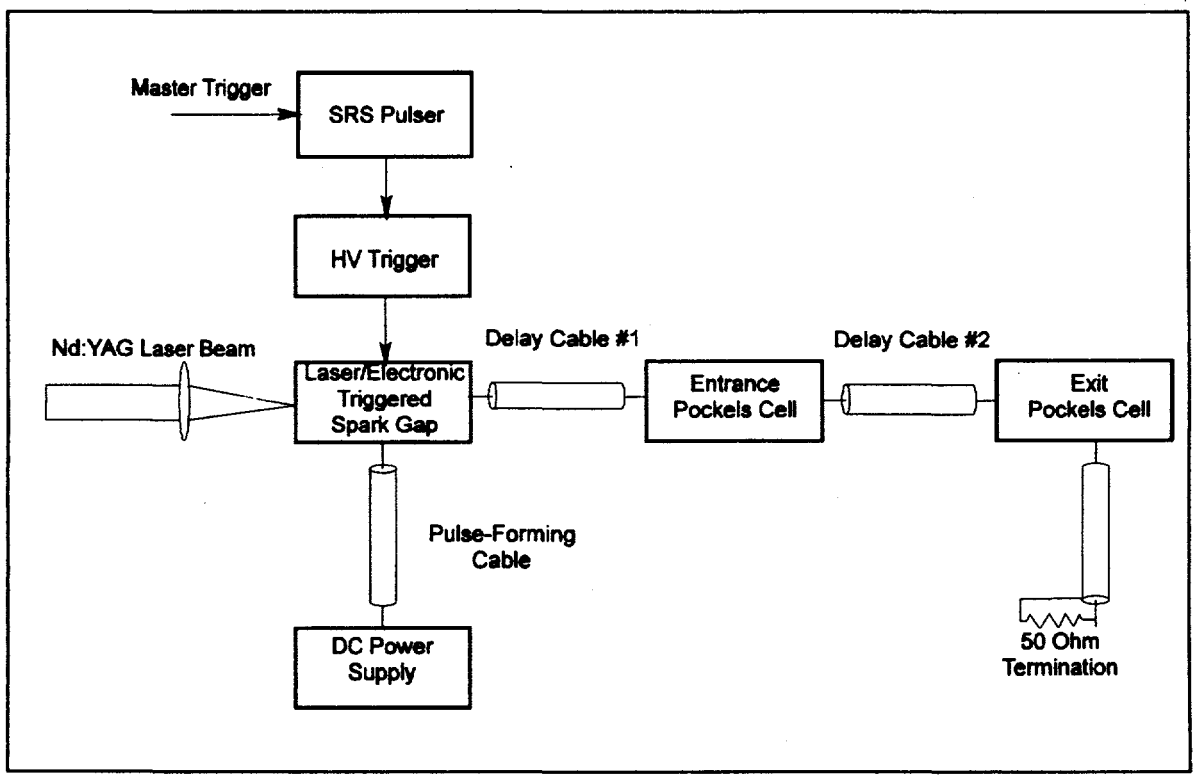

Fig.15

Block diagram of regenerative amplifier

budget constrains lead to arranging the RP optic path inside the same large-aperture amplifier that will be installed anyway as the primary component of the ATF laser upgrade.

The operation sequence for the regenerative preamplifier as illustrated by Fig.14 is as follows. Linearly polarized seed pulse is introduced along the optic axis of RP via reflection from the surface of the polarizing beamsplitter set at Brewster angle. The beamsplitter is designed to reflect s-polarized light and transmit p-polarized light. After a double pass through a λ/4-plate the laser beam polarization is switched 90° and transmitted by the beamsplitter. While the amplified pulse is doing its first round trip inside the RP cavity, a HV control pulse reaches the Pockels cell #1 that becomes to act as a λ/4-retarder (8 kV is required for a 5 cm long CdTe crystal). Thus, when the amplified laser pulse reaches the Pockels cell #1 for the second time, it gets an additional 90° polarization rotation that compensates the action of the λ/4-plate. That means that the amplified beam stays p-polarized and, hence, is trapped inside the RP cavity for as long time as the HV potential is kept at the cell #1 electrodes. After the laser pulse is amplified in multiple trips up to the required energy, it shall be released from the RP cavity. We arrange it by using Pockels cell #2 that, in two passes, that rotates the laser polarization 90°. After it, s-polarized beam is reflected from the beamsplitter in its original direction of propagating before it has been deflected and trapped in the RP cavity. The same control HV pulse that operates PS#1, after the proper cable delay is used to control PS#2. Block-diagram of the RP setup is shown in Fig.15. All the key components required for the RP arrangement are presently available at the ATF including two Pockels cells, a 16-kV DC power supply, and a spark gap equipped with the electronic triggering unit having a 5 ns switching time and jitter (according to the specifications). This time is short enough to compare with a round trip time through the RP cavity being ~20 ns. Much more stable triggering (<1 ns) may be obtained using laser initiation of the spark gap. Laser pulse of 1-2 mJ energy splitted from the Nd:YAG pulse used to control the semiconductor switching should be adequate for this purpose.

After the gain characteristics and other parameters of the amplifier are finalized, the length of the pulse-forming and delay cables will be determined by the simulations of the amplification process similar as were used in Paragraph 3.1. Assuming the round trip time through the RP cavity ~20 ns and 10 passes to go, the length of both cables may be chosen at ~100 ns (~30 m).

4.4 Large-Aperture Amplifier

1-10 GW output of the regenerative preamplifier will be further increased via several passes through the large-volume, high-pressure amplifier. With its high stored molecular excitation energy that may be released in a form of coherent laser radiation and the large aperture needed to transmit this radiation through the optical window, this device is the most energetic part of the upgraded laser system being responsible for delivering the ultimate design parameter - peak power at the terawatt level. Development of this device is the major effort and investment in the course of the presented here upgrade program.

Prior to developing this proposal, all efforts have been made in researching of the scientific resources and world-wide market potentials to create such device in the most efficient way. The approach to development of the terawatt-class x-ray preionized amplifier adopted here is the result of this search and represents, to our belief, the most reliable and economic way of developing a device with the desired parameters.

In Section 3 we considered different aspects and alternatives to developing the terawatt class amplifier. Summarizing results of this analysis we compile in Table 7 requirements on the

amplifier design. While meeting the ultimate goal of the ATF laser system upgrade (≥1 TW), these requirements, to the best of our knowledge, are not in a contradiction with technological and economical feasibility. Indicating required parameters within certain margins rather than their firm values adds flexibility to the project management when budget constrains are somewhat uncertain. In separate columns of the table we show also the most "desirable" values of parameters, which are sometimes at the edge of technical feasibility, and "comfortable" values which are more affordable and may be met with less efforts while not strongly compromising the project goals. The "comfortable" values are more realistic and, therefore, are regularly used in illustrations throughout the text.

As follows from Table 7, our preference is given to 5-atm multi-isotope option over alternatives using a regular mixture at a higher pressure. The reasons for this are as follows:

Table 7

Requirements to Terawatt-Class CO_2 Laser Amplifier Design

Parameter	Range	Desirable	Comfortable
Laser Pulse Duration (ps)	3-10	3	5
Gas Pressure (atm)	5-10	10	5
Regular/Multi-Isotope	R/M	M	M
V_{out} (MV)	0.5-1.0	1.0	0.75
Interelectrode Spacing (cm)	5-10	10	8
Discharge Volume (l)	5-15	15	8
ξ (%)	15-30	30	25-30
E_{dep} (kJ)	3.5-12	6	6
Discharge Pulse (μs)	0.25-0.5	0.25	0.5

Both approaches have their own complications. The high-pressure approach is cost driving due to the requirements of a powerful and fast HV pulser with V_{out}≈1 MV, corresponding problems with electrode isolation, and enforced vessel and optic windows design to withstand 10-atm pressure. The use of the 5-atm multi-isotope mixture considerably reduces construction cost while increasing operation costs. Another problem associated with lower gain in the multi-isotope mixture may be partially surpassed by using higher ξ mixtures. The decisive factor in choosing the multi-isotope option is a higher prospective peak power (see Table 6).

Fig.16 presents a block-diagram of the amplifier components. They include three primary components: discharge cell with the electrode manifold, pulse power source and x-ray source. The design of these components, most critical for the successful performance of the project, is discussed in the next three paragraphs. We start with the x-ray source which is, in a sense, least dependent upon the particular design of other amplifier components.

4.4.1 X-Ray Source

The reasons for choosing the x-ray preionization technique for a high-pressure, large-aperture CO_2 amplifier has been explained in Paragraph 3.5. Here we consider in more details technical aspects of this technique and specify requirements to the x-ray source to be installed into the ATF amplifier.

When talking about the x-ray sources, the general concern is regarding potential safety hazards. Our preliminary study show that the following factors, in their combination, contribute to satisfy the BNL safety requirements which call for the dose of ≤5 mRad/hr at minimum distance from the amplifier accessible by the personnel (1 m in the room without radiation interlock):

a) limited corona cathode current (~1 kA at 100 kV of the applied voltage);

b) low repetition rate (<0.1 Hz);

c) collimated in vertical direction x-ray flux;

d) massive HV electrode and thick high-pressure vessel walls;

e) possibility of placing the amplifier in a radiation interlocked room.

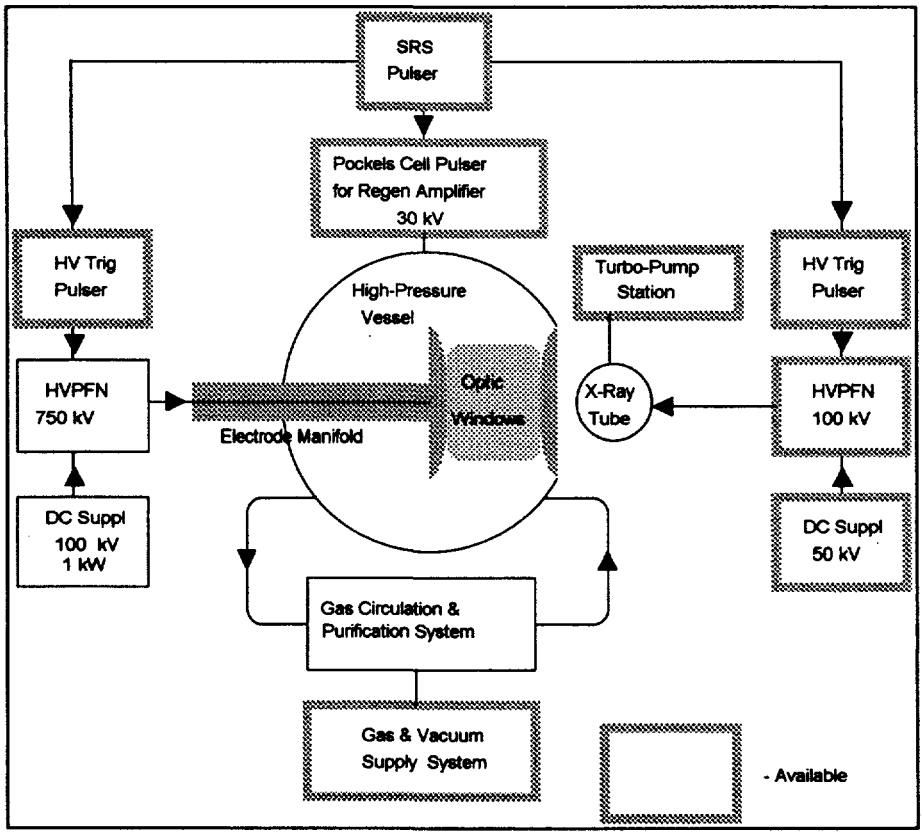

Fig.16

Amplifier block-diagram

In simple and robust x-ray tubes, electrons are emitted from a corona or explosive cathodes by applying a ~100 kV negative potential resulting in an accelerating electric field developed between the cathode and target. For the uniform preionization of a big gas volume, a flat cathode is configured according to the geometry of the discharge area (in our case, 100x10 cm^2). Electrons originating from the cathode are accelerated and then stopped at the target, producing bremsstrahlung x-rays. X-rays penetrate through the target, x-ray tube window, and nearest (ground) main discharge electrode into the discharge volume and ionize the gas.

X-rays produced by electron bombardment of a high-Z target have a broad spectrum with a cut-off at the accelerating potential and a peak at ~70% of the accelerating potential. When choosing the accelerating potential we should satisfy two conflicting requirements:

First, x-ray energy should be high enough to prevent a significant attenuation in the target, tube window, electrode and across the interelectrode gap. The last requirement is important to ensure a reasonably uniform volume ionization of the gas.

On the other hand, to produce an efficient gas ionization, we need soft x-rays (see plot A in Fig.17). Note that x-ray absorption in gas is proportional to P and ξ.

The optimum x-ray energy that satisfies both these requirements ensuring the sufficient gas ionization depends upon the choice of the window material that shall be considered next.

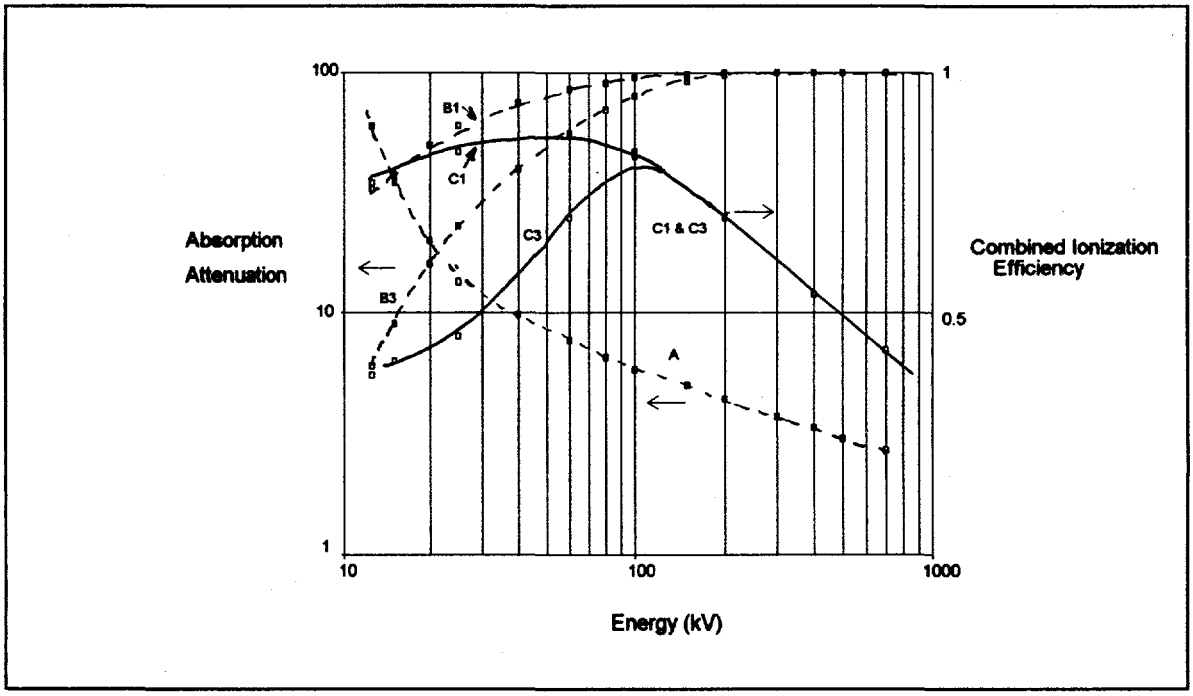

Fig.17

X-ray ionization efficiency curves: A - x-ray absorption in the amplifier gas; B1 and B3 - x-ray attenuation in , correspondingly, 1 mm and 3 mm thick aluminum; C1 and C3 - efficiency curves presenting combinations of , correspondingly, curves A and B1 or A and B3.

The optimum target material is one that efficiently stops the electrons but transmits the produced x-rays without significant attenuation. These two requirements are again in mutual contradiction because high-Z materials which are good for electron stoppage have also a high x-ray absorption.

However, the radiation ranges (penetration depth) are much shorter for electrons than for x-rays of a similar energy. That is why thin foils of a high-Z material, such as the commercially available 8-μm Ta (Tantalum) foil, are usually used as the targets. An additional problem with using thin films is the reduced life time because of the thermal loading due to the electron energy deposition. This problem is regularly solved by using special designs of the support metal structures for the foil. Another approach utilizes high-Z metal layers, such as Au, deposited onto a relatively thick wall of a low-Z material with a high thermal conductivity and x-ray transmission, such as Al. In the last case, the target may serve also as an x-ray window separating the vacuum x-ray tube from the ambient atmosphere or from a high-pressure gas, when the x-ray tube is accommodated inside the discharge cell. Mechanical requirements on the window will determine its thickness. For the preferred configuration (see below), the x-ray window should be designed to withstand an external 6 atm pressure. A window that holds such pressure but still has a low x-ray attenuation should be of a honeycomb structure with thinned down to 1-2 mm areas. The best candidates for such a window are Be (Z=4) and Al (Z=14). Because of a low Z, Be has an extremely low attenuation and is preferable if certain technological problems are resolved. Al-Mg alloy is much cheaper material presenting an acceptable compromise for a practical device. Curves B and C in Fig.17 show the x-ray attenuation by the window and ground electrode, both made of Al of a total thickness 3 mm (Curve B) or 2 mm (Curve C). The product of Curves A and B (or C) gives a combined ionization efficiency for the x-rays of various energy and helps to specify the optimum accelerating potential which is around 100 kV. We see, that the reduction of the window and electrode thickness leads to the increased soft x-ray transmission and shifts the optimum accelerating potential towards smaller numbers.

To determine the initial electron density produced via x-ray preionization, we need to integrate the efficiency curve over the x-ray spectrum and over the preionization pulse duration. For typical conditions with a 100-kV, τ=1 μs preionization pulse, the produced x-ray dose in the interelectrode space and the initial electron concentration are, correspondingly, 10-20 mRad/cm^2 and ~10^8 cm^{-3} that is adequate for a uniform glow discharge to be developed between the electrodes.

At the acceleration potential 100 kV and typical cathode current 1 A/cm^2, the acceleration gap between cathode and target with a 100x10cm^2 cross section represents a 100 Ohm load. With a τ =1 μs impedance matched discharge, the circuit inductance should be $L \leq R\tau/2$=50 μH and C_{shock}=2 τ/R=20 nF. The principal diagram of the HV pulser used to apply an electric potential to the electron emitter of the x-ray tube is shown in Fig.18. It is a three-stage Marx generator charged from a 75-kV DC power supply. With ~500 J of the stored electric energy in the Marx banks and 3-6 ppm repetition rate, the required power of the DC power supply is 100-200 W. The HV triggering unit is initiated by the TTL signal provided by a master low-voltage (SRS) pulser. The same pulser, synchronized with the ATF linac's rf field and Nd:YAG laser serves to maintain the proper triggering sequence for all other components of the CO_2 laser system including oscillator, Pockels cells of the regenerative preamplifier, and main amplifier discharge.

Via current leads and feedthroughs, a HV potential is delivered inside the vacuum chamber of x-ray tube. To maintain proper vacuum conditions inside the vacuum chamber, the x-ray tube is equipped with a turbo-pump station. Small controlled helium leak is generally required for corona-discharge cathode operation.

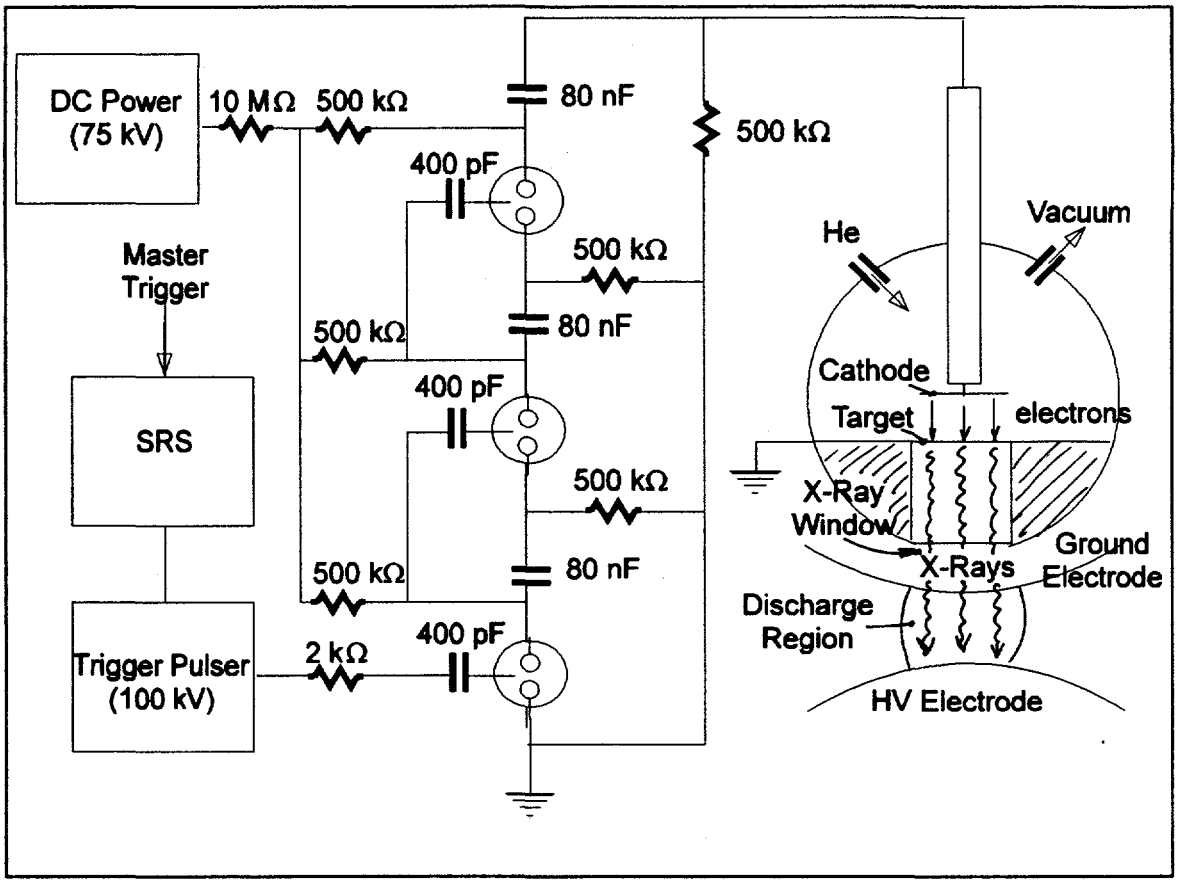

Fig.18

Block-diagram and principal electric scheme for x-ray preionizer

4.4.2 Discharge Cell

The amplifier discharge cell is essentially a high-pressure vessel that comprises discharge electrodes with current feedthroughs, accommodates optical windows for transmitting the amplified laser radiation through the interelectrode region, anticipates means for the uniform gas recirculation through the discharge, and is compatible with or accommodates a source of the x-ray flux used to preionize the interelectrode space.

Electrodes and Preionizer Configuration

The design of the discharge cell starts with considering the preferred configuration of electrodes and preionizer assembly. Among several alternatives to consider, there are:

a) a single HV electrode (other electrode is grounded), or two, positive and negative, HV electrodes (binary scheme);

b) preionization through the electrode or from a side.

There are pros and cons to any of these options in their combinations.

Sideways x-ray tube positioning results in essentially nonuniform preionization across the discharge region (primarily due to the x-ray flux divergence). Even with two x-ray tubes placed symmetrically at both sides of the discharge region, there is still the problem with unwanted

practically excludes a possibility of using metal vessel or/and requires a strong electric insulation of the x-ray tube. For these reasons we eliminate the configuration with the side ionization and look more attentively into another alternative. This is an option where the x-ray source is placed behind the electrode or two x-ray tubes are placed behind both electrodes. Until a reliable solution for preventing the electric breakdown from the back of the HV electrode towards the x-ray tube and its circuitry is found, we can not consider this option for a practical design. Other related cost-saving option with a "slave" x-ray tube where a portion of the HV electrode potential is branched onto the x-ray cathode (if negative) or target (if positive) is not flexible enough to allow a sufficient preionization of the discharge volume prior the peak potential is erected. The result of it is a possibility of the breakdown or sparking. Rejecting the scheme where the x-ray source is placed behind the HV electrode we automatically eliminate the binary discharge approach.

A single HV electrode and a preionizer behind the grounded electrode seems the most reliable and experimentally proven scheme. When properly collimated and masked, the x-ray flux illuminates uniformly and symmetrically the central portion of the interelectrode space. This reduces the probability of electric breakdown at edges of the HV electrode and simplifies the requirements for its perfect shaping. X-ray illumination through the ground electrode is also safe against HV breakdown towards the metal x-ray tube. X-rays transmission into the discharge area is possible by using a mesh ground electrode or even smooth thinned-wall aluminum electrode. Delivery of the total discharge voltage onto one HV electrode instead of splitting it between two electrodes in a binary scheme does not look like a very complicated problem for the range of V_{out} =0.5-0.75 MV. At least it has a more straightforward solution than other problems associated with alternative combinations of electrodes and x-ray sources mentioned above.

Requirements on High-Pressure Vessel

According to the choice of the amplifier design parameters specified in Table 7 and further discussed below, the high-pressure vessel design shall satisfy the following requirements:

a) compatible with isotopic mixture;

b) 5-atm maximum working pressure;

c) withstand mechanical shock with a 6 kJ energy deposited into the discharge;

d) accommodate HV and ground electrodes with the flat area of 100x10 cm^2, allow for profiled edge extended 10 cm beyond the flat area along the electrode perimeter;

e) interelectrode distance adjustable continuously or stepwise between 5-8 cm;

f) electric isolation of the HV electrode from the ground for a 750 kV pulse;

g) compatible with x-ray source positioned behind the ground electrode;

i) means for a laminar gas ventilation of the interelectrode space at a volume rate compatible with the gas circulation circuit (~100 s*l*/min);

k) accommodate end flanges with optical windows;

l) ease of mounting and components service;

m) ports for observation and detector positioning;

n) low inductive resistance to the discharge current;

o) EM noise protection;

p) safety features: x-ray shielding, electrical grounding and external electric insulation.

Some of the requirements listed above are subject to further clarification at the preliminary and critical design stages. For instance, such parameters as interelectrode spacing, working pressure, or stand-off voltage depend upon characteristics of the HV pulser which will be finalized before its procurement.

Compatibility with the isotopic mixture sets certain restrictions on possible choices of the materials for the high-pressure vessel. The problem is that the isotopic gases are rather expensive. In order to keep the operation costs for the ATF laser system at a reasonable level, a prolonged life time and recycling of the isotopic gases shall be ensured. That presumes that all measures shall be taken to prevent a pollution or desorption of the isotopic gases that is most likely to occur at the internal surface of the high-pressure vessel. As the most resistant to outgasing or unwanted reactions with the isotopic oxygen, we consider: corrosion resistant metals, especially stainless steel, and such dielectric materials as glass, quartz, teflon, ceramics. Composites, such as fiberglass, traditionally used as structural materials for high-pressure discharge tubes, are not desirable for our application because of their high-vacuum incompatibility (porous structure, outgasing) and a partial decomposition under the UV and x-ray radiation of the discharge. That is why the proposed below designs for the high-pressure vessel (see Fig.20, 21) are based on using stainless steel or such vacuum-compatible dielectric materials as glass or ceramics.

Optical Windows

End flanges of the discharge cell shall be equipped with optical windows transparent to IR and visible radiation with apertures to permit transmission of laser beams sized and oriented according to the adopted optical set-up of the amplifier shown in Fig.9. Here we redraw this design in scale (see Fig.19). For a convenience of the demonstration, we distort horizontal and vertical proportions (scaled sketch is then compressed 5-times horizontally). The following apertures are required in order to transmit laser beams through the amplifier cell according to the proposed optical set-up:

a) 10 cm (wide) by 8 cm (high) apertures centered along the prime horizontal axis of the discharge region;

b) Apertures of 4 cm (wide) by 8 cm (high) centered along the axes that intersect the prime optical axis in the center of the discharge region at angles of a $\pm 5^0$ in a horizontal plane. Vertical elongation of these apertures permits transmission of several beams of a small diameter at different vertical levels. That may be useful if five or more amplification passes are required to attain the desirable terawatt power.

Because of the requirements of a low optical attenuation at 10 μm and a high mechanical strength to withstand a 5-atm pressure differential, it is reasonable to use individual properly oriented and sized windows for every listed above aperture other than to use single big windows covering all apertures at once.

As we remember, the primary restriction in the output laser energy upscale is the optical damage of the output window. That is why it is strongly preferred to use a Brewster window (extended surface due to the oblique incidence) at the output 8-cm aperture. It may be more economical and convenient to use normal anti-reflection (AR) coated windows at every other aperture. Polarization insensitive AR-coated windows are necessary for the apertures reserved for the regenerative amplifier cavity. NaCl (or other salt) and ZnSe are the best candidates as the window materials. NaCl is cheaper than ZnSe but mechanically less strong (requires bigger thickness and care against cracking) and sensitive to fogging due to the air humidity (needs heating or/and other protection).

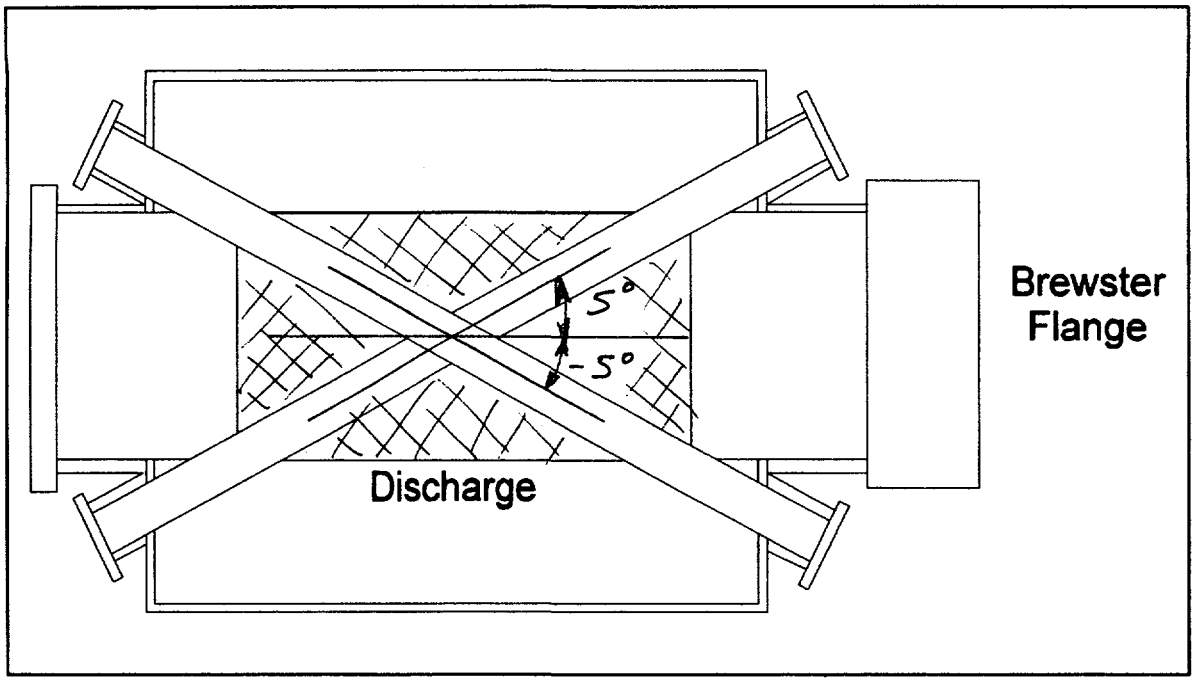

Fig.19

Top-view schematic of the amplifier configuration and optic widows.

Ventilation Ports

With high-repetition rate gas lasers, the required fast gas exchange between the shots inside the interelectrode region is a serious technical problem to be addressed. High-repetition rate, high power lasers require also high average-power HV sources and correspondingly scaled heat exchangers, catalytic regenerators, circulation pumps, etc. All these problems may be resolved, but they are cost-driving as well as require a large space for laser and supply systems. The ATF does not have such space. Also for presently envisioned scientific application of the ATF CO_2 laser system a high repetition rate is not the primary goal. Reduction of the repetition rate to 3-6 ppm helps to reduce the required power of HV DC supplies to 1 kW and to use compact and relatively inexpensive blower, catalytic converter, etc. With such low repetition rate and the discharge volume ~8 *l*, gas exchange rate at the level of 100 sl/min looks adequate (see below). However, even with such relatively slow gas flow certain precautions to avoid turbulent nonuniformities of gas within the discharge area shall be taken. According to one of proposed designs of a metal discharge cell illustrated by Fig.20, gas enters and exits the discharge cell through symmetric gas distribution manifolds attached to the gas ports of the discharge cell. In another proposed design of a dielectric discharge cell, similar gas manifolds still may be used. However, we would rather consider here a novel gas exchange method that supposedly provides much higher efficiency of gas recovery and looks technically simple. The idea of the method is based on understanding that the decomposition of CO_2 gas in discharge occurs mostly in a narrow region near the cathode where the electric field is strongest. In the discharge volume the electric field is partially screened by the positive space charge of slow ions. Hence, pumping out the gas through the cathode surface will help to remove the products of the CO_2 decomposition (CO and O_2) as well as products of other secondary chemical reactions (Nitrogen Oxides) much more efficiently than when these products

are already mixed with a bulk gas inside the vessel. This method is similarly more efficient to remove a heated gas from the interelectrode space, especially if the gas intake is also arranged through the anode surface. Thus, it is presumed that a flat region of a HV electrode has multiple small holes drilled for gas ventilation. Such holes with properly smoothed edges should not effect the electric field uniformity and the discharge stability. Actually, it is known that micro-turbulence and electrode surface micro-roughness even sometimes benefit the stability of pulsed discharges.

Discharge Cell Configurations

Based on the above discussion, we propose here two different designs of a high-pressure discharge cell with x-ray preionization. The first more traditional and straightforward design shown in Fig.20 is based on using a metal, preferably stainless steel, high-pressure cylindrical vessel with end flanges designed according to Fig.19. The size of the cell is defined by the dimensions of the electrode manifold, x-ray tube, dielectric stand-off's, and by breakdown distance across the gas. All dimensions and shapes should be designed to withstand full charge shock potential from the HV pulser even at no x-ray ionization across the discharge region.

Assuming that the curved edge of properly shaped HV electrode extends 10 cm beyond the perimeter of a 100x10 cm^2 flat area and a 20 cm breakdown-safe distance from the HV electrode to metal wall, we estimate the cell length to be 160 cm, not including the end flanges. The minimum internal diameter of the cell defined by the similar considerations as its length is 70 cm. It is desirable not to extend the diameter considerably above this size because of severe pressure stress and in order to reduce gas consumption having in mind the high cost of isotopes. The diameter of the cell depends to a big extent upon the design and positioning of stand-off's and the x-ray tube. The dimensions and shapes sketched in Fig.20 are taken to the best of our knowledge based on available information. Two or three stand-off's support the HV electrode and deliver an electric potential from the HV pulser. There is no possibility to use more stand-off' according to this design.

Welded stainless steel is not the best structural material for a high-pressure vessel. That is why it is overlaid externally with a composite (fiberglass) shell. This dielectric shell will serve also as an additional protection against the HV exposure as long as the metal cell is also a conductor for the return discharge current. To protect against EM radiation, a metal ground screen may be put on top of the composite shell. The estimated inductance of the 70-cm diameter metal discharge cell is ~150 nH; gas volume 600 *l*.

The second proposed design of a dielectric discharge cell shown in Fig.21 may look more risky and extravagant, but has certain advantages over the plain metal cell, including:

a) low gas volume;

b) low inductance;

c) screened against EM radiation, no stray potential at the enclosure;

d) more efficient gas circulation scheme.

A possibility of using a compact dielectric vessel without bulky feed-through's, with thin vacuum-compatible walls is due to using an external metal container with SF_6 gas at the same 5 atm pressure as the laser gas mixture inside the cell. As a result, there is not permanent stress upon the dielectric vessel. We may consider such a vessel to be welded and composed of ceramics and glass. the external enclosure may be built of any construction metal, including cast iron. To avoid dielectric wall rupture, filling and pumping out of gas in both volumes will be done synchronously with permanent automatic control of the pressure differential.

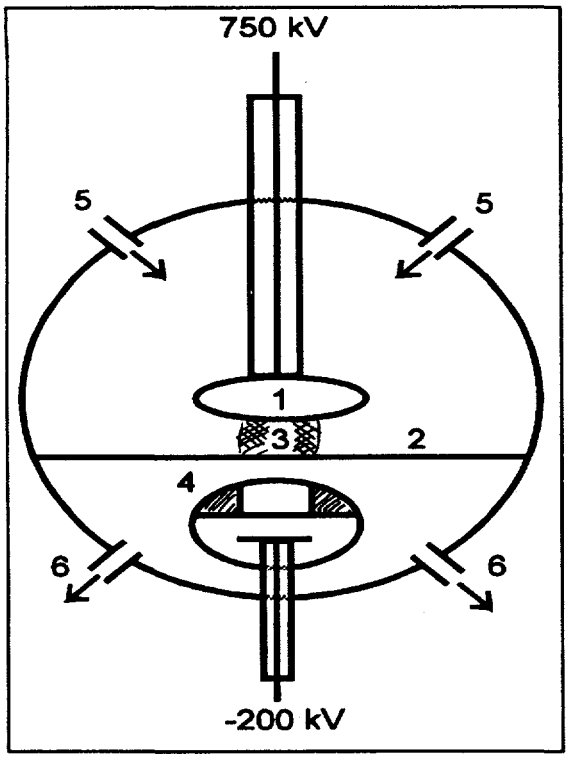

Fig.20

Design of metal discharge cell:

1 - HV electrode; 2 - ground mesh electrode; 3 - discharge region; 4 - x-ray gun; 5 - gas-in; 6 - gas-out

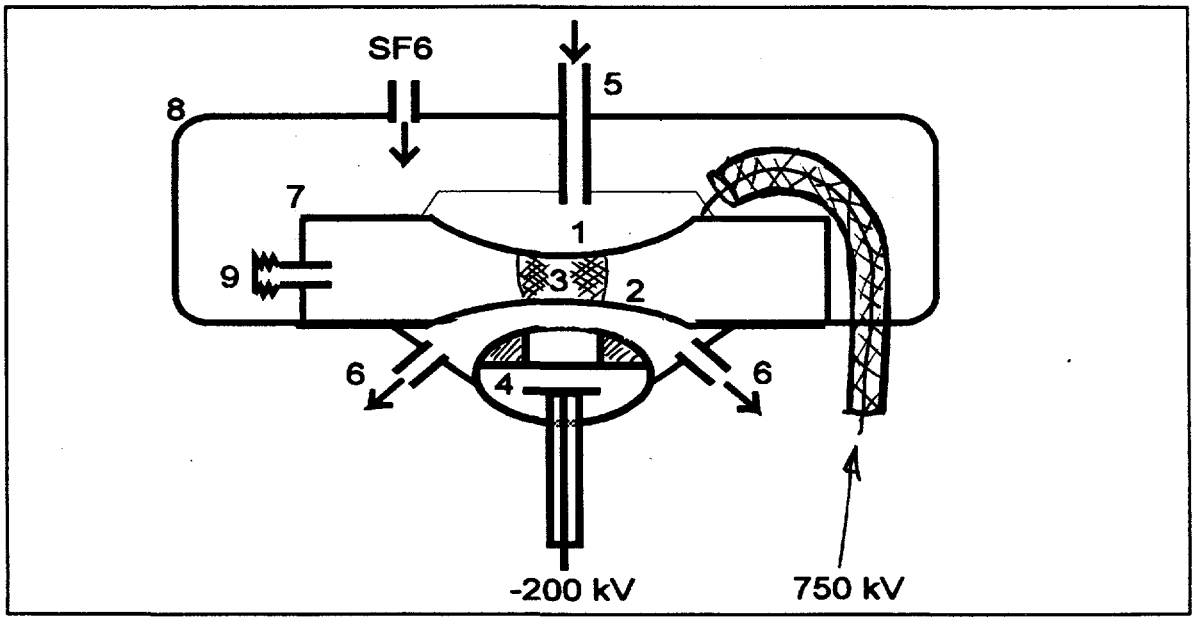

Fig.21

Design of dielectric discharge cell: 1 - HV mesh electrode; 2 - ground mesh electrode; 3 - discharge region; 4 - x-ray gun; 5 - gas-in (dielectric pipe); 6 - gas-out; 7 - dielectric inner cell; 8 - metal container; 9 - relief membranes

The HV electrode is connected to the HV pulser via a bundle of low-inductance cables. The total impedance of the discharge cell is ~60 nH, gas volume ~200 *l*. The only concern regarding the rigidity of the dielectric vessel is due to a pressure shock resulting from the energy deposited into the discharge. Dissipation of 5 kJ into a 200 *l* volume may result in a 100-150 torr pressure jump inside the dielectric vessel. To relieve this stress, a number of relief membranes may be anticipated along the dielectric walls. These membranes may be made of a thin teflon. silicon rubber or other vacuum compatible and flexible materials. Two possible options are bellow or balloon-type expandable membranes; the first one is sketched in the drawing.

4.4.3 Pulsed Power

A HV pulser is designed to generate and deliver to the discharge cell a HV pulse to sustain a high-current discharge during the time interval defined by Eq.(9) and permitting the total electric energy loading defined by Eq.(7). Eq.(6) defines $V_{out}=2V_s$. Hence, when the gas mixture and discharge dimensions are chosen (e.g., P, ξ, S, and d are specified), we can determine the key parameters of the discharge circuit using formulas from Paragraph 3.5.

As has been discussed above (see Table 7), the optimum choice of physical parameters for the amplifier are considered to be: P=5 atm, ξ=25%, S=1000 cm^2, and d=8 cm. Using these parameters, we get: V_{out}=700 kV by Eq.(6), $E_{dep}\geq$5 kJ by Eq.(7), $\tau_{10\text{-}90}\approx$0.5 μs by Eq.(9), $20\leq C_{shock}$[nF]$\leq$60 by Eq.(8) and Eq.(13) under the assumption that $R_{disch}\approx$5 Ohm. The upper limit for C_{shock} is not much important at this point because, trying to keep energy requirements on the HV pulser as low as reasonable, we would better choose C_{shock} close to its low limit, e.g., $C_{shock}\approx$20 nF. The required circuit inductance is estimated by Eq.(12) at $L\approx$500 nH. For better understanding of the inductance limitations, let us address Fig.8 which shows the dependence of the energy deposition time upon the circuit parameters. We see that the minimum pulse duration is $\tau_{10-90}\approx 2\sqrt{LC_{sh}}$. For specified above $\tau_{10\text{-}90}$ and C_{shock}, we get $L\leq$3 μH. This is necessary but not enough. From Fig.8 it follows also, that the minimum discharge duration is attained when $\sqrt{L/C_{shock}}$ is in the range of (0.5-1.5)R_{disch} (impedance matching). This brings us to the requirement $L\leq$1 μH. The sharp increase of the normalized discharge duration to the left from the minimum in Fig.8 indicates that the last requirement is pretty firm, and our final choice would be L=0.5-1 μH. The total inductance of the circuit is the sum of the inductance of the HV pulser, discharge cell and current leads:

$$L = m(L_c + L_s) + 4\pi \times 10^{-7}\left(\frac{\pi D^2}{16h} + \frac{l}{2\pi N}\ln\frac{R}{r}\right), \qquad (14)$$

where L_c and L_s are, correspondingly inductance of a single capacitor and a spark gap, m- number of the HV generator stages, D is diameter of the discharge cell, h - length of discharge, R and r, correspondingly, radii of external and internal conductors in a coaxial cable, l - cable length, and N - number of cables in a bundle. We may estimate the discharge cell inductance ≤120 nH, inductance of the cable bundle ~100 nH, $L_c+L_s\approx$50 nH, and for m=8, the total inductance $L\approx$600 nH - well within the required range.

For the present conceptual design we consider an 8-stage Marx generator with a 100 kV charge voltage and a single-stage capacitance C=150 nF. According to the energy loading and repetition rate, at least 1 kW DC power supply is needed to charge the capacitor bank in 20 sec. The

principal electrical schematic of the Marx generator and a block diagram of its control system are shown in Fig.22. The control system includes: HV triggering unit initiated by TTL signal from the master SRS pulser, gas flow control panel to supply nitrogen or synthetic air to 8 spark gaps of the pulser and to the triggering unit.

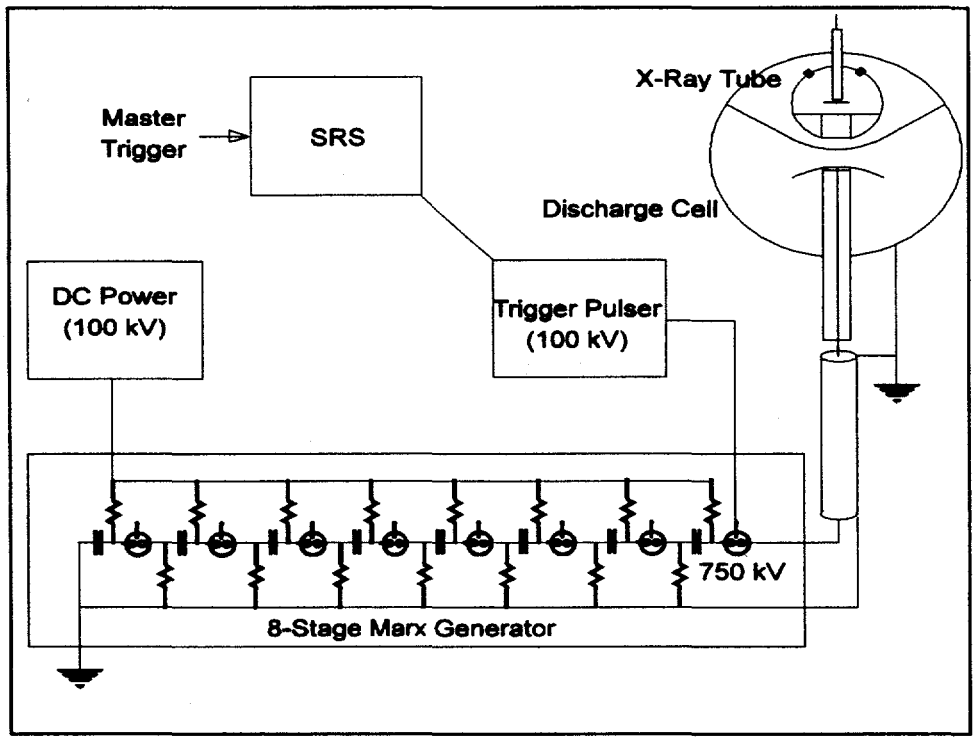

Fig.22

Electric schematic for pulse-forming network for the amplifier discharge

Although we tentatively choose a Marx generator scheme for the HV pulser illustration, there is a multiple choice of other schemes including: C-C transfer, L-C inversion, their double-sided versions, etc. Among the advantages of different schemes are: higher HV peak facilitating the initial ionization in C-C scheme, less number of spark gap required in L-C scheme, two-times reduction of the HV pulse inductance and a double loaded energy in double-sided schemes. The particular choice of the system will be worked out with the designer of the HV pulser.

4.5 Gas System

The gas system serves to maintain proper gas conditions (pressure, gas components proportion, exchange rate, purity) in the discharge cells of the ATF CO_2 laser system including: 1-atm oscillator discharge cell, 18-Torr oscillators smoothing tube, 5-atm big-volume amplifier, x-ray vacuum tube. Fig.23 presents the general diagram of the gas system. It includes subsystems for vacuum pumping, gas fill, and closed loop gas recirculation and purification system (CLGCPS).

Gas and vacuum subsystems include: high-pressure gas cylinders with regulators, gas supply lines, gas manifolds to control proportion, pressure and flow rates of the gas components introduced into the discharge cells, roughing vacuum pumps with oil and water traps, turbo-pump for x-ray tube and quadrupole mass-spectrometer, vacuum pipes with valves connecting vacuum pumps to discharge cells, pressure gauges and overpressure relief valves.

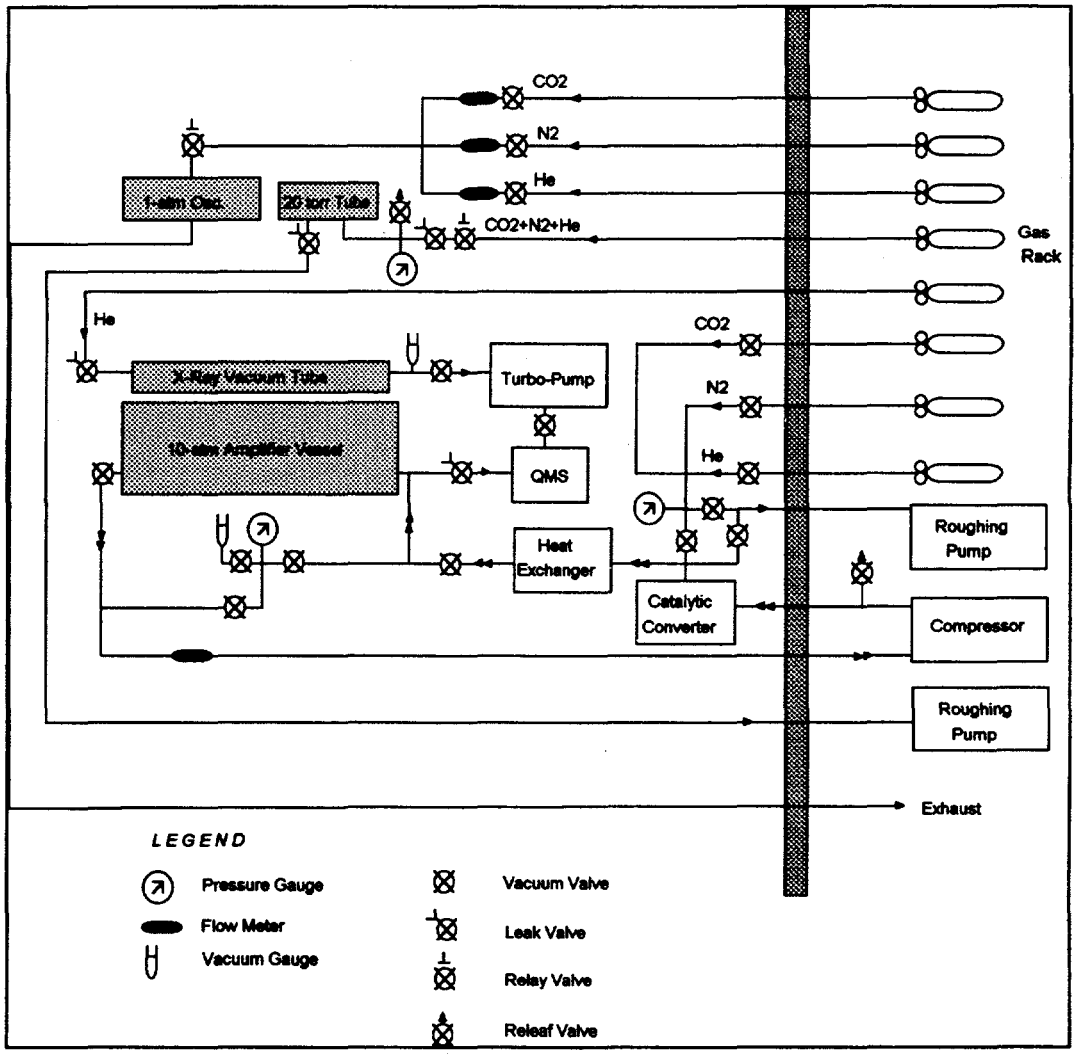

Fig.23

Gas and vacuum system for the ATF CO_2 laser

The CLGCP serves to circulate the laser gas mixture through the amplifier discharge cell and to recover the mixture components degraded in the discharge. The CLGCPS is connected to the input and exit ports of the discharge cell. It includes: gas compressor, catalytic converter, heat exchanger, mass-spectrometer and other diagnostic equipment, CO_2 isotope recovery unit, and tubing.

The components of the gas system are located in following parts of Bldg. 820: gas cylinders in the outside gas hutch, roughing pumps in the outside pump cabinet, energized components of the closed loop subsystem in the high-bay area, gas and vacuum tubing, detectors and valves in Rooms #1, #2 and other locations listed above.

Gas and vacuum subsystems are presently operational at the ATF, and just minor modifications will be required in the course of the ATF laser system upgrade (mostly, extension of gas and vacuum supply lines to Room #1). In the present paragraph, we will concentrate more on the

design features of CLGCPS, that should be build together with the big-volume amplifier, and especially on its key elements: compressor, catalytic converter and isotope recovery unit.

Gas heating and CO_2 decomposition in the discharge necessitates gas exchange in the amplifier discharge region. High energy loading into the amplifier discharge requires relatively fast gas replacement making impractical the exhaust ventilation as used in a low-energy CO_2 oscillator. That is why the closed loop recirculation and gas recovery system is used in the amplifier. It helps to prolong a single-fill gas life-time to several thousands shots. When slow unreversable gas degradation occurs, gas may be released from the CLGCPS and replaced with new portions. When using the isotopic CO_2, the requirements to the extended life time of the gas mixture, or at least of its isotopic components, become more stringent. That is why the additional isotope recovery unit is incorporated into the CLGCPS. This unit permits a separation of the isotopic gas from other gas components with its further purification (possibly at the manufacturer's site) and recycling into the CLGCPS.

The understanding of the gas degradation process is required to properly design the CLGCPS components. Decomposition of the CO_2 molecules under the electron bombardment is a common problem with the CO_2 discharge lasers:

$$CO_2 + e^- \rightarrow CO + O + e^-.$$

This process initiates a chain of secondary chemical reactions in a discharge volume resulting in the production of molecular oxygen and a family of nitrogen oxides:

$$O + O + M \rightarrow O_2 + M,$$
$$N_2^* + O \rightarrow NO + N_2,$$
$$N_2^* + O \rightarrow N_2O,$$
$$NO + O \rightarrow NO_2.$$

These products have high constants of electron attachment in reactions:

$$O_2 + e^- \rightarrow O + O^-,$$
$$NO + e^- \rightarrow N + O^-,$$
$$NO_2 + +e^- \rightarrow NO + O^-,$$
$$N_2O + e^- + M \rightarrow N_2O^- + M,$$

correspondingly, $k \approx 10^{-11}$ cm^3s^{-1} for O_2, and $k \approx 10^{-9}$ cm^3s^{-1} for N-oxides. That results in the electron density reduction causing the discharge instabilities and arcing.

To avoid arcing, it is required to keep the partial pressure of O_2 and N-oxides below 1% and 0.01%, correspondingly. Catalysts help to control O_2 and N-oxides concentrations via sponsoring endothermic reactions:

$$2CO + O_2 \rightarrow 2CO_2,$$
$$2NO \rightarrow O_2 + N2,$$
$$2NO + 2CO \rightarrow N_2 + 2CO_2,$$
$$N_2O + CO \rightarrow N_2 + CO_2.$$

In platinum catalysts like the one presently used in the ATF UV-preionized amplifier, the catalytic action is based upon a dissociative chemisorption of O_2 on platinum surface. The adsorbed atomic oxygen can react with either chemisorbed or gas-phase CO to form CO_2 which desorbes from the platinum surface. In a similar way, the catalyst helps in removing N-oxides. This or similar catalytic converter will be used in the upgraded CLGCPS.

To monitor the impurities in the CO_2 amplifier, a quadrupole mass-spectrometer (QMS) will be used according to the procedure already adopted at the ATF. QMS data collected so far on the effect of the gas mixture degradation in discharge are useful to estimate the required gas circulation

impurities concentration in the 3-atm ATF CO_2 laser amplifier during the period when the discharge was activated with the repetition rate 5 ppm. Ultimately, degradation of the discharge became noticeable resulting in a persistent arcing between the main electrodes. The fast drop of the impurities concentration when a warm catalyst was valved-in demonstrates the ability of the catalyst to reverse the trend of O_2 and N-oxides accumulation with a return to initial partial concentrations. What is actually important for us to learn from these data is the number of discharges before the gas degradation became noticeable. This number is ~100. Assuming that the rate of impurities production is proportional to the electric energy loaded into the discharge and that the adverse impurities effect depends upon their fractional dilution, we arrive at the proportion for the allowed number of shots in the projected amplifier: $\Sigma=100\, E_1V_2P_2/E_2V_1P_1$.

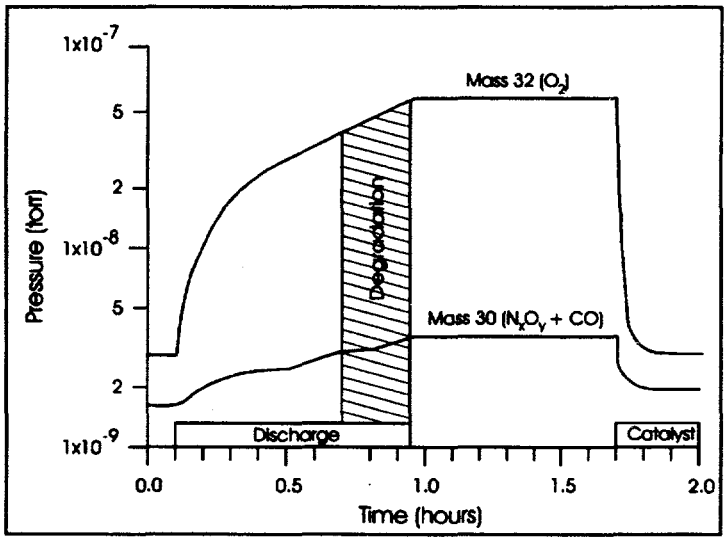

Fig.24

Catalytic regeneration in the CO_2 amplifier

Taking for the present and projected amplifier, correspondingly, E_1=0.5 kJ, V_1=40 *l*, P_1=3 atm and E_2=5 kJ, V_2=400 *l*, and P_2=5 atm, we get Σ=150. Hence, we set a requirement that the compressor should produce such mass-flow through the catalyst (that is considered to be ~100% efficient) that the stationary concentration of impurities maintained will never exceed the critical concentration attained in the system without catalyst after 150 shots. With the compressor pushing gas through the catalyst at a standard volume productivity S[*l*•atm/min] we can write a kinetic equation for the number of the impurity molecules M

$$\frac{dM}{dt}=Ef\zeta-\frac{MS}{VP}, \qquad (15)$$

where f is the discharge repetition rate and ζ is the efficiency of the impurities formation in the discharge. At the stationary conditions (saturation), $M=Ef\zeta PV/S$. Using Eq.(15), the number of impurity molecules observed after 150 shots without catalyst is $M=150E\zeta$. Hence, the condition for maintaining the saturated impurity concentration below the critical level is

$$S>PVf/150=(5\text{ atm})\times(400\ l)\times(6\text{ ppm})/150=80\ l\bullet\text{atm/min}.$$

The isotope recovery unit is intended to separate the isotopic mixture of CO_2 gas from N_2, He and any impurities accumulated in the course of the prolonged closed-loop laser operation and/or wall material outgasing and leaks that can not be eliminated by the catalytic converter. The operation of the proposed cryogenic isotope recovery unit is illustrated by Fig.25 and is described as the follows.

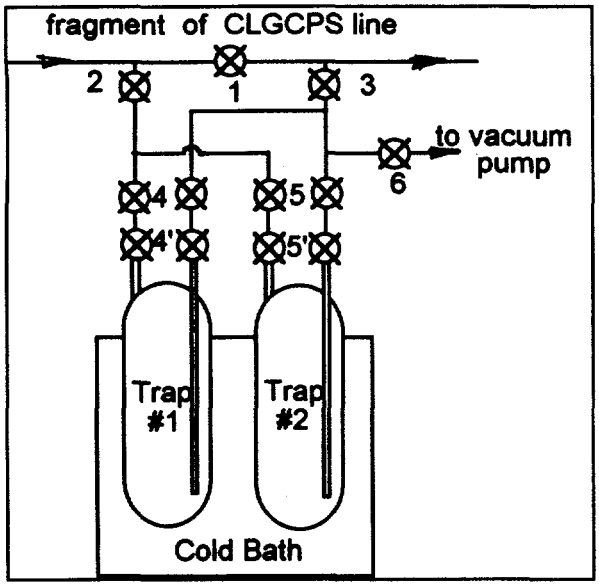

Fig.25

Principal diagram of Isotope Recovery Unit

The cryogenic isotope recovery unit consists of two cold traps with means for temperature adjustment in the range of 200-145 K and system of valves. When employing the recovery unit, the cold bath temperature is initially set slightly above the dew point of the CO_2 at its working concentration (e.g., 181 K for 0.5 amagat). Then we close or partially close valve #1 and, by opening valves ##2, 3, 4, and 4', introduce gas circulation through the cold trap #1 permitting freezing out of all volatile impurities with boiling points above CO_2 (e.g., water, oil, etc.). Isolate trap #1 from the CLGCPS. Decrease the cold bath temperature to ~147 °K, which corresponds to the CO_2 saturated concentration 0.01 amagat. By opening valves ##5, 5' permit CO_2 freezing out in trap #2. Isolate trap #2 from the CLGCPS. return the recovery unit to room temperature. Pump out the CLGCPS and the content of trap #1. Introduce trapped CO_2 gas back into the CLGCPS or disconnect trap #2 and send trapped CO_2 for processing to the manufacturer.
The technical details of the isotope recovery unit will be worked out with the designer.

4.6 Control System

The ATF CO_2 laser control system includes monitoring devices primarily located at the master control post, detectors for optical , electrical and gas diagnostics located throughout the entire laser system, other special optic instruments (spectrum analyzer, autocorrelator) located on the control table in Room #2, data acquisition devices located primarily at the master control post, and computer control devices located in Room #2 and in the ATF Control Room.

The master control post for the ATF CO_2 laser system is located in Room #2. It includes panels that accommodate controls (switches, regulators) and display devices necessary for normal operation of the system. Rack-mounted control electronics (oscilloscopes, pulse generators, etc.) are accommodated in a standard 19" rack positioned next to the control panels.

Were possible, the control and data acquisition functions of the control panel and rack-mounted electronics will be duplicated by the computer control and data acquisition system. The upgraded computer control system is envisioned as an extension of the existing CO_2 laser computer control system illustrated by Fig.26. The efficiency of this system has been demonstrated during the ATF experiments.

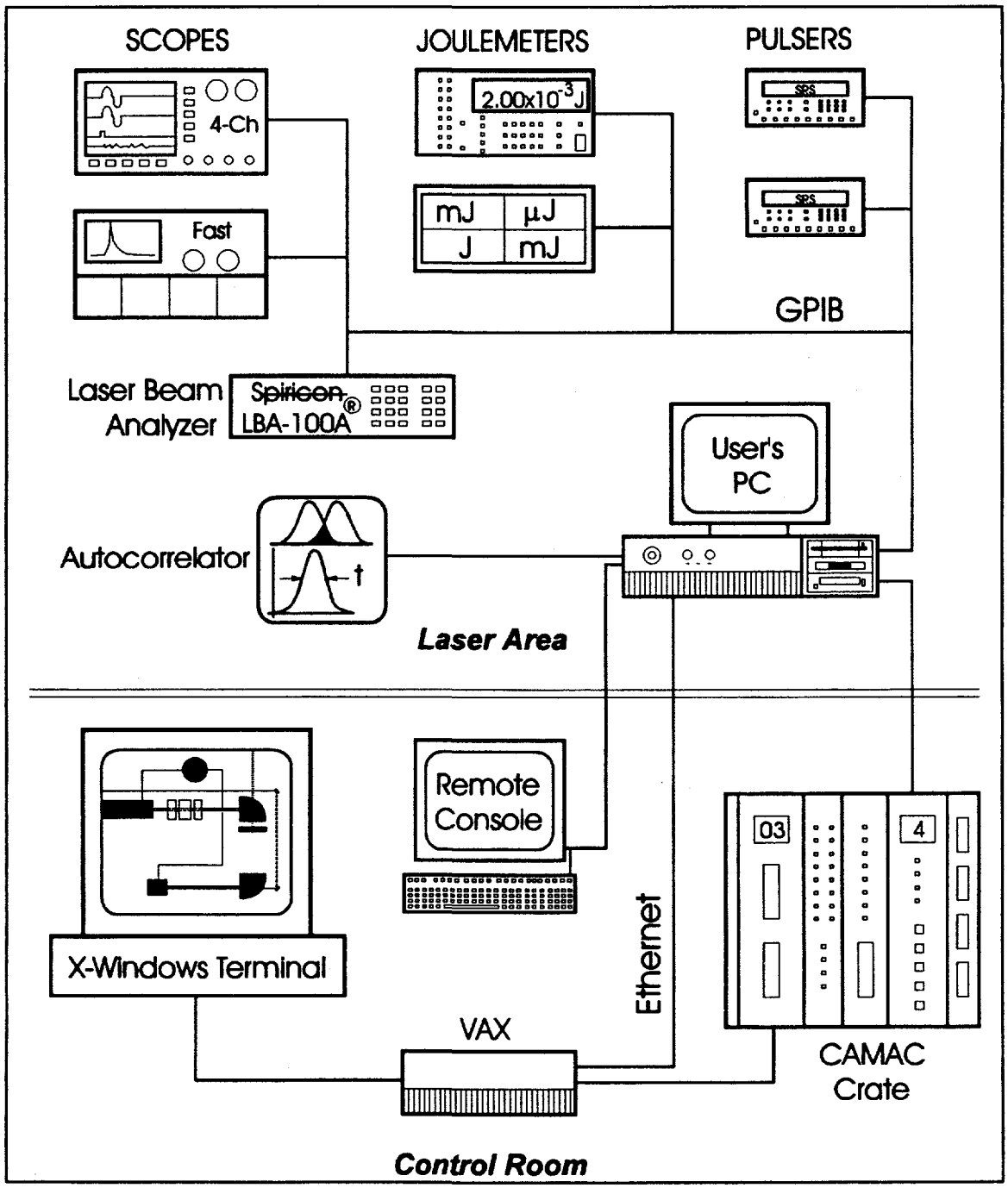

Fig.26

Block diagram of the present computer control system for the ATF CO_2 laser

Computer control via exploiting the GPIB compatibility of various laser control devices makes it possible to operate the system remotely from the Control Room where the control posts for the ATF linac and current experiments are also located. To serve as the central interface for the CO_2 laser is the National Instruments AT-GPIB interface card installed into the IBM PC equipped with the Intel 80486 33-MHz processor. This card enables the PC to control the flow of information to and from each device connected to the GPIB network. As shown in Fig.26, our GPIB configuration presently encompasses seven devices, which are connected to the PC's GPIB card. Not shown in the diagram is the triggering system that was devised to enable the remote triggering of the GPIB devices and the CO_2 Laser System in synchronization with the Nd:YAG laser system and the ATF linac control system.

Tying all of this diagnostic and triggering hardware together is the software package LabVIEW from National Instruments. Running under the Microsoft Windows 3.1 operating environment, LabVIEW provides the means to program the PC with ordered routines and instructions for GPIB and triggering purposes. Instead of having to know and write out source code, the operator need only logically connect icons within the programming environment. The multitasking capabilities of Windows are exploited by LabVIEW to allow the simultaneous display of several virtual instruments. In our case, both pulsers, one of the joulemeters (Molectron JD2000, 2 channel energy ratiometer), and the four-channel digitizing storage oscilloscope (Tektronix TDS 420) have been routinely viewed and operated simultaneously with the timing card at work.

Accommodations have also been made to allow direct communication between the central control PC, the ATF VAX, and users PC for the purpose of data correlation among these systems. That gives the possibility to the user, e.g., during the laser acceleration experiment, to collect automatically data needed for further processing. Such parameters as: laser peak power available from the control PC, linac's magnet settings and the position of the laser delay translator from the VAX, etc., may be downloaded to the users PC together with the e-beam energy spectrum and other important for the experiment data.

These and additional features will be integrated into the modified control system structure which will be finalized at the further design stages of the ATF CO_2 laser system upgrade.

Section 5

Project structure and management

In the preceding sections we discussed the physical approach to the upgrade of the ATF CO_2 laser system to the terawatt level and what the upgraded system looks like. In the present Section we suggest the answers to the following practical questions: who will perform the upgrade (Paragraph 5.1), when it may be completed (Paragraph 5.2), and how much it may cost (Paragraph 5.3).

5.1 Project Organization

According to the design approach to the upgrade of the ATF CO_2 laser system, the main efforts are directed towards the development and integration into the system of a large-aperture x-ray preionized CO_2 laser amplifier and the appropriate reconfiguring of the ATF laser system (e.g., moving Nd:YAG laser to the e-gun). The tasks associated with this upgrade are listed in Fig.27 together with their cost estimate which is discussed in the last paragraph. According to the nature and content of the particular task or its subtask, assignments are done for design, manufacturing, assembly and tests. These assignments are based on the following primary considerations:
a) capability of handling the job at the proper technical and quality level,
b) availability or degree of completion of the particular system or component,
c) cost saving.

It is also presumed that BNL is the leading organization in the technical management of the upgrade project. This is reasonable, taken into account such factors as: experience gained in development of the present laser system, availability at BNL a number of components necessary for the fulfillment of the project, diversity of project tasks, and broad capabilities of the BNL staff and services that will be involved into the project.

Less evident is an answer to the question: who should be responsible for technical management of the biggest cluster of the laser system upgrade tasks - design, manufacturing and installation of the large-aperture amplifier. Presently, BNL is in the middle of a procurement process for a High-Power, High-Pressure CO_2 Laser Amplifier (RFP 765507, see Appendix). However, there is a possibility that no one submitted bid on the integrated amplifier unit satisfies all of BNL technical, quality and cost requirements. In this case, BNL should be prepared to take a responsibility for technical management of this part of the project. This Section is written with such a possibility in mind.

Block-diagram of the projected amplifier in Fig.16 shows its components. It illustrates that the ATF, already equipped with some of the required components, is well prepared to handle the project. These components are actually parts of the present CO_2 amplifier that will be decomissioned. Components marked in Fig.16 may be used directly or after minor modification. Note also, that Gas Circulation and Purification System from the present amplifier may also be used at the first stage of the laser system upgrade.

Practically, there are just a few unavailable components, but they are the most critical parts of the projected amplifier. They are: a discharge cell, HV pulser with DC power supply, and x-ray tube. Among them, there are three parts that require special expertise in design and manufacturing, and they should be procured from suppliers, who have such expertise. These components are: x-ray

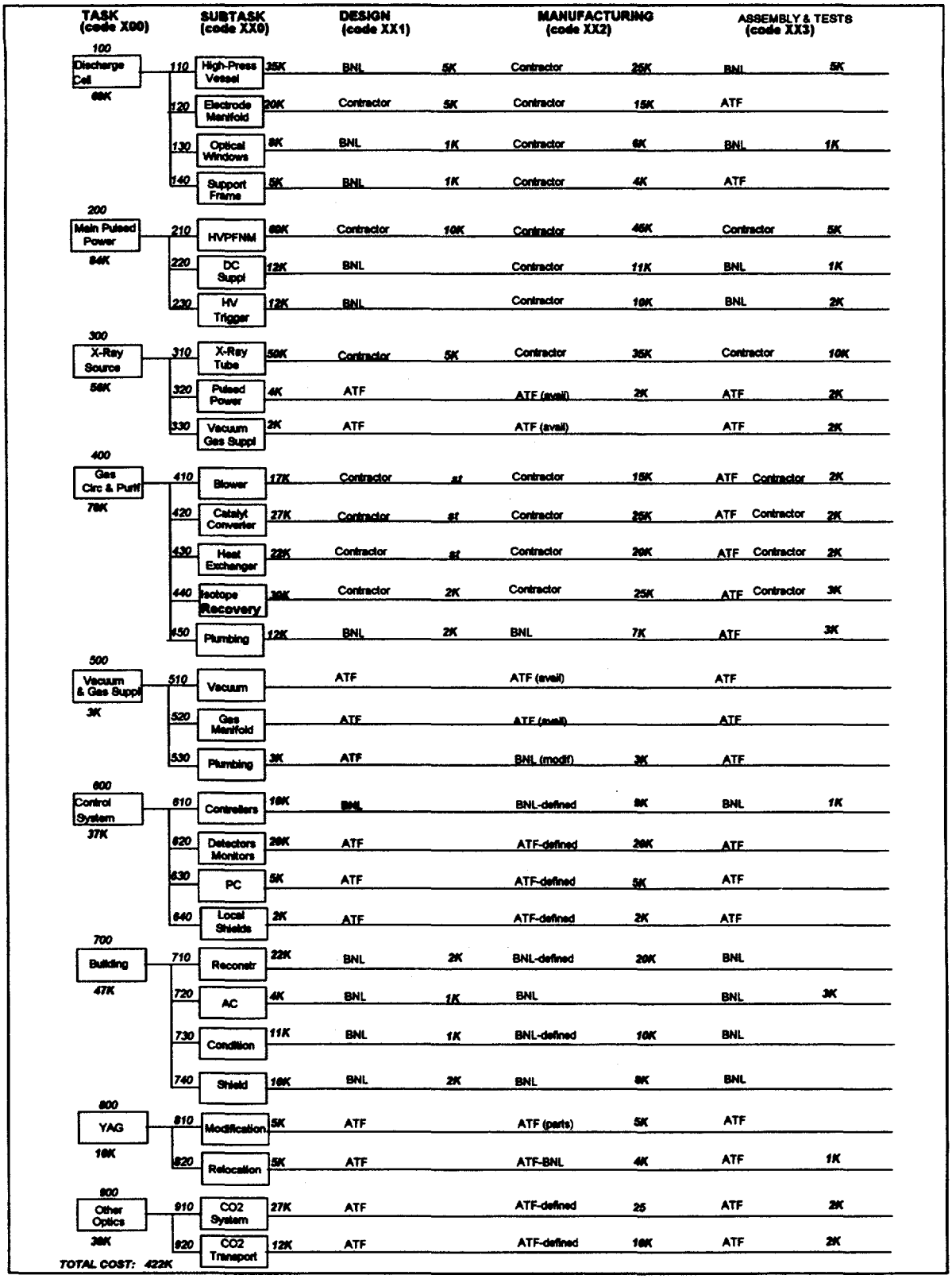

Fig.27

Project tasks and cost estimate

tube, specially profiled electrodes of the discharge cell, and HV pulser. Proper design and performance of these elements are crucial for the success of the present project. That is why choosing contractors for these components will be the most important procurement decision in the course of this program. Manufacturing and/or procurement of other components, such as a high-pressure vessel, discharge cell optics and 100-kV DC power supply, do not present special problems.

Project organization chart shown in Fig.28 gives the overview of the personnel and resources involved into the project. In addition to the ATF and NSLS personnel responsible for the major project tasks, the chart includes contactors for mentioned above critical amplifier components as well as contractors involved in other tasks listed in Fig.27, e.g., Gas Circulation and Purification System and Building Reconstruction. It is also assumed that some tasks may be performed on a collaborative basis. For instance, such collaboration may be negotiated under the sponsorship of the Joint (USA-Russia) Committee on Fundamental Properties of Matter where Laser Particle Accelerators Studies are already included into the program.

Another valuable resources for the project come from the ATF technical support team, NSLS designers and technical services, BNL plant engineering and other services.

We conclude the discussion of the project organization plan with the statement that BNL has the adequate scientific and technical potential, including personnel and facilities, to manage the Terawatt Laser Upgrade project in cooperation with conractors which will be selected and named later.

5.2 Project Staging and Schedule

The task sequence within the project and their scheduled completion time will be determined by such factors as the budget constrains (currency flow rate), intermediate goals to attain, logical hierarchy of tasks (precursors-successors), and required minimum shut-down time for the ATF experiments that use CO_2 laser. In planning the project schedule, we assume that the budget constrains and required intermediate research studies may not permit us to reach the ultimate goal of the upgrade - terawatt peak power level - as a single ongoing effort. In this case, a certain staging of the project is desirable. The logic is that at the end of each project stage, that may be completed in a reasonably short period of time or at least with a short shut-down time involved, the CO_2 laser is available for the experiments at a higher level of performance.

Two stages of the CO_2 laser upgrade may be anticipated. At the first stage, new laser amplifier should be developed and integrated into the reconfigured ATF laser system. Operating with a regular gas mixture, CO_2 laser system will be capable to deliver at least 250 GW, 30-ps or shorter laser pulses. In the course of the second upgrade stage, switching to multi-isotope gas mixture and shorter laser pulses shall be attempted permitting to attain a several terawatt peak power level in as short as a 3-ps pulse.

Our tentative schedule summarized in Fig.29 and presented in more details in Fig.30 and Fig.31 is close to this scenario with just a minor exception. We still anticipate Stage 1 as the most critical part of the project that requires major reconfiguring of the ATF laser system and 2-3 months shut-down time. During this shut-down, the Nd:YAG laser will be moved into the newly built hutch and the CO_2 amplifier will be replaced with the new one. However, in order to balance budget more uniformly over the period of the project (as according to the expected currency flow), noncritical tasks have been moved from Stage 1 to Stage 2. As a result, at the end of Stage 1, we still have an

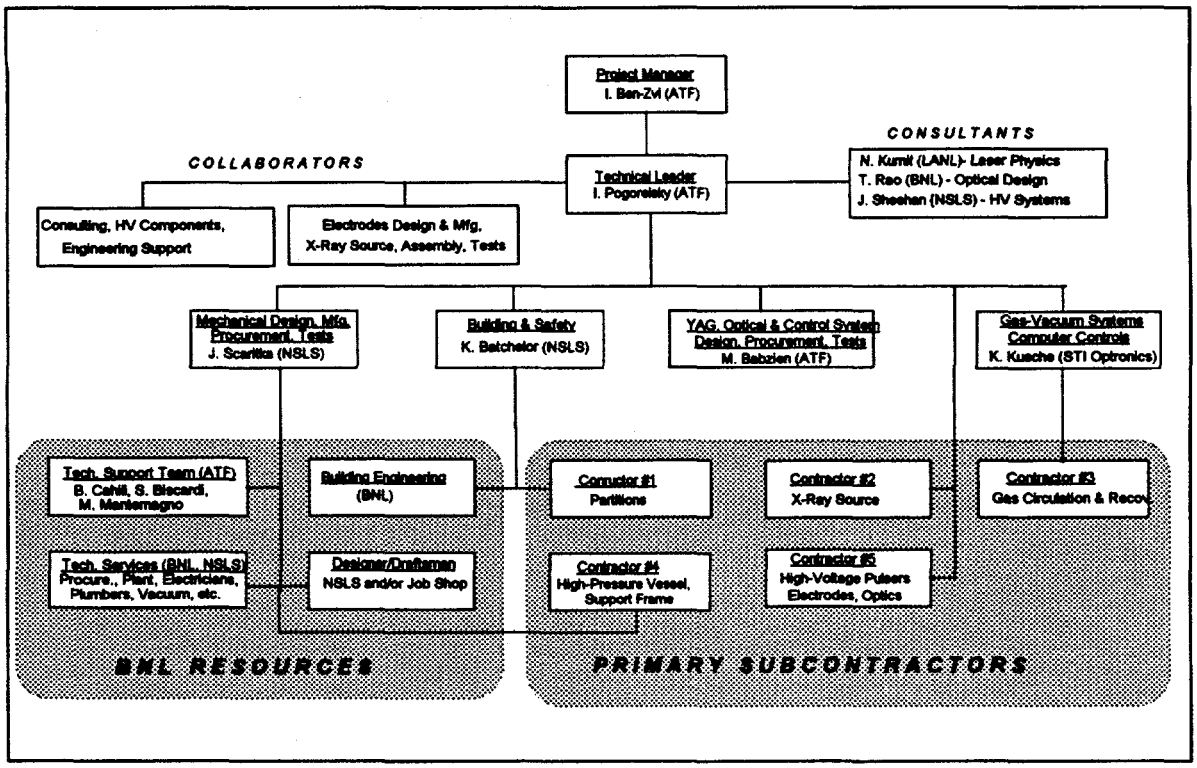

Fig.28

Project organization chart

Table 8

Proposed Staging for CO_2 Laser System Upgrade

Parameter	Stage 1	Stage 2
Pressure (atm)	3.5	5
DC Voltage (kV)	75	100
DC Power (kW)	0.12	1-2
Shock Voltage, V_{out} (kV)	500-550	700-750
Load Energy (kJ)	3	6
Gas Exchange Rate (sl/min)	25	80-100
Repetition Rate (ppm)	0.5-1	3-5
Laser Pulse Duration w/regular gas (ps)	50	30
Laser Pulse Duration w/isotope gas (ps)	NA	5
Output Power w/regular gas (TW)	~0.1	~0.25
Output Power w/isotope gas (TW)	NA	~2

operational system of a significantly higher output peak power to compare with the present ATF CO_2 laser system. However, rebuilding of the CO_2 laser system at the end of Stage 1 is incomplete and further "evolutionary" improvements will be continued through Stage 2. We call these improvements "evolutionary" because they do not require serious construction work or shut-down and may be introduced over the extended period of time. The "incomplete" character of Stage 1 is further illustrated by Table 8 where parameters of the CO_2 laser system after Stage 1 are compared with those after the completed upgrade.

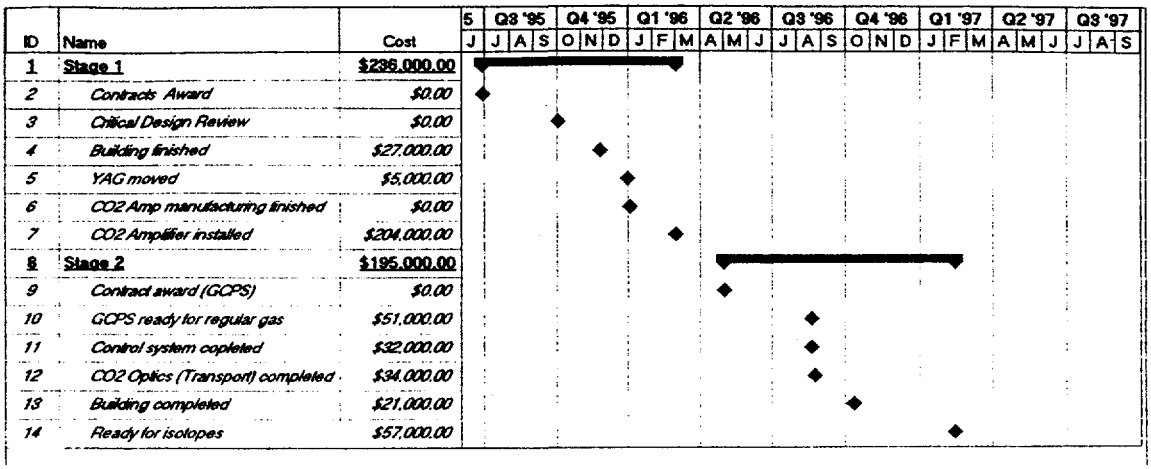

Fig.29

Project staging

The possibility to postpone the completion of jobs, which have been moved from Stage 1 to Stage 2, stems from the availability at the ATF of components that may be temporarily used. The examples of such possible substitutions are:

- 75-kV, 120-W DC power supply instead of the projected 100-kV, 1-2 kW power supply;
- 3.5-4 atm, 25 sl/min gas circulation and purification system instead of the projected 5-atm, 80 sl/min system.

Other examples of jobs that may be postponed until the completion of Stage 2 are:

- completion of the control and diagnostics system; e.g., the PC-controlled remote operation function may be implemented later;
- air filtering, conditioning and some other building improvements;
- high-power laser beam transport line (bigger diameter mirrors, mounts, etc.).

Naturally, Stage 2 involves a certain amount of research on extending the life-time of a gas mixture and generating short picosecond pulses to seed into the amplifier. The required upgrade research and necessary modifications will be done in parallel and not in a contradiction to the normal operation of the laser system as a part of a regular activity of the ATF personnel.

Stage 2 may be started shortly after a completion of Stage 1, as shown in the preliminary schedule in Fig.29, or after longer lap time, or its duration may be extended. During this time, the laser system will be still available for the application experiments.

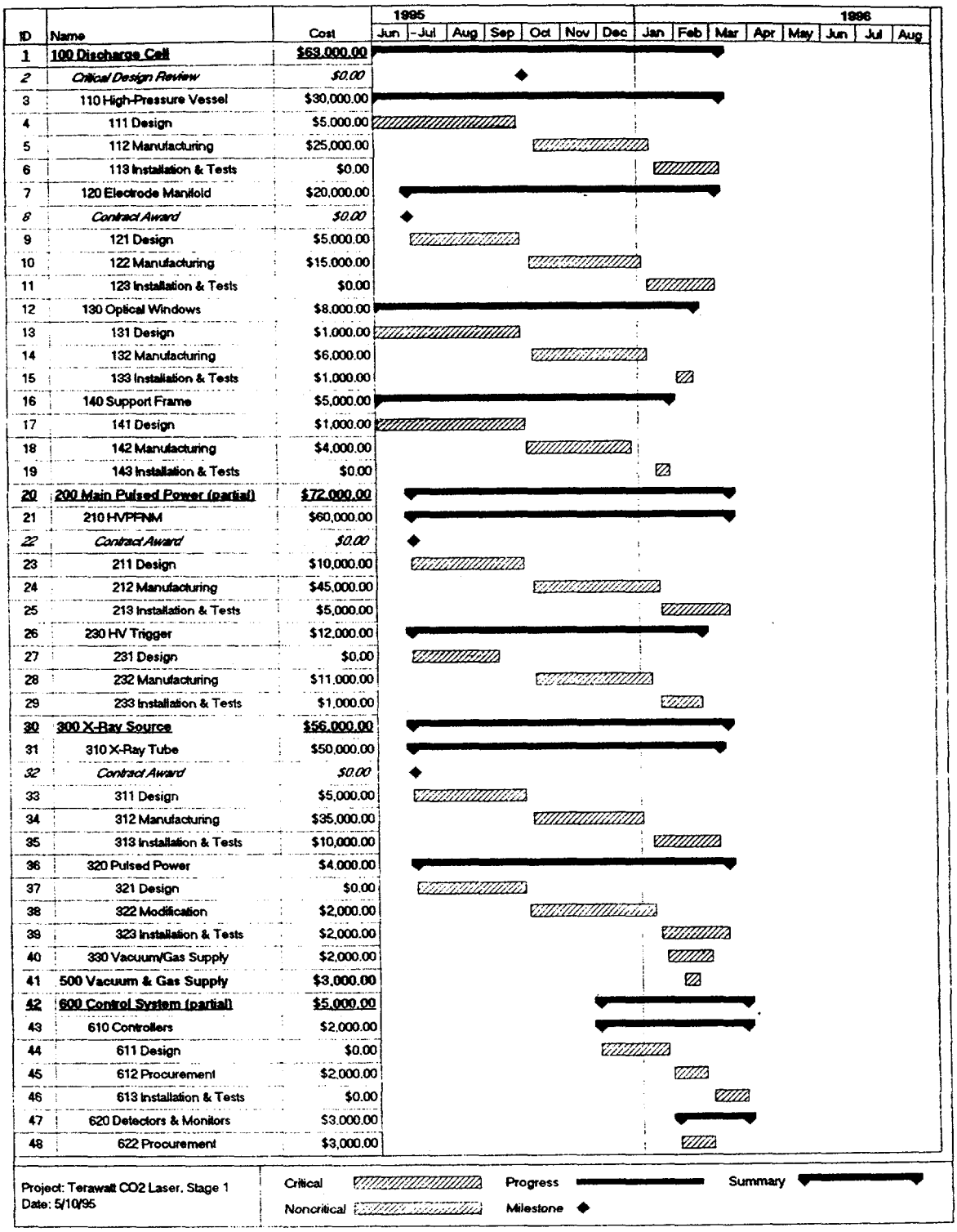

ID	Name	Cost
1	100 Discharge Cell	$69,000.00
2	Critical Design Review	$0.00
3	110 High-Pressure Vessel	$30,000.00
4	111 Design	$5,000.00
5	112 Manufacturing	$25,000.00
6	113 Installation & Tests	$0.00
7	120 Electrode Manifold	$20,000.00
8	Contract Award	$0.00
9	121 Design	$5,000.00
10	122 Manufacturing	$15,000.00
11	123 Installation & Tests	$0.00
12	130 Optical Windows	$8,000.00
13	131 Design	$1,000.00
14	132 Manufacturing	$6,000.00
15	133 Installation & Tests	$1,000.00
16	140 Support Frame	$5,000.00
17	141 Design	$1,000.00
18	142 Manufacturing	$4,000.00
19	143 Installation & Tests	$0.00
20	200 Main Pulsed Power (partial)	$72,000.00
21	210 HVPFNM	$60,000.00
22	Contract Award	$0.00
23	211 Design	$10,000.00
24	212 Manufacturing	$45,000.00
25	213 Installation & Tests	$5,000.00
26	230 HV Trigger	$12,000.00
27	231 Design	$0.00
28	232 Manufacturing	$11,000.00
29	233 Installation & Tests	$1,000.00
30	300 X-Ray Source	$56,000.00
31	310 X-Ray Tube	$50,000.00
32	Contract Award	$0.00
33	311 Design	$5,000.00
34	312 Manufacturing	$35,000.00
35	313 Installation & Tests	$10,000.00
36	320 Pulsed Power	$4,000.00
37	321 Design	$0.00
38	322 Modification	$2,000.00
39	323 Installation & Tests	$2,000.00
40	330 Vacuum/Gas Supply	$2,000.00
41	500 Vacuum & Gas Supply	$3,000.00
42	600 Control System (partial)	$5,000.00
43	610 Controllers	$2,000.00
44	611 Design	$0.00
45	612 Procurement	$2,000.00
46	613 Installation & Tests	$0.00
47	620 Detectors & Monitors	$3,000.00
48	622 Procurement	$3,000.00

Fig.30 (a)

Project schedule, Stage 1

ID	Name	Cost
49	623 Installation & Tests	$0.00
50	700 Building	$27,000.00
51	710 Reconstruction	$22,000.00
52	711 Design	$2,000.00
53	712 Manufacturing	$20,000.00
54	720 AC	$5,000.00
55	721 Design	$2,000.00
56	723 Installation & Tests	$3,000.00
57	800 YAG	$10,000.00
58	810 Modification	$5,000.00
59	811 Design	$0.00
60	812 Manufacturing	$5,000.00
61	813 Installation & Tests	$0.00
62	820 Relocation	$5,000.00
63	821 Design	$0.00
64	822 Manufacturing	$4,000.00
65	823 Installation & Tests	$1,000.00
66	900 Other Optics (partial)	$5,000.00
67	910 CO2 System	$5,000.00
68	911 Design	$0.00
69	912 Procurement	$5,000.00
70	913 Installation & Tests	$0.00

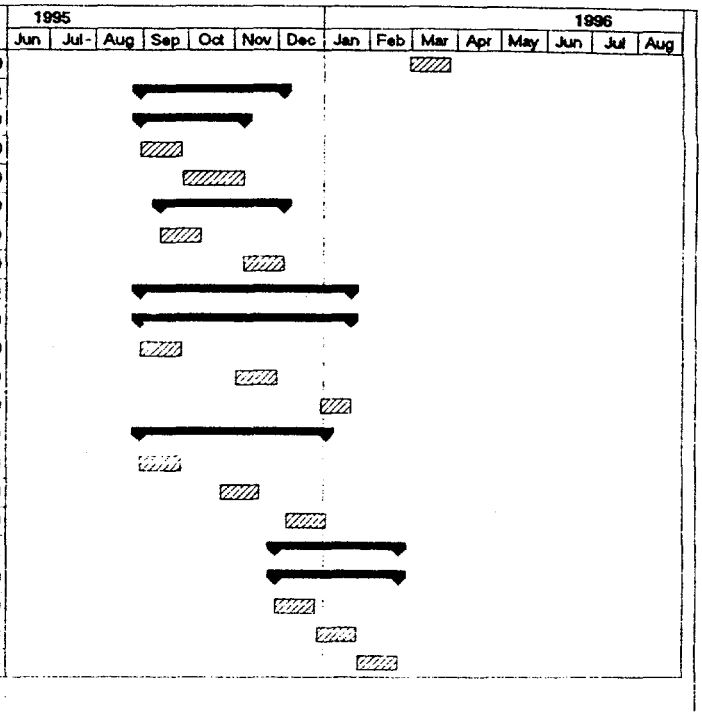

Fig.30 (b)

Project schedule, Stage 1 (continued)

ID	Name	Cost
1	200 Main Pulsed Power (completio	$12,000.00
2	220 DC Supply	$12,000.00
5	400 Gas Circulation & Purification	$108,000.00
6	*Contract Award*	*$0.00*
7	410 Blower	$17,000.00
10	420 Catalytic Converter	$27,000.00
13	430 Heat Exchanger	$22,000.00
16	440 Catalyst Recovery Unit	$30,000.00
20	450 Plumbing	$12,000.00
24	600 Control System (completion)	$32,000.00
25	610 Controllers	$8,000.00
28	620 Detectors & Monitors	$17,000.00
31	630 PC	$5,000.00
34	640 Local Shields	$2,000.00
38	700 Building (completion)	$21,000.00
39	730 Air Condition	$11,000.00
43	740 EM Shield	$10,000.00
47	900 Other Optics (completion)	$34,000.00
48	910 CO2 System	$22,000.00
52	920 CO2 Transport	$12,000.00

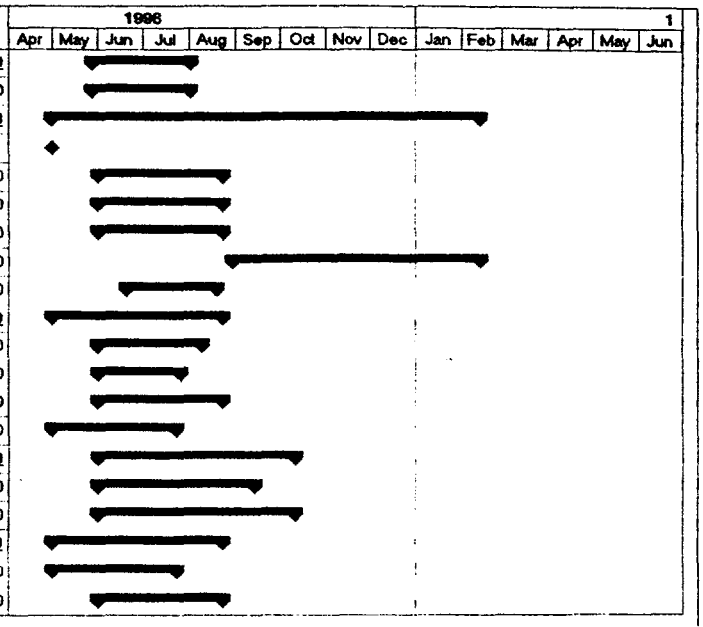

Fig.31

Project schedule, Stage 2

The proper planning of Stage 1 that involves the major structural modification to the ATF laser system is most crucial now and is considered here in more details. In the presented in Fig.30 proposed schedule for the fist stage, we actually arrange chronologically relevant tasks listed in Fig. 27. This schedule is arranged according to our understanding of the logical sequencing of tasks and sub-tasks, our best estimate of the time required for completion of every task, and under the assumption that budgetary considerations introduce no further delays to the schedule.

The critical milestone at the beginning of Stage 1 is the completion of the procurement and awarding the contracts on the major amplifier components. These components that shall be built by the outside contractors, who are proficient in the field, are: x-ray tube, HV pulser for the main discharge, and electrode manifold. We put tentatively the date 7/1/95 for this milestone. If it moves, all the successor tasks move accordingly.

We presume in the schedule that BNL is responsible for design and manufacturing (or procurement) of other amplifier components scheduled within Stage 1, e.g., high-pressure vessel with optical windows, support frame, etc. Designing of these components may start prior the contracts award. That will give BNL an opportunity to clarify the components compatibility issues before the contracts award. Note that basic requirement on the amplifier components are already specified to the potential contractors in RFP which shall be referred as an official document within the present procurement.

Completion of the amplifier component design is defined by another milestone - Critical Design Review, after which manufacturing may start. One or two preliminary design reviews may be needed before CDR, as anticipated in RFP (Appendix).

After manufacturing and necessary tests at the contractor's site, the amplifier components are ready for installation at the ATF. To that moment (~25 weeks after the contracts award), Nd:YAG laser should be already moved from Room #1 into the newly built hutch at the front end of linac.

Correspondingly, construction and relocation (tasks 700 and 800) shall be scheduled in a prior time. However, the beginning of these jobs may depend upon the ATF funding introducing another contingency into the schedule.

Upon the clarification of all external factors involved, schedule may naturally vary. However, the present preliminary scheduling is still adequate for the Conceptual Design document and may serve as a guidance for building more detailed and correlated plan in the future.

5.3 Comments on Cost Estimate

Cost is one of the most attentively considered issues. However, its estimate is inherently least predictable as long as the project involves development of state-of-the-art nonstandard laser components. It is not like we are not aware of a market situation in the field. Actually, pretty extensive study on this subject has been done during the last two years. However, prices vary in a wide range from company to company, float in time (unfortunately upward), and may depend upon requirements and restrictions imbedded into the procurement process. That is why it is difficult to predict with a good accuracy the contract cost before it is negotiated. Contract costs assigned to the tasks in Fig. 27 and further in Table 8 are estimated close to the lowest known market prices having in mind certain budget constrains imposed. If we succeed inegotiating contracts at the bottom cost level without sacrificing the product performance and quality. in it, when the whole project, including the rest of the tasks with lower contingency comes out to ~450K.

BROOKHAVEN NATIONAL LABORATORY
Associated Universities, Inc.
Upton, New York 11973

Accelerator Test Facility Specification
X-ray Preionized High-Pressure CO_2 Laser Amplifier

QA CATEGORY A - 2		
OUTSTANDING ECN's		

REVISION CONTROL SHEET

LETTER	DESCRIPTION	DATE	WRITTEN BY	APPROVED BY	TYPED BY
A	First Issue	11-16-94	J. Skaritka	I.Pogorelsky	LJL

BROOKHAVEN NATIONAL LABORATORY
ASSOCIATED UNIVERSITIES, INC.
UPTON, N. Y.
Form 1803

JOB NUMBER	DRAWING NUMBER	SIZE	REV

Table of Contents

1.0 SCOPE

1.1 General Description

This specification details the requirements for the fabrication, assembly, inspection and test of the CO_2 Laser Amplifier (Amplifier) for the Accelerator Test Facility (ATF) of Brookhaven National Laboratory (BNL).

Where this specification fails to take advantage of special facilities or processes available to the supplier, changes to this specification which do not adversely affect function may be negotiated at or before the Critical Design Review (CDR).

1.2 Acronyms and Abbreviations

The Acronyms and Abbreviations referenced in this document are listed in Appendix A.

2.0 APPLICABLE DOCUMENTS

The following documents, of the issue in effect at the time of the contract, form a part of this specification to the extent specified herein. In the event of a conflict between the documents referenced herein and the contents of this specification, the contents of this specification shall take precedence.

Copies of BNL documents required by suppliers in conjunction with specified procurement functions shall be obtained from the BNL procurement office by the Contract Administrator (CA) or as directed by the ATF Cognizant Project Engineer (PE)..

Copies of descriptions and manuals to the parts and components supplied by the ATF shall be obtained from the ATF Contract Administrator. Procurement of all other governing documents is the responsibility of the supplier.

2.1 BNL (ATF) Documents

2.1.1 Statement of the Work for the Terawatt CO_2 Laser Amplifier, BNL Document WC #765507

2.1.2 Quality Assurance and Quality Control Requirements

2.1.3 Description of the ATF CO_2 laser system

2.1.4 ATF floor plan

2.1.5 Environmental Safety and Health Standard Sections

1.3.4 Operational Safety Limits.
1.4.0 Compressed Gas Cylinder Safety.
1.4.1 Pressurized Systems for Experimental Use.
1.4.2 Glass and Plastic Windows for Pressure Vessels.
1.5.0 Electrical Safety.
1.5.2 Design Criteria for Electrical Equipment.
1.6.0 Material Handling Equipment.
1.10.0 Hazard Information Placards.
2.3.1 Lasers.
2.3.2 RF and Microwaves
2.4.0 Noise
3.1.0 Standards for Radiation Protection, BNL RADCON Manual Table 2.3

2.2 Non-BNL Documents

2.2.1 National Electric Code

2.2.2 OSHA Parts 1900 to 1910

2.2.3 ASME Pressure Vessel Code, Section 8

2.2.4 ISO 9000 Quality Standard

2.2.5 MIL-I- 45208 Quality Specification

2.3 Source of BNL Documents

The documents may be obtained from the ATF Contract Administrator.

2.4 Source of Non-BNL Documents

Non BNL documents are readily available at libraries or organizations which have prepared them.

2.5 Specification Revision

Revision to this specification can only be authorized by the Principal Project Scientist (PS) and implemented by the cognizant Project Engineer (PE). Originals of the specification revision shall remain on file in the NSLS design office.

3.0 FABRICATION REQUIREMENTS

3.1 General

3.1.1 The amplifier consists of the following primary components:

a. Discharge cell with electrode manifold for the main discharge as defined in section 3.2.

b. X-ray preionizer as defined in section 3.3.

c. High voltage pulse forming network (HVPFN) as defined in section 3.4.

3.1.2 Auxiliary components

a. DC high voltage power supplies for main discharge and x-ray preionizer as defined in section 3.5.

b. Closed loop gas circulation and purification system as defined in section 3.6.

c. Gas supply and vacuum system as defined in section 3.7.

d. Control panel as defined in section 3.8.

3.1.3 The system shall operate with 60 Hz primary power source.

3.1.4 Standards for Radiation Protection

The amplifier shall conform to standards defined in the BNL ES&H Standard Section 3.1.0 and the BNL RADCOM Manual Ref. Table 2.3.

3.2 Discharge Cell

The discharge cell consists of:

a. Electrode manifold.

b. High pressure vessel.

c. Mechanical supports.

3.2.1 Electrode Manifold

The electrode manifold is used to maintain a uniform pulsed electrical discharge in a gas volume comprised within the manifold.

3.2.1.1 Electrode Manifold Shape and Dimensions

3.2.1.1.1 The electrodes shall comprise a planar region of dimensions (10-12)cm x (100-120) cm.

3.2.1.1.2 The interelectrode distance shall vary continuously or step-adjustable between 5-10 cm.

3.2.1.1.3 The peripheral regions of the electrodes shall be contoured to help fit the discharge plasma within the aforementioned volume, and to develop a monotonically graded electric field on the edges in order to prevent field-induced arc formation.

3.2.1.2 Electrode Manifold Feedthroughs

3.2.1.2.1 Both, cathode and anode, of the electrode manifold shall be mounted on insulated feedthroughs to permit a +/- 500 kV floating pulsed potential between either electrode and ground.

3.2.1.2.2 The feedthroughs shall permit up to 100 kA current commuted to the electrodes in 1μs pulse with a repetition rate 0.1 Hz.

3.2.1.3 Compatibility to X-Ray Preionizer

The electrode manifold shall be designed to facilitate a uniform penetration of the interelectrode volume with x-rays generated by the preionizer.

3.2.2 High Pressure Vessel

The high pressure vessel provides separation of the gas discharge volume from ambient atmosphere, supports feedthroughs of the electrode manifold, and provides optical communication through the discharge region in the visible and IR spectral regions.

3.2.2.1 The high pressure vessel configuration shall be designed to accommodate the electrode manifold and x-ray preionizer and provide appropriate distances through the gas and along the dielectric surfaces in order to prevent high-voltage break-down.

3.2.2.2 The vessel shall have ports for optical windows and axial gas circulation.

3.2.2.3 Provisions in the high pressure vessel design shall be made to ensure turbulence-free gas flow through the discharge region at a rate of 200 l/min.

3.2.2.4 Vessel construction shall provide access to the electrode manifold and x-ray preionizer for maintenance and repair.

3.2.2.5 Standard Compliance

The high pressure vessel design shall conform to the BNL ES&H Standard Sections, 1.4.0, 1.4.1, 1.6.0, 1.10.0 and Sec. 8 of ASME pressure vessel code.

3.2.2.6 Pressure and Vacuum Tightness and Mechanical Stability

3.2.2.6.1 Design Pressure

The vessel shall be mechanically designed for normal operation at 10 atm of internal pressure, plus the shock impulse generated by loading up to 20 kJ of electric discharge energy into the gas volume.

3.2.2.6.2 Leak Tightness

The vessel shall be leak-free in the entire range of 10^{-3} through 7,600 Torr of internal pressure at the level indicated in the Discharge Cell Test Procedure.

3.2.2.6.3 Mechanical Stress Limits

Design stress shall not exceed 70% of the materials yield strength or 50% of the materials ultimate strength. For any load bearing member of the pressurized system.

3.2.2.6.4 Safety Standards

The vessel shall comply with the BNL ES&H Standard Sections 1.3.4, 1.4.1, and the limits imposed by the ASME pressure vessel code section 8 which ever is conservative for the specific application.

3.2.2.7 High Pressure Vessel Material

The internal vessel surface in contact with a laser gas mixture shall be constructed of inert, low gas desorption material compatible with prolonged closed-loop operation of the Amplifier, compatible with x-ray irradiation, and compatible with isotope ^{18} O. (Reduction of ^{18} O concentration shall not exceed 10% in 10,000 amplifier shots.) Identical requirements are applied to gaskets materials used for vacuum sealing of the discharge cell.

3.2.2.8 Optical Windows

3.2.2.8.1 Side flanges of the vessel shall be equipped with optical windows transparent to visible and IR radiation with apertures to permit transmission of laser beams sized and oriented in the following ways. (See reference drawings Appendix C.)

a. Aperture of 8 cm diameter centered and directed along the prime optical axis of the discharge region.

b. Aperture of 4 cm diameter centered on the axis intersecting the prime optical axis in the central point of the discharge region at an angle of 5° formed in a plane parallel to the electrode surface (preferably in a horizontal plane).

c. Aperture of 2 cm diameter intersecting the optical axis in the central point of the discharge region at the angle of -5° formed in a plane parallel to the electrode surface

3.2.2.8.2 Window material and its thickness shall be chosen to produce a minimum optical attenuation to the IR laser beam (less than 3%/pass), high optical damage threshold (above 0.5 J/cm^2 in a single shot with a 10-ps CO_2 laser test pulse), and to withstand a 10-atm vessel pressurization as well as impulse shock produced by electrical discharge of up to 20 kJ energy loading.

3.2.3.8.3 The window design shall comply with the BNL ES&H Standard Sections 1.3.4 and 1.4.2.

3.2.3 Mechanical Supports

3.2.3.1 Mechanical supports shall be attached to the floor and hold the assembled high-pressure vessel in rigid position connected to HVPFN, gas circulation system and other subsystems. Mechanical supports shall be designed to permit convenient access to vessel ports and flanges for operation, maintenance, leak test, and repair.

3.2.3.2 The mechanical supports shall comply with the BNL ES&H Standard Section 1.6.0.

3.2.4 Discharge Cell Safety Features

3.2.4.1 The discharge cell radiation shield shall satisfy BNL requirements ES&H Standard Sections 2.3.1, 2.3.2, 2.4.0 and 3.1.0 for complete protection against x-ray and other electromagnetic non-laser radiation being generated in the course of the amplifier operation. The residual

radiation shall not present any hazards to the personnel working in the laser room. The permissible radiation level at 1 m distance from the equipment is less than 5 millirad/hr.

3.2.4.2 Discharge cell electrical shield and grounding shall be designed to minimize stray EMP radiation and extra current loops in order to eliminate cause of any disorder to the sensitive electronic equipment located in the laser room and shall comply with BNL ES&H Standard Sections, 2.3.2.

3.2.4.3 The discharge cell shield together with electrical interlock system shall prevent any possibility of personnel exposure to electrical shock. It shall comply with National Electric Code and BNL ES&H Standard Sections 1.5.0 and 1.5.2.

3.2.4.4 Mechanical design of the pressurized discharge cell shall comply with the BNL ES&H Standard Sections 1.4.0 and 1.4.1. an overpressure relief valve shall be implemented to protect against cavity rupture.

3.2.4.5 The amplifier acoustic noise emission shall be within safe levels and shall comply with BNL ES&H Standard Section 2.4.0.

3.3 X-Ray Preionizer

3.3.1 General

The x-ray preionizer shall provide a broad x-ray beam uniformly irradiating the discharge region comprised by the electrode manifold accommodated inside the discharge cell. By applying a 30-100 KeV potential to the electron emitter, an accelerating electric field is developed between the emitter and target. Electrons originated from the emitter are accelerated by the amount of the potential drop and then stopped at the target, producing x-rays of the same energy. X-rays penetrate through the target and nearest main discharge electrode into the main discharge volume and ionize the gas.

3.3.2 It is the responsibility of the contractor that X-ray dose magnitude and distribution provided by the preionizer satisfy conditions for stable and uniform discharge. These conditions shall be verified according to the test procedure described in sections 5.4 and 5.5.

3.3.3 Provisions shall be made for appropriate insulation of the emitter from ground and from the electrode manifold.

3.3.4 Provisions shall be made for high-vacuum pumping of the preionizer chamber and for controlled gas flow introduced into the chamber..

3.3.5 The preionizer life-time shall be guaranteed by the contractor to be not less than 1 x 10^6 shots. Provisions shall be made for easy removal of the preionizer for maintenance and repair.

3.3.6 The preionizer shall comply with the BNL ES&H Standards Sections 1.3.4, 1.5.1, 1.5.2, and 3.1.0.

3.4 High-Voltage Pulse-Forming Network (HVPFN)

HVPFN consists of two parts: a HVPFNM used to energize the main discharge in a gas discharge cell, and a HVPFNP used to apply a potential to the electron emitter of the x-ray preionizer.

3.4.1 High-Voltage Pulse-Forming Network For Main Discharge (HVPFNM)

3.4.1.1 General

The HVPFNM shall be designed to deliver a 500 kV or higher voltage pulse to the electrode manifold and to sustain a high-current discharge during a time period of 0.2-1.0 microseconds permitting the total loading of not less than 6 kJ into the gas mixture CO_2:N_2:He with a molecular content of 15% and minimum PxD=50 atmxcm, where P is the total pressure and D is interelectrode distance.

3.4.1.2 HVPFNM Type

A typical type of HVPFN shall be designed as a multi-stage Marx generator. An alternative type of HVPFNM, if suggested by the contractor, shall satisfy herein requirements. Standard electronic parts shall be used where possible and provisions for easy maintenance and repair of the HVPFNM shall be made.

3.4.1.3 HVPFNM Life Time

The HVPFNM and its components shall be designed and chosen to meet the requirements of prolonged operation life time between replacement or repair of its sensitive parts. The required life time for the HVPFNM components under the normal operating conditions before their replacement or refurbishing is: 1 x 10^6 shots for spark gaps, 5 x 10^6 shots for other components. As a proof of the expected life time, contractor shall present either a manufacturer specification for standard components or prior test results for any nonstardard components used.

3.4.1.4 HVPFNM Safety Features

The HVPFNM shall meet National Electric code and OSHA 1910-147 standards and shall be equipped with dual independent interlocks which activate an emergency energy dump. The HVPFNM shall comply with the BNL ES&H Standard Sections 1.5.0 and 1.5.2.

3.4.1.5 HVPFNM Control System

The HVPFNM control system is a part of the HVPFNM assembly and includes:

a. Triggering unit

b. Spark gaps gas flow control panel

c. Diagnostics

3.4.1.5.1 HVPFNM Triggering Unit

The HVPFNM triggering unit supplies high voltage pulses to trigger the HVPFNM spark gaps. The initiation of the triggering unit is synchronized with other components of the ATF laser system by TTL pulses. Short rise time and duration of the trigger pulse shall ensure a reliable triggering of the discharge with a time jitter less than +/- 20 ns.

3.4.1.5.2 HVPFNM Gas Flow Control Panel

The HVPFNM gas flow control panel accommodates a manifold of gas valves, flow meters, pressure gauges, and low/high pressure security interlocks. The control panel is connected with flexible conduit to the HVPFNM main unit and air/gas supply, and shall permit a convenient mounting at the control panel location.

3.4.1.5.3 HVPFNM Build-in Diagnostics

The HVPFNM build-in diagnostics shall provide monitoring of the main discharge voltage and current characteristics.

3.4.2 HVPFN For X-Ray Preionizer (HVPFNP)

3.4.2.1 General

The HVPFNP is used to apply a potential to the electron emitter of the x-ray

preionizer. The optimal accelerating potential for material penetration and gas ionization lies between 30-100 keV.

3.4.2.2 HVPFNP Triggering Unit

The HVPFNX triggering unit shall permit an advanced initiation of the x-ray flux before the main discharge starts. X-ray pulse timing jitter shall not exceed 10% of the optimal delay time between the preionization and main discharge. A TTL synchro-pulse will be provided by, ATF master-clock pulse generator.

3.4.2.3 HVPFNP Life Time

The HVPFNP life time requirements are the same as those for HVPFNM described in paragraph 3.4.1.3.

3.4.2.4 HVPFNP Safety Requirements

The HVPFNP safety requirements are the same as those for HVPFNM described in paragraph 3.4.1.4.

3.4.2.5 HVPFNP Gas Flow Control Panel

The HVPFNP gas flow control panel is arranged the same as the HVPFNM control panel described in paragraph 3.4.1.5.2. Both panels may be conveniently integrated into a single unit.

3.4.2.6 HVPFNP Built-in Diagnostics provides monitoring of the discharge voltage and current characteristics displayed on an oscilloscope.

3.4.2.7 The contractor shall consider a HVPFNP simplification and even elimination by replacing it with a pulse-charged capacitor connected between the emitter and ground. In that case, the emitter is located inside the anode of the main discharge electrode manifold. The positive potential supplied to the anode by the HVPFNM serves to accelerate electrons in the x-ray preionizer.

3.5 High-Voltage DC Power Supplies

3.5.1 The output voltage and power of DC power supplies for the HVPFNM and HVPFNP are determined by the design of HVPFNM and HVPFNP and by the repetition rate of the amplifier. The Contractor shall specify those parameters at the time of the PDR.

3.5.2 DC power supplies shall be equipped with control panel with voltage switches,

regulators and meters.

3.5.3 DC power supplies shall comply with the National Electric Code and OHSA safety standards and shall be equipped with interlocks that will activate an emergency energy dump. Any possibility of electrical shock due to a human contact, with DC power supplies or their cabling, wiring shall be excluded.

3.5.4 On/off switches of the DC power supplies, slow-discharge relief switches, and voltage regulators shall be controlled locally from the control panel in the laser room, and remotely, through the ATF computerized remote control and data acquisition system that shall be located in the ATF Control Room .

3.5.5 The buyer can exercise the option to provide its own DC power supplies at the time of amplifier assembly at the ATF. The contractor shall supply all required diagnostic test equipment for testing of the amplifier by the contractor prior to shipment to BNL.

3.6 Closed Loop Gas Circulation and Purification System (CLGCPS)

The CLGCPS serves to circulate laser gas mixture through the discharge cell and to recover the mixture components degraded in the discharge.
The CLGCPS is connected to the input and exit gas ports of the discharge cell. The CLGCPS includes:

a. Gas compressor

b. Catalytic converter

c. Diagnostic system

d. Tubing

e. CO_2 isotope recovery unit

f. Heat exchanger

3.6.1 General

At the option of the contractor the CLGCPS shall be supplied as G.F.E., by BNL. The contractor shall accommodate such a system as described in the following sections. If the contractor elects not to supply the CLGCPS then any interface requirements must be supplied to BNL by the contractor at the time of the PDR. All elements of CLGCPS shall be rated for operation at 10 atm of pressure; it shall be high-vacuum compatible and high-purity non-reactive gas compatible. Design of the CLGCPS shall be supported with gas-dynamic computations for flow rate, pressure and temperature through the CLGCPS.

3.6.2 Compressor

The compressor will produce a positive pressure differential for gas displacement through the discharge cell and closed loop circuit. Capacity shall be adequate to permit a proper gas exchange between two consecutive amplifier shuts (10 seconds), that is 100 l/min or more. The compressor, its supports and enclosure shall ensure low vibration and noise levels. Pressure and vacuum requirements for compressor are the same as the general requirements of the CLGCPS (see 3.6.1)

3.6.3 Catalytic converter

Catalytic converter serves to recombine into the original gas components byproducts of CO_2 gas dissociation and consecutive chemical reactions which occur within the main discharge. Contractor chooses among the options to transmit a total gas flow through a catalytic converter or to branch through it a certain portion of a total gas flow. Contractor shall present prior test results and/or calculations serving in support to any design option chosen. Pressure and vacuum requirements for catalytic converter are the same as the general requirements of the CLGCPS (see 3.6.1).

3.6.4 Gas diagnostics

Gas diagnostics includes: pressure gauges, flow meters, and thermocouples located in critical points throughout the CLGCPS and quadrupole mass-spectrometer. Detectors used shall provide digital or analog signals for remote display and computerized data acquisition. Overpressure relief valve and other safety signal and emergency shut-down devices shall be installed throughout the system. Quadruple mass-spectrometer equipped with a turbo-pump station is available at the ATF.

3.6.5 CLGCPS tubing

CLGCPS tubing, valves, and ballast volumes shall be designed to accommodate CLGCPS devices listed herein, provide connections to gas discharge cell and gas/vacuum supply system, and to comply with gas-dynamic calculations for CLGCPS. All ports shall have standard flanges compatible with all other related CLGCPS devices.

3.6.6 Isotope Recovery (CO_2 Separation) System

Isotope recovery (CO_2 separation) system will be developed separately and is not included into this specifications. However, two 1" ID valved-off ports shall be implemented in the CLGCPS tubing system to redirect gas for isotope recovery in the future.

3.6.7 Heat Exchanger

The amplifier's main discharge, compressor and catalytic converter operation are affected by gas temperature . Provisions shall be more to ensure that gas temperature at the entrance to the discharge cell is less that 40° C.

3.7 Gas supply and vacuum system

3.7.1 General

At the option of the contractor the gas supply and vacuum system may be supplied as G.F.E. by BNL as an up-graded version of the device that is currently in operation at the ATF. If the contractor elects not to provide the gas supply and vacuum system then any interface requirements must be supplied to BNL by the contractor at the time of the PDR.

The gas supply and vacuum system includes a subsystem for gas fill and vacuum pumping the discharge cell and the high vacuum system for x-ray preionizer.

3.7.2 Gas and vacuum system for gas discharge cell

Gas and vacuum system for gas discharge cell includes:

a. high-pressure gas cylinders with regulators,

b. gas supply lines,

c. gas manifold to control proportion and pressure of gas components introduced into the CLGCPS,

d. roughing vacuum pump with oil and water traps,

e. turbo-pump for vacuum conditioning of the discharge cell and CLGCPS,

f. vacuum pipes with valves connecting vacuum pumps to CLGCPS,

g. pressure gauges and overpressure relief valves.

The gas supply and vacuum system will be provided by the buyer during the period of the amplifier assembly and installation at the ATF. The contractor is responsible to use his own gas supply and vacuum system to conduct in house acceptance tests of the amplifier in accordance with the contract, S.O.W. and this specification.

3.7.3 High Vacuum System

High vacuum system is used to maintain low operating pressure and for vacuum

conditioning of x-ray preionizer. It includes a high-vacuum turbo pumping station and leak valve to introduce a slow flow of a working gas. ATF will consider installation of its own turbo-station to pump out the x-ray preionizer. In that case, in-shop tests and procured components as defined in section 3.7.1 and interface details shall be supplied to BNL at the time of the PDR.

3.8 Control Panel

Control panel shall be located in the vicinity of the amplifier in the laser room. It accommodates control and display devices necessary for normal operation of the amplifier and its subsystems including: controls and displays for HVPFNM, HVPFNP, DC power supplies, remote controls and displays for CLGCPS, gas supply and vacuum systems. Rack-mounted control electronics (oscilloscopes, pulse generators, etc.) will be accommodated in a standard 19" rack placed next to control panel. As stated above, some of the control and data acquisition functions of the control panel and rack mounted electronics will be duplicated by the ATF computer control and data acquisition system. For that purpose, appropriate connectors or spare space shall be anticipated at the back or side wall of the control panel.

4.0 CONTRACTOR TESTS

4.1 General

All tests and checks are discussed herein according to the task sequence and according to the Statement of the Work (SOW) # 765507.

4.2 Gas Discharge Cell and X-Ray Preionizer Tests

The discharge cell with x-ray preionizer covered by this specification must be subjected to vacuum and pressure tests at the contractor's plant after all manufacturing operations are completed according to SOW sub-task 3.1.2.1. Tests, according to methods described in sections 5.1 and 5.2, shall be done in assembled operational configuration of the discharge cell and x- ray preionizer with electrodes, feedthroughs, and internal insulation elements installed. Discharge cell is subject to pressure test up to 15 atm.

4.3 Amplifier Assembly Tests

The amplifier assembly that is in compliance with this specification and completed according to SOW #765507, section 3.1.2.3 must be subjected to radiological, electrical, and optical tests at the contractor's plant. Tests shall be done according to the methods described in sections 5.3-5.6. Test shall be conducted by the contractor at their premises before delivery of the amplifier to the buyer. The results of tests must be documented. The buyer may witness any or all of these procedures at their discretion.

4.4 Amplifier Final Tests

Upon installation at the ATF according to SOW #765507 section 3.1.3, the amplifier must be subjected to vacuum, pressure, electrical, optical, and gas dynamic tests at the buyer's site. Tests shall be done according to the methods described in sections 5.1-5.6.

4.5 Documentation of Test Results

4.5.1 Project Log and Data Notebooks

The subcontractor shall maintain a project log and data notebook. The notebook shall define all major test procedures as indicated in section 5.0 of this specification and resulting raw data of each test. Examples of all pertinent computations, test results to satisfy the requirements of section 4.0 and daily notes detailing individual results shall be included.

4.5.2 Witness Points

The domestic subcontractor shall contact the buyer a minimum of five (5) working days prior to any major subsystem and system acceptance tests that are outlined in SOW #765507 or this specification.

4.5.3 Test Results

Test results that are obtained shall reside in the project log.

4.5.3.1 Sub-Component Acceptance Test Reports

All acceptance tests of major subcomponents shall be summarized and presented in report form.

4.5.3.2 General Diagnostic and Incoming Inspection

All test results and incoming inspections results shall reside in the data notebook.

4.6 Quality Assurance Provisions

The quality control provisions as defined in applicable paragraphs in the BNL QA 101 document shall be fully implemented and adhered to by the contractor.

4.6.1. The Quality Assurance Provisions are outlined in the BNL QA 101 document that is found in Appendix B.

5.0 TEST PROCEDURES

The contractor shall prepare written test procedures for Sections 5.1 through 5.6 and submit them to BNL for approval. An individual test procedure shall be submitted for review not less than 10 working days prior to the start of the specific test. Alternative test procedures shall be considered by BNL only if specified test procedures are determined too costly or impractical through negotiations between BNL and the contractor.

5.1 Vacuum Leak Testing

Internal cavities of the discharge cell and x-ray preionizer are subject to leak test after all cleaning, baking and outgasing operations have been completed. Contractor must have in its disposal a helium mass spectrometer leak detector with a detection sensitivity of 10^{-8} cc/sec as measured on a calibration helium leak. Cavities shall be termed leak-tight when total leak rate does not exceed 10^{-7} cc/sec while using a helium mass spectrometer leak detector. Subsequent to delivery, buyer will perform its own vacuum leak testing in the same manner at its own site as part of the acceptance testing, in order to verify the vacuum and mechanical integrity of the amplifier cavities.

5.2 High Pressure Tests

The amplifier cavity shall be pressure tested to 150% of its operating pressure and conform to the ASME Pressure Vessel Code section 8.0 and to the BNL ES&H standard sections 1.4.1 and 1.4.2. The preliminary pressure test shall use a hydraulic fluid (water) to apply hydrostatic pressure to the amplifier cavity when optical windows are temporarily replaced with metal flanges. Appropriate cleaning/drying must be performed after testing is complete. The final test procedure for the amplifier cavity with optical windows installed shall be written by the contractor and will be submitted for approval prior to start of pressure testing.

5.3 X-ray Dose Tests

5.3.1 X-ray dose distribution measurements in the space between the main electrodes of the discharge cell shall be performed. Measurements shall be made in several locations using the x-ray probe inside the discharge cell in order to provide characterization of x-dose distribution inside the interelectrode volume. Measurements may be performed in air at one atmosphere pressure.

5.3.2 Measurements shall demonstrate single-shot x-ray dose in the central point of the interelectrode volume to be less than 15 mRad/cm^2 pulse . Dose drop above the edge of the flat electrode surface should not exceed 20% of the middle point dose magnitude.

5.3.3 X-ray dose rate measurements in the vicinity of the discharge cell. Sensitivity of the x-ray dosimeter and number of shots shall be chosen to demonstrate the required low level of irradiation 5 mRad/hr. at the distance of 1 m from the discharge cell and

preionizer. Measurements shall be done at normal operating conditions at full charge of capacitor banks of the preionizer and main discharge.

5.4 Electrical Discharge Tests

Discharge tests shall be conducted at normal operating conditions of the discharge cell at total gas pressures of 5 atm. and 10 atm. and at variable molecular content between 15% and 30%. Discharge tests include:

5.4.1 Establishing a proper timing between preionization discharge and main discharge in order to produce a stable discharge.

Time jitter of the preionization and main discharge shall be demonstrated to be less than 20 nanoseconds.

5.4.2 Measurement of voltage and current characteristics of the preionizer and main discharge.

Upon the electric measurement made for the main discharge, specific energy loading in the discharge shall be calculated. This value shall be demonstrated to be not less than 100 J/l.atm for aforementioned pressure and molecular content ranges

5.4.3. Spatial envelope and uniformity of the discharge region

The spatial envelope and uniformity of the discharged region shall be tested by photography of the discharge made through the output optical window of the discharge cell. Microdensitometer trace of the photographic image made through the middle of the discharge region in the direction along the electrode plane shall demonstrate less than 20% drop of the discharge luminescence intensity at the edges of the electrodes flat regions.

5.5 Optical Gain Tests

Small signal gain (SSG) in the discharge cell shall be measured as a function of time and highwidth position across the interelectrode region. CW CO_2 laser beam shall be directed parallel to the amplifier optical axis. Output signal measured by the IR power detector and displayed on an oscilloscope presents a time-evolution of gain during the discharge. Peak SSG shall be demonstrated to be not less than 2.5%/cm. Gain non-uniformity across the interelectrode area shall not exceed ±10%.

5.6 Gas Dynamic Tests

5.6.1 Measurement of a pressure drop across the discharge cell at normal operating conditions with gas circulating through the discharge cell and CLGCPS. It shall be

demonstrated that the pressure drop on the discharge cell is below 20% of the total pressure increment developed by the compressor of the CLGCPS.

5.6.2 Measurement of spatial and time uniformity of the gas flow through the discharge region.

These tests shall be done by a time resolved interference methods. As an alternative method, probing of the interelectrode region with a HeNe laser beam may be used. In this case, deviations of the laser beam from its static position will be a measure of the gas flow nonuniformity and instability. Test result will be considered satisfactory if the laser beam angular deviation in any point of the interelectrode region does not exceed 0.3 milliradian.

6.0 DELIVERY, SHIPPING AND INSTALLATION REQUIREMENTS

6.1 Preparation of Shipment

The subcontractor shall package all major subcomponents in appropriate shipping containers. The components shall be wrapped in plastic that will effectively prevent environmental moisture or road debris from penetrating the component packaging. Desicate shall be supplied as required to assure a non-condensing atmosphere inside the shipping container.

6.2 Rigging

6.2.1 Appropriate lifting eyes and support points shall be designed and installed on all sub components or subassemblies of components weighing 100 pounds or more.

6.2.1.1 All components shall be designed so as to utilize the existing doors and hallways of the ATF using generally available means of rigging and/or transport. A drawing showing the floor plan and access corridors of building 820 can be found in Appendix "C".

6.3 Building Integrity

All sub components shall be designed and packaged so as to allow uncrating on the floor of building 820 and final assembly may be made in the CO_2 room without significant changes to the room or building 820. A drawing showing a partial floor plan of building 820 can be found in Appendix "C".

6.4 Shipping

6.4.1 The contractor shall hire the services of an exclusive use carrier to transport the laser amplifier assembly FOB, Building 820, Brookhaven National Laboratory, Upton, NY 11973.

6.4.2 Carrier

6.4.2.1 Domestic Carriers

The carrier shall use a trailer with an air ride type active suspension system to minimize shock and vibration to the amplifier assembly during transport.

6.4.2.2 International Carriers

The international carrier shall transport by air the laser amplifier FOB Kennedy Airport, New York, NY, USA.

Appendix A.

Acronyms and Abbreviations

(ATF) Accelerator Test Facility
(BNL) Brookhaven National Laboratory
(CDR) Critical design Review
(PE) Project Engineer
(SOW) Statement of the Work
(PS) Project Scientist
(NSLS) National Synchrotron Light Source
(HVPFN) High voltage pulse forming network
(DC) Direct Current
(IR) Infrared
(ASME) American Society of Mechanical Engineers
(EMP) Electro-magnetic pulse
(HVPFNM) Maindischarge High Voltage Pulse From Network
(HVPFNP) X-ray Preamplifier High Voltage Pulse Forming network
(TTL) Transistor-Transistor Logic
(OHSA) Occupational Health and Safety Act
(CLGCPSPS) Closed Loop Gas Circulation and Purification System
(SSG) Small signal gain
(G.F.E.) Government Furnished Equipment

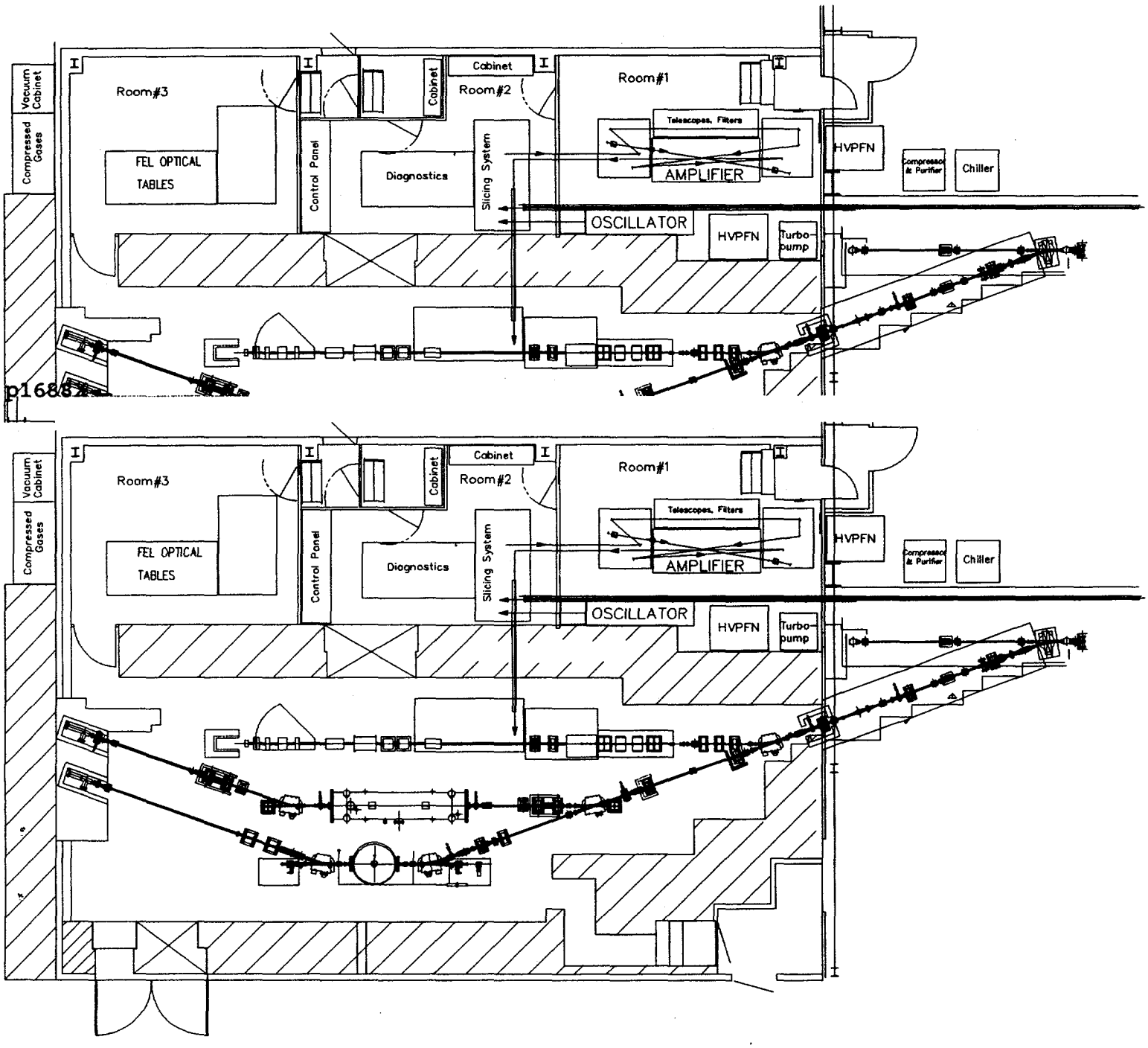
Vacuum Cabinet
Compressed Gases
Room#3
FEL OPTICAL TABLES
Control Panel
Cabinet
Cabinet
Room#2
Diagnostics
Slicing System
Room#1
Telescopes, Filters
AMPLIFIER
HVPFN
Compressor & Purifier
Chiller
OSCILLATOR
HVPFN
Turbo-pump
Vacuum Cabinet
Compressed Gases
Room#3
FEL OPTICAL TABLES
Control Panel
Cabinet
Cabinet
Room#2
Diagnostics
Slicing System
Room#1
Telescopes, Filters
AMPLIFIER
HVPFN
Compressor & Purifier
Chiller
OSCILLATOR
HVPFN
Turbo-pump

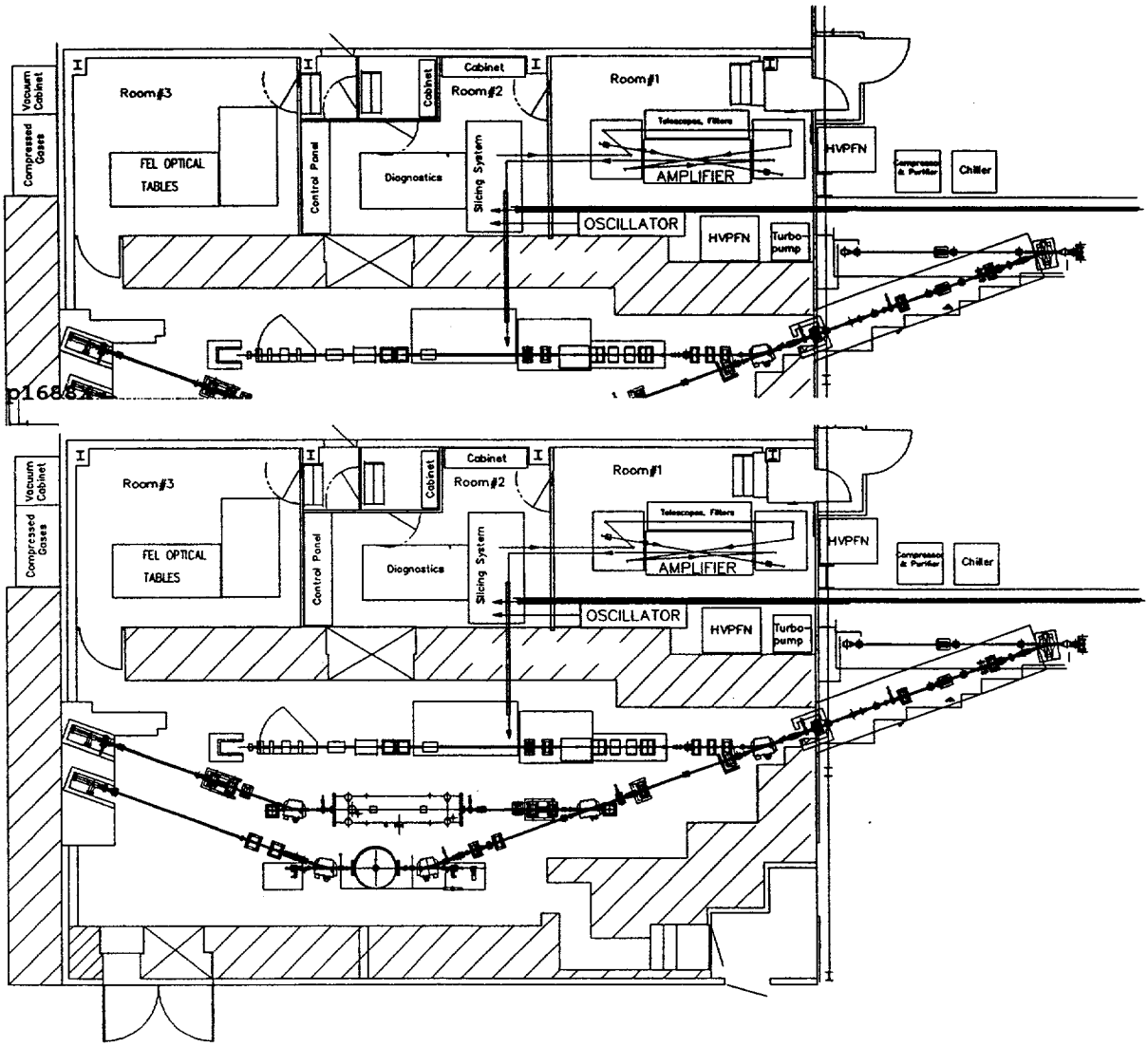
Vacuum Cabinet
Compressed Gases
Room#3
Cabinet
Cabinet
Room#2
Room#1
Telescopes, Filters
HVPFN
Compressor & Purifier
Chiller
FEL OPTICAL TABLES
Control Panel
Diagnostics
Slicing System
AMPLIFIER
OSCILLATOR
HVPFN
Turbo-pump
Vacuum Cabinet
Compressed Gases
Room#3
Cabinet
Cabinet
Room#2
Room#1
Telescopes, Filters
HVPFN
Compressor & Purifier
Chiller
FEL OPTICAL TABLES
Control Panel
Diagnostics
Slicing System
AMPLIFIER
OSCILLATOR
HVPFN
Turbo-pump